AN INVESTIGATION INTO COMBINING ELECTRICAL IMPEDANCE MAMMOGRAPHY WITH 3D ULTRASOUND FOR BREAST CANCER DETECTION

By

NEVIS BEQO

Submitted For The Degree Of
Doctor Of Philosophy

BIOMEDICAL RESEARCH
SCHOOL OF ENGINEERING AND INFORMATICS
UNIVERSITY OF SUSSEX
BRIGHTON
UK

November 2012

DEDICATION

To my parents for teaching me to always ask questions and go in the pursuit of science to find my answers.

To the 100th Anniversary of the Independence of Albania.

DECLARATION

I hereby declare that this thesis has not been and will not be submitted in whole or in part to another University for the award of any other degree.

Signature:.....

Nevis Beqo

UNIVERSITY OF SUSSEX

NEVIS BEQO - PHD BIOMEDICAL ENGINEERING

AN INVESTIGATION INTO COMBINING ELECTRICAL IMPEDANCE MAMMOGRAPHY WITH 3D ULTRASOUND FOR BREAST CANCER DETECTION

SUMMARY

Worldwide, breast cancer accounts for 22.9% of all cancer incidences in women, causing 458,503 deaths per annum [WHO 2008]. The most common screening method is X-ray mammography, an ionising method, which has many technical and age group limitations and has come under scrutiny for accuracy and safety on many occasions.

Electrical Impedance Mammography (EIM) is a novel, non-invasive, non-ionising imaging modality based on bioimpedance. Initial test results show it as very promising; however the image resolution is quite low. Ultrasound imaging is widely used for high-resolution medical imaging and clinical diagnostics. Ultrasound is non-invasive and is effective in imaging soft body tissue, including subcutaneous structures and organs, but fails to distinguish tissue type.

Merging the information of the above modalities and integrating them in an automated device offers a safe, non-invasive, fast, higher accuracy, breast cancer detection method for all age groups. To explore the proposed system, the work was divided into cumulative integrative stages: investigation of the technical challenges of a real world breast scanner device for each modality and the combination of both, including engineering, repeatability, safety and ergonomics, to adhere to medical device standards; data acquisition systems design, signal processing and calibration; image geometry correction; 3D image reconstruction; volumetric merger and visualisation; validation with dual modality scans on phantoms and *in-vivo*; DICOM image porting.

These two modalities were successfully combined in a unified automated breast scanner that can accommodate and scan 95% of women (breast volume up to 1200cc) in a safe and comfortable way. Data acquisition and scan time achieved is five minutes per breast. The image results achieved from this research complement each other by integrating the boundary information of Ultrasound with the impedance data and tissue discrimination of EIM, therefore potentially providing a more complete and accurate cancer diagnostic method. The images were successfully ported into the DICOM radiology imaging standard therefore becoming platform independent. This work concluded with over twenty academic publications and two filed patents on the technology of a breast scanner and on the methodology of its imaging.

ACKNOWLEDGEMENTS

This project has been a very enjoyable experience and I have been privileged to work with so many talented and determined people. My greatest thanks are for my two esteemed supervisors Dr Wei Wang and Prof Christopher R. Chatwin for their guidance and support, their open door policy and their wealth of knowledge. The advancement of this project would not have been possible without the support of the DTI (Department of Trade and Industry) of the United Kingdom.

There are so many people I would like to thank for their support in hardware, software, training, guidance, clinical support or simply just being there for me. The list is so long that I wouldn't know where to begin. It would be only fair to include everybody and that is why I am including a list with of all the Companies and Institution in alphabetical order, with my greatest gratitude:

- BRIGHTON AND SUSSEX HOSPITALS NHS TRUST – PARK CENTRE FOR BREAST CARE
- BRIGHTON AND SUSSEX MEDICAL SCHOOL – CLINICAL IMAGING SCIENCES CENTRE
- CREATE-3D LTD
- DE MONTFORT UNIVERSITY – BIOMEDICAL ENGINEERING RESEARCH
- DIAGNOSTIC SONAR LTD
- OXFORD UNIVERSITY HOSPITALS NHS TRUST – JOHN RADCLIFFE CANCER CENTRE
- SWINDELL & PEARSON LTD – INTELLECTUAL PROPERTY ATTORNEYS
- TECHNOLOGY STRATEGY BOARD OF THE DEPARTMENT FOR BUSINESS, INNOVATION AND SKILLS, UK
- UNIVERSITY OF SUSSEX – BIOMEDICAL ENGINEERING RESEARCH
- WEEDON ELECTRONICS LTD

FALENDERIME

Falenderoj perzemersisht Komandant Mevlanin, Presore Shaden dhe Enrin me Blerinen per mbeshtetjen e tyre.

Nje falenderim te vecante ja dedikoj te bukures Dasara.

TABLE OF CONTENTS

LIST OF TABLES

LIST OF FIGURES

ACRONYMS

3D:	Three-Dimensional
AJCC:	American Joint Committee on Cancer
APT:	Applied Potential Tomography
BIS:	Bioimpedance Spectroscopy
CE:	Conformité Européenne (European Conformity)
COTS:	Commercial Off The Shelf
CT:	Computed Tomography
CAT:	Computed Axial Tomography
DAQ:	Data Acquisition
DAS:	Data Acquisition System
DBT:	Digital Breast Tomosynthesis
EIM:	Electrical Impedance Mammography
EIT:	Electrical Impedance Tomography
EIS:	Electrical Impedance Spectroscopy
FDA:	Food and Drug Administration
FFT:	Fast Fourier Transform
FN:	False Negative
FP:	False Positive
GPL:	General Public Licence
HIFU:	High Intensity Focused Ultrasound
IEC:	International Electrotechnical Commission
IFU:	Instructions For Use
ISO:	International Organization for Standardization

LDPE:	Low-density Polyethylene
LVDT:	Linear Variable Differential Transformer
MHRA:	Medicines and Healthcare products Regulatory Agency
MIT:	Magnetic Induction Tomography
MNR:	Modified Newton Raphson
MRI:	Magnetic Resonance Imaging
MUX:	Multiplexer
NEMA	National Electrical Manufacturers Association
NI:	National Instruments
NIROT:	Near Infrared Optical Tomography
OEM:	Original Equipment Manufacturer
PC:	Personal Computer
PCI:	Peripheral Component Interconnect
PCB:	Printed Circuit Board
PET:	Positron Emission Tomography
PPV:	Positive Predictive Value
PTFE:	Polytetrafluoroethylene
PXI:	PCI eXtensions for Instrumentation
RAA:	Risk After Action
ROC:	Receiver Operating Characteristic
ROI:	Region of Interest
SNR:	Signal to Noise Ratio
TN:	True Negative
TNM:	Tumour Node(lymphatic) Metastases
TP:	True Positive

SYMBOLS

A	Amplitude
A_0	Amplitude at reference location
α	Relaxation factor
C	Membrane capacitance
f	Frequency
F_r	Relaxation frequency
j	Complex number
l	Distance sound travels
λ	Wavelength
$NaCl_{(aq)}$	Sodium chloride dissolved in water e.g. saline
Ø	Diameter
R	Resistance of extracellular space
R_e	Reflected energy
R_∞	Resistance at high frequencies (to infinite)
R_0	Resistance at low frequencies (to zero)
ρ	Material density
S	Resistance of intracellular space
θ	Resolution
V	Acoustic velocity
Z	Impedance
Z_a	Acoustic impedance

CHAPTER 1

- INTRODUCTION

1.1 BACKGROUND

Early stage diagnosis and medical imaging are proving to be invaluable in the fight against cancer (Tabar and Dean, 2010). According to the World Health Organisation in their 2008 GLOBOCAN report "Worldwide, breast cancer accounts for 22.9% of all incidences in women, causing 458,503 deaths (Ferlay et al, 2010). The 2007-2010 Breast Cancer Facts & Figures of the American Cancer Society show that the death rate is reduced by 22-44% if the cancer is diagnosed at an early stage (Duffy and Tabar, 2002). Facts like these are the reason why routine mammography screening is highly recommended and has been introduced in many countries. Tabar et al, 1985), (Hellquist et al, 2011).

Currently, there are a few well-established technologies that are in common use in hospitals and clinics, assisting clinicians every day in their diagnostic work. Some of the most used are: X-Ray Mammography, (MRI) Magnetic Resonance Imaging, X-ray (CT) Computed Tomography or (CAT) Computed Axial tomography, Ultrasound Imaging, (PET) Positron Emission Tomography, (SPET) Single-Photon Emission computed Tomography etc. (Cherry, 2006), (Hassan and El-Shenawee, 2011). Each technology has managed to position itself in a particular area of Radiology-diagnostics based on the triangle of: Cost-Speed-Results. That is not to say that the areas of use and applications do not overlap. Recently the combination of two or more technologies (modalities) has been found to yield better scan results, therefore providing a more accurate and informed diagnosis (Cherry, 2006) (Kelly et al, 2011).

In the fight against cancer other new scanning and imaging technologies are emerging. Some of them are in prototype/research stage, whilst some have already gone through clinical trials evaluation. These new technologies are targeting well-known areas and challenging the commercial dominance of the 'well-established' ones by either offering; lower equipment and operation costs; faster scans and analysis; better results in specific diagnosis; or increased safety for patients and medical personnel. Worth mentioning are: (DBT) Digital Breast Tommosynthesis, (PAT) Photoacoustic Tomography, Breast Thermography, EIT (Electrical Impedance Tomography), MIT (Magnetic Inductance Tomography, (NIROT) Near Infrared Optical Tomography etc. (Griffiths et al, 1988),

(Cook et al, 1994), (Hartov et al 2000), (Brown et al, 2001), (Tromberg et al, 2008) (Dobbins et al, 2009), (Hassan and El-Shenawee, 2011).

Detecting cancer faster and safer and as a result saving human lives, is the noble driving force behind the development of these technologies. In addition there is also a major commercial incentive. The July 2011 report on diagnostic imaging from market research company 'Markets and Markets' suggest that the global diagnostic imaging market is expected to reach $26.6 billion by 2016. The report also points out that 'fusion imaging' or 'technology combination' such as PET+CT, SPECT+CT, MRI+PET are attracting a lot of interest and are fuelling the trend.

An integral part of medical imaging is also the DICOM (Digital Imaging and Communications in Medicine) Standard. DICOM had become the international standard for viewing, storing and transferring information on all scans from MRI, CT, DBT, PET and Ultrasound for all kinds of scans (Source NEMA.org – National Electrical Manufacturers Association). This unified imaging standard, as recognised by ISO 12052:2006, makes it possible that scanners, servers, workstations, printers etc. from different manufacturers can be fully compatible with hospital PACS (Picture Archiving and Communication System). The standardisation and expansion of DICOM in hospitals and the Medical Imaging Market makes it imperative that any new imaging technology must offer compatibility in order to facilitate acceptance from PACS trained clinical personnel.

1.2 RAISON D'ÊTRE

Current most used breast cancer diagnosis technologies (e.g. X-Ray, MRI etc.) offer a great deal of support to clinicians in their diagnostic work. However there are many limitations that these technologies face, which subsequently translate into diagnosis uncertainty (Pisano et al, 2005).

Imaging technologies can offer the ability to identify a ROI (Region of Interest) and depending on patient, lesion location, technology etc., are limited to the size of cancer they can detect (Baert, 2008) (Kelly et al, 2010). A further examination by biopsy or histopathology and the involvement of qualified and experienced pathologists is then

required. This 'double-procedure' affects the diagnosis in a negative way, by delaying the outcome of the results or increasing false-positive occurrences; 40% for imaging and 26% False Negatives from biopsy (Bayford, 2006).

In terms of patient numbers for breast cancer screening, X-Ray mammography takes centre stage (Dean and Tabar, 2010). MRI offers higher accuracy but is very expensive therefore it is reserved for women with a probability of 20% or higher of developing breast cancer in their lifetime, e.g. women with a strong family history of breast cancer or those who are likely or identified carriers of the BRCA1/BRCA2 gene mutation. MRI can also return a high number of False Positives by picking up breast changes that are not cancer, as confirmed by unnecessary biopsy (Viehweg et al, 2000).

Mammography is reasonably cheap and has been used for many years, therefore becoming a gold standard. However criticism towards it has increased, not only about its effectiveness but also due to its ionising technology (x-rays). It might actually cause more harm than good, i.e initiating mutation and increasing cancer probabilities. Also one of the major limitations of Mammography is its inability to visualise radiographically dense breasts. Density is a risk factor for both False Positives and False Negatives (Fletcher and Elmore, 2003). Breast density variation can be as result of age, ethnicity, weight, stage of menstrual cycle, number of births, etc. (Boyd et al, 2007). Women below 50 years of age have higher density in their breasts than older women. However high density may also be present at high levels even in older women and this has been shown in 40-60% of women who have had mammograms. (Kolb et al, 1998). This causes a problem for mammogram diagnosis. On mammograms, film and digital, dense breast tissue can mask more than half of invasive breast cancers (Pisano et al, 2005). In the breast, higher levels of fibrous connective and glandular tissue than fatty tissue will translate to denser breasts. Statistically, women with dense breast tissue have 4-6 times higher chances of developing breast cancer in their lifetime (Boyd *et al*, 2007). This is a 'catch 22' situation; women with high breast density have a higher risk for breast cancer and at the same time mammography cannot distinguish their cancers at an early stage, furthermore x-rays can cause breast cancer.

Breast Biopsy, the incision and removal of tissue from the breast (sometimes multiple times in the session) with a specialised needle, can be a very painful and traumatic

experience for the patient. The tissue is then sent to a lab for examination under the microscope or chemical analysis. FNA (Fine Needle Aspiration) uses a 20-22 gauge needle (0.6 - 0.9 mm diameter) and is less traumatic than Core biopsy, where the needle can be a gauge 11 (3 mm in diameter) (Verkooijen, 2002). At the moment biopsy is deemed necessary and as the last step into confirming a breast cancer in the event of a positive diagnosis from the mammogram (Joy et al, 2005). If the lump is big and can be identified by palpation then a freehand needle biopsy is performed. In any other case, biopsy has to rely in some kind of imaging modality in order to guide the clinician to the ROI (Region of Interest). These are mainly ultrasound guided, stereotactic or vacuum-assisted.

Some new imaging technologies on their own or in combination with proven ones could offer the possibility of higher diagnosis accuracy, lower costs, increased safety in breast cancer etc. One of them is EIT (Electrical Impedance Tomography) and its derivative for breast cancer screening named EIM (Electrical Impedance Mammography). EIM is a non-invasive, safe technique that measures the distribution of electrical impedance in the breast. It uses no ionising radiation and does not rely on any contrast agents, therefore making it a candidate for mass screening.

1.3 Original System Engineering Contributions to EIT + ultrasound Combined System

The research and personal contributions presented in this PhD thesis are concentrated on the investigation of EIT in the current proposed form of mammography, and its evolution - co-imaging with ultrasound, as a valid medical diagnostic technology. The thesis is presented from the point of view of medical physics and instrumentation, including the identified challenges and proposed solutions from in-house investigations and from the clinical environment. The analysis is done using current Systems Engineering Theory methodology. Focusing on - that this is a new technology, which is ultimately targeted for the diagnosis of breast cancer in humans, and will require human operation, albeit trained personnel. This is expressed in the proposed ergonomics, the human-machine interaction and the safety analysis of the technology and apparatus. It is now almost 30 years since EIT was identified to have the potential to be used as a mainstream medical device. However, apart from the technology validity, an EIT device as a whole has to satisfy a set of international directives in order for it to be

certified as a commercial entity. Otherwise it will always remain a technology bound to research labs and with no apparent benefit to humanity. Assessments on IEC 60601 and ISO 14971 for EIT and Ultrasound have been investigated. Parts are presented in the thesis and further tailored for the proposed designs. The original contributions are:

- EIM System Architecture, with the introduction of a novel Data Acquisition and System Control platform based on PXI architecture.
- Control of the whole environment from a laptop computer with integrated system software for: scanner position, water heating, liquid delivery, automated cleaning and of course, software customised multi frequency signal generation, data logging and post-processing, data compression and management etc.
- Open architecture system design to accommodate many instrumentation modalities i.e. ultrasound, FPGA, signal conditioning, signal generator, DAQ, image, motion.
- Performance analysis on the EIM system; this includes the identification of air bubbles on electrodes; artefacts; noise spikes; patient contact issues and ergonomics; signal corruption; breast boundary detection; repeatability; phantom types etc.
- Ultrasound investigation for a 3D scanner design that can accommodate a human breast with the prospect of merging the data with the EIM scans.
- Investigation and material testing for the 3D Ultrasound scanner and auxiliaries.
- Successfully combining a dual modality EIM + Ultrasound scanner, fulfilling the specifications and analysing the method of how to scan a breast in a repetitive and safe way, including clinical protocol. Design and patent awarded.
- Investigating ways of compensating the loss of 4 EIM electrodes due to the ultrasound transducer positioning; including superposition or 'bridge' electrodes.
- Data visualisation software and test rigs for both EIM and Ultrasound.
- Convert and display images with full compatibility to the medical DICOM standard, including digitisation and conversion errors, interpolation and registration.
- Risk assessment, of an EIT and Ultrasound based medical device, for acceptance to IEC/ISO standards and in turn for MHRA approval and further on CE Marking.
- Location coordinates extraction and motion controller for targeted dosing possibilities, including semi invasive HIFU. Design and patent applied for.
- Possibility of nipple effect (mask) removal in EIT scans.
- 3D EIM shape information and data transfer to custom meshing.
- EIM resolution increase using multiple scanning and superposition.
- Intracavity EIT and Ultrasound design for cancer diagnosis.

1.4 CONTENT OF THE CHAPTERS

The thesis consists of seven chapters plus bibliography and the appendix with some selected publications.

Chapter 1 starts with an introduction and background on the breast cancer problem. It also introduces some of the common imaging modalities for breast cancer diagnostics, in clinics and research, making way for the reasons behind the need for more innovations especially EIM (Electrical Impedance Mammography) and EIM + Ultrasound.

Chapter 2 presents information on the human breast and current imaging modalities. Introducing statistical analysis and reasoning why ultrasound, although not a flag bearer, does offer a lot of imaging support for breast cancer.

Chapter 3 offers a risk assessment of the system according to medical instrumentation standards. The reason for this part of the research is the preparation for the next stage when this project goes to clinical trials in a hospital.

Chapter 4 starts with the introduction of Electrical Impedance Tomography, its concepts, systems and methods derived from a literature review. It continues with an analysis of the Mk4 system and its architecture, concluding with some performance tests.

Chapter 5 does an analysis of ultrasound imaging and how it was used to achieve 3D scanner prototypes for breast imaging. It continues with tests and performance investigations and concludes with the best method selected.

Chapter 6 merges the information and the architecture of EIM in Chapter 4 with the 3D Ultrasound scanner designs in Chapter 5. It introduces the challenges of dual modality and their solutions. It concludes with dual modality visualisation using custom software and the evolution of data conversion into DICOM.

Chapter 7 opens the discussions and summarises the findings. It then expands on the overall project conclusions, achievements and way forward. Finalising with project derivatives and proposed future work from the research and the methods investigated.

The bibliography used in this thesis follows Chapter 7.

In the Appendix are presented the project's British and international patent publications.

CHAPTER 2

- BREAST CANCER DIAGNOSIS

2.1 INTRODUCTION

Breast cancer causes 458,503 deaths annually, according to World Health Organisation and the report of Ferlay et al in 2010. This chapter will expand on the classifications of breast cancers. It will follow with a statistical analysis on the efficiency of the current diagnostic methods with focus on the benefits of ultrasound and multimodality in general. The chapter also offers a report to the ergonomic question in scanning the breast, in preparation for the prototype scanners that will be revealed in the chapters to follow.

2.2 CANCER DIAGNOSIS

2.2.1 CLASSIFICATIONS

Cancer is the abnormal growth of cells in a particular part of the body, and in the case of breast cancer it normally originates from the lobules, the milk production glands, or the ducts that connect the lobules. A classification is drawn depending on where the cancer started and whether is contained or is spreading:

- (LCIS) Lobular Carcinoma In Situ - originates inside the lobules, but does not expand through the lobule walls. It is not referred as a cancer but neoplastia and x-ray cannot see it. In most cases it will not become invasive but there is a risk.
- (DCIS) Ductal Carcinoma In Situ - originates inside the ductal walls, but has not expanded. It should be treated immediately so that to reduce the chance of spreading. It is removed with surgery or even with more drastic mastectomy.
- (ILC) Invasive Lobular Carcinoma - this is when the cancer originating from the lobules has expanded on the breast tissue or even further. ILC counts for 10-15% of breast cancer cases. The method of treatment is surgery followed by therapy (radio, chemo, biological, hormone etc).
- (IDC) Invasive Ductal Carcinoma - the cancer has spread from the milk ducts into the surrounding tissue and can even continue to spread into the lymphatic channels or blood vessels and to other parts of the body. IDC accounts for 70-80% of breast cancers.

2.2.2 STAGES

The gravity of the cancer invasiveness is subject to the stage of the disease. Stages can also be specific to the type of cancer in question. The American Joint Committee on Cancer (AJCC) has developed the most commonly used stage system called TNM and this is followed with the I-IV numerical system (Tobias et al., 2010). TNM is an acronym and stands for T-tumour size; N-lymph node association; M-metastases spread. The numerical system that follows is from Knowles and Selby, 2005, and Cancer Research UK, 2011.

- Stage I
  - Stage I-a – Cancer up to 2cm but contained in the breast.
  - Stage I-b – Cancer cells identified in the lymph nodes.
- Stage II
  - Stage II-a – Cancer in lymph nodes spread in the armpit or breastbone or cancer between 2-5cm but no cancer in lymph nodes.
  - Stage II-b – Cancer between 2-5cm and lymph nodes affected or is bigger than 5cm but no lymph nodes.
- Stage III
  - Stage III-a – Cancer over 5cm with a few lymph nodes or no cancer but many lymph nodes affected.
  - Stage III-b – Chest wall and/or skin start to be affected with ulcers.
  - Stage III-c – many lymph nodes are now affected.
- Stage IV – the cancerous cells have metastasised to other parts of the body e.g. chest, bones, lungs and other organs.

If breast cancer is diagnosed at an early stage then the survival rate is higher. The Office for National Statistics (ONS) provides the following cancer survival rate in England for patients diagnosed 2005-2009:

- 95.8% survival rate if cancer diagnosed within the first year
- 85.1% survival rate at 5-10 years
- 77% at over 10 years

The survival rate drops sharply if the cancer is aggressive and diagnosed in Stage IV:

- 13% at 5 years
- 10% at 10 years

However it is very difficult to identify the early stage, as this usually does not cause any pain, discomfort and might not have any symptoms at all. A list of tell-tale signs is provided from clinicians on what women should look for:

- Palpate the breast and under the arm regularly and check for any lumps or abnormalities that were not there before
- Changes in the size, shape or skin of the breast; texture, colour, sensitivity
- Nipple discharge/tenderness or inversion

2.2.3 LOCATION

A study on the laterality, location and histology of 224,137 cases of invasive breast cancers and 34,712 *in situ* cases, was done from the Department of Health of California between 1988-1999 (Kwong, 2003). The study shows that for *in situ* cases cancer occurrences are 52% on the left breast and 48% on the right. The occurrences for invasive cancers are 50.8% on the left breast and 49.2% on the right. There seems do be no explanation why there is a higher occurrences on the left breast (Kwong, 2003).
The study continuous to expand on the locations of the cancer in the breast, by dividing it in 4 quadrants and central (areola) region.

Figure 2.1 and Figure 2.2 show maps of the locations and percentages of breast cancer occurrences *in situ* and invasive respectively. The upper-outer quadrant seems to be by far the most affected area of the breast. The study points out that this is true for both breasts and women from all ethnic groups and all ages.

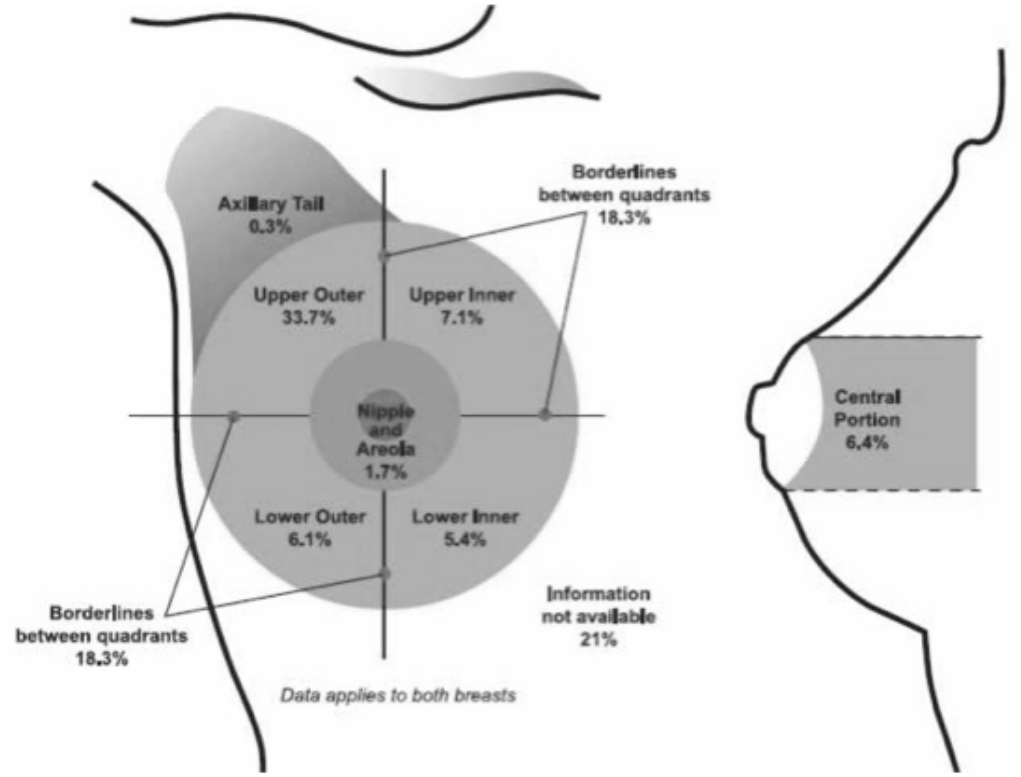

Figure 2.1 Locations and percentages of *in situ* breast cancer occurrences (Kwong, 2003).

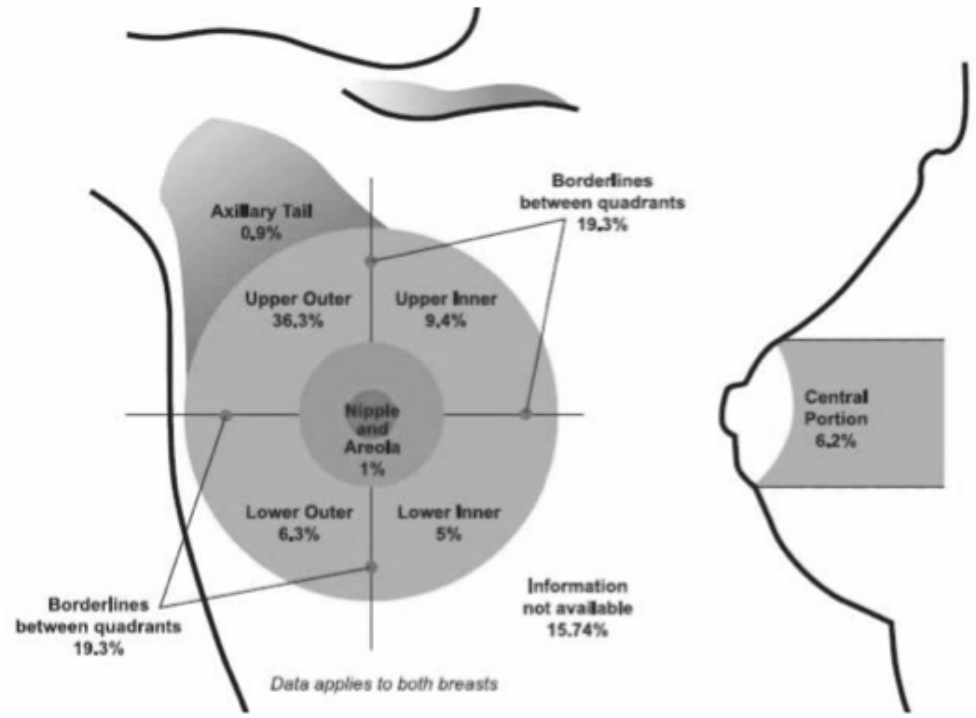

Figure 2.2 Locations and percentages of invasive breast cancer occurrences (Kwong, 2003).

2.3 STATISTICAL ANALYSIS

Medical equipment must follow sets of procedures before and after they enter the market. This can be in the form of Clinical Trials or Statistical studies and in some countries are a prerequisite from governmental bodies; eg MHRA in the UK and FDA in the USA. They permit the collection of data to evaluate in more depth many factors on the device and its performance. The data information aids in improving safety, protocol, human factors and the quite necessary statistical analysis on the device's efficiency. Some of the commonly used statistical measures are:

1. Sensitivity is the percentage of correctly identified cases, given by the ratio of True Positives (TP, correctly identified cases) over the sum of True Positives and False Negatives (FN, missed cases):

$$Sensitivity = \frac{TP}{TP + FN} \tag{2.1}$$

2. Specificity is the percentage of correctly identified non-cases (cases that do not have the disease) and is given by the ratio of True Negatives (TN, correctly identified non-cases) over the sum of True Negatives and False Positives (FP, wrongly flagged non-cases):

$$Specificity = \frac{TN}{TN + FP} \tag{2.2}$$

3. Precision a.k.a. Positive Predictive Value (PPV) is the percentage of correctly identified positive cases:

$$Precision = \frac{TP}{TP + FP} \tag{2.3}$$

4. Accuracy is the percentage of correct results out of the whole test population:

$$Accuracy = \frac{TP + TN}{TP + FP + FN + TN} \tag{2.4}$$

Berg et al, published in 2004 a study comparing the most used breast cancer detection techniques on a test population of 258 patients with breast cancer. 177 of them had confirmed malignant tumours, and 81 benign tumours. Table 2.1 presents the results.

Table 2.1. Performance comparitive table of breast cancer detection techniques.

Modality	Sensitivity	Specificity	Precision	Accuracy
Clinical examination	50.3% (89/177)	92% (75/81)	94% (89/95)	63.6% (164/258)
Mammography	67.8% (120/177)	75% (61/81)	85.7% (120/140)	70.2% (181/258)
MRI	94.4% (167/177)	26% (21/81)	73.6% (167/227)	72.9% (188/258)
Ultrasound	83.0% (147/177)	34% (28/81)	73.5% (147/200)	67.8% (175/258)
Mammo + clinical ex.	77.4% (137/177)	72% (58/81)	58.6% (137/160)	75.6% (195/258)
Mammo + ultrasound	91.5% (162/177)	23% (19/81)	72.3% (162/224)	70.2% (181/258)
Mammo + clinical ex. + ultrasound	93.2% (165/177)	22% (18/81)	72.4% (165/228)	70.9% (183/258)
Mammo + clinical examination + MRI	99.4% (176/177)	7% (6/81)	70.1% (176/251)	70.5% (182/258)

Another study of 245 women with positive family history and that were under breast cancer surveillance was done from Sim et al in 2004 and is shown in Table 2.2.

Table 2.2 Sensitivity and specificity comparison Study 2.

Modality	Sensitivity	Specificity	Precision	Accuracy
Mammography	53.9%	85.7%	n/a	n/a
MRI	93.3%	63.6%	n/a	n/a
Ultrasound	83.3%	65.5%	n/a	n/a
Mammo + ultrasound	92.9%,	62.5%,	52.0%	71.7%

Another method of representing statistical data in clinical trials is the use of the ROC (Receiver Operating Characteristic) curve, which is a graphical representation of Sensitivity vs 1-Specificity. The closer the data is to the top left corner the better it is.

The data in Figure 2.3 is from Berg et al, 2008 and their results confirm that adding ultrasound to mammography will diagnose 1.1 to 7.2 cancers per 1000 high-risk women, but it will also increase the number of False Positives.

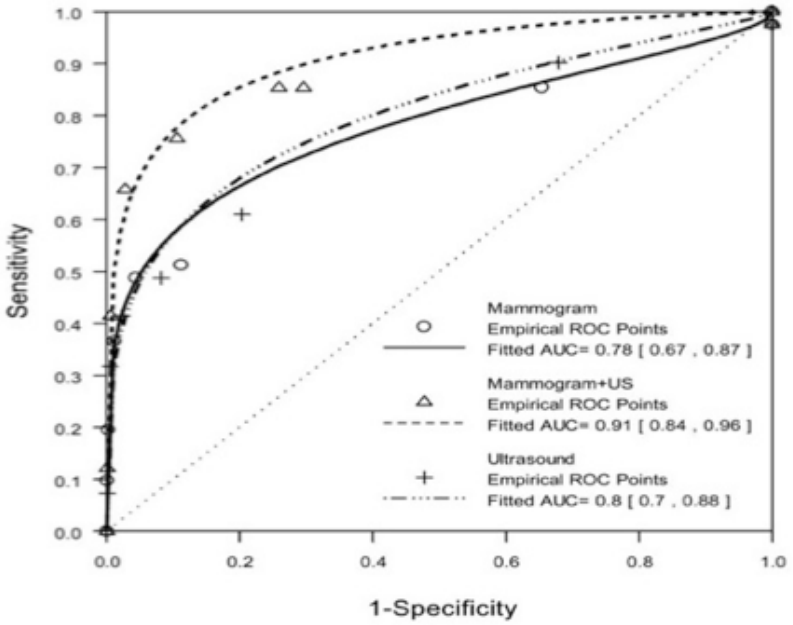

Figure 2.3 ROC curves based on clinical trials; solid line - mammography; dashed and dotted line - ultrasound; dashed line - combined mammography and ultrasound, which is the highest, i.e. the best. (Berg et al, 2008).

2.4 Breast Cup Size

As mentioned in Chapter 1, human factors were a big part of the project. In order to anticipate the breast scanning method, some design specifications had to be established for the scanner head. The scanner head or the patient interface is where the patient will place one breast at the time in a warm saline water bath, for it to be scanned. The machine has to cater for a large percentage of the female population.

There is a large variation in women's breast shapes and sizes; in fact even on the same person it is not uncommon that the left and the right breast size differ and there is general variation during the menstrual cycle (Wood et al, 2008). For the determination of the brassier size two measurements are given: The band or frame size and the cup size. Therefore it is common to hear terms like for example: Cup size=36C. Where '36' is the 'band' and 'C' is the 'cup'. The fact is that cup size keeps varying; in the UK, 34B was the average size in the 1990s and then it became 36C in the 2000s (Lantin, 2003).

Measuring a bra size:

(This measurement is done in inches as this is still the common UK and US method of breast measurement).

1. Wrap a measuring tape around the chest, under the bust
2. Expel the air from the lungs to get the closest chest measurement
3. If the measurement is an odd number e.g 31, add 5, so 31+5=36
4. If the measurement is an even number e.g. 32, add 4, so 32+4=36 (Note: here is the first question mark raised about the accuracy of this method).
5. Now, wrap a measuring tape around the bust. Breath normally.
6. Bust measurement is e.g. 38 inches.
7. Take the difference of the band measurement from bust measurement. E.g. 38-36=2
8. A bust-band difference table is used to extract the cup size, as shown in Table 2.3
9. The difference 2 corresponds to Cup 'B', therefore the final measurement is '36B'

Table 2.3 Corresponding cup size related to bust-band difference.

Difference Bust-Band Size (Inches)	Corresponding Cup Size
<1	AA
1	A
2	B
3	C
4	D
5	DD
6	F
7	G

Why is the extra numbers added?? This was a marketing ploy. Just after World War II, the perceived ideal female measurements were: 36-24-36. As demand increased the manufactures needed the chest sizes, and by adding 4 or 5 inches to the band number they had the chest measurement and at the same time they made the product more appealing to women as they were now closer to the "ideal size".

Discussed in more detail in Chapter 4, the scanning method used is based on the breast being submerged into a warm saline water bath. The scanner has a fixed aperture of 18cm diameter and a cylinder can be moved up and down bringing the scanning plate closer to the breast as shown in Figure 2.4.

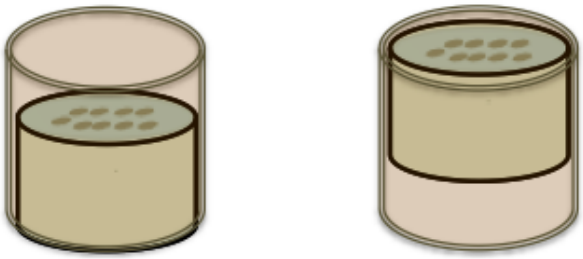

Figure 2.4 The scanner head showing the inner cylinder at its lowest point on the left and at its highest point on the right.

The plate is brought close to the breast and slightly pushing it upwards so that there is good contact of its surface with the breast. Note: this plate is still below the bed line, i.e. if the person were to sleep in the prone position, therefore it causes no discomfort at all. The scanner plate displacement from the base line (bed level) is controlled based on the Table 2.4:

Table 2.4 Bra volume to scanner adaptation

Cup size	Bra volume (cm^3 or cc)	Depth
A	330.8	1.3cm + 20%
B	441.9	1.74cm + 20%
C	568.2	2.23cm + 20%
D	715.5	2.8cm + 20%
DD	881.8	3.46cm + 20%
F	1068.4	4.2cm + 20%
G	1278.1	5.02cm + 20%

*20% tolerance to compensate non-full cylinder shape of the breast.

Diameter = 180mm = 18cm
Radius = D/2 = 90mm = 9 cm
Surface area = πR2 = 254.47cm2
Cylinder pitch = 1mm/rev
Volume = 254.47cm2 * 0.1cm/rev = 25.447cm3/rev = 254.47ml/rev
Max range = 6cm = 60mm
Max volume = 254.47cm2 * 6cm = 1526.82cm3
Comfortably measure up to a G Cup

However this method is not the most accurate. Another chart and bra measurement from manufacturers points out that the same bra volume can correspond to different bra sizes; e.g. 34A, 32B and 30C have the same volume of 310 cc. Therefore the best method of positioning the scanner plate to the breast size would be a custom measurement of the breast, using Archimedes principle of water displacement when the breast is inserted into a fully filled scanner head.

2.5 CONCLUSION

In this chapter, it was revealed why breast cancer is such a major issue and why it requires major considerations. Research was performed on how breast cancer is classified and what are the stages of the disease. Major points extracted for EIM detection are the size and location of the cancer at certain stages. Statistical analysis and mapped location provided the foundation for setting further diagnosis specifications.

The chapter also covered the major diagnosis techniques, currently used in clinics and hospitals. Not considering the side effects and the poor performance of mammography in dense breast, looking at the statistical data, using dual modality in general, and adding ultrasound specifically, increased the sensitivity of detecting breast cancer. The diagram in Figure 2.5, demonstrates perfectly the abilities of each imaging modality and where they can benefit with added value from each other.

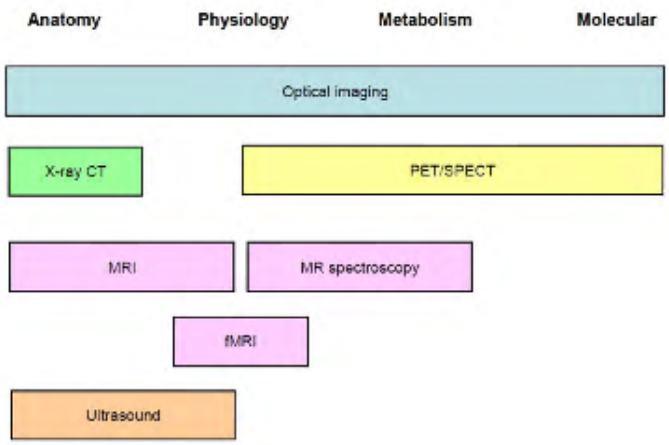

Figure 2.5 Functional utility of medical imaging methods (Analoui, 2011 SPIE).

In general, MRI offers higher specificity but lower sensitivity. Mammography is the opposite with lower specificity but higher sensitivity. Ultrasound on its own seems to be in the middle range for both, but that is not a good thing. MRI is very expensive, while mammography is cheaper but cannot image dense breast. The bottom line is that there is no one-for-all solution, therefore new modalities can overcome the missing gap and dual-modality will complement any diagnostic results.

An investigation into breast sizes, how different they can be and how to ergonomically adapt this information in a potential scanner was also performed. The specifications are for a scanning method in a water bath with minimal discomfort to the patient in the prone position, while at the same time satisfying the requirements of the imaging algorithm.

CHAPTER 3

- RISK ASSESSMENT OF AN EIT DIAGNOSTIC DEVICE

3.1 INTRODUCTION

The International Electro-technical Commission system for conformity testing and certification of Electrical Equipment (IECEE), oversees the 'Certification Body' CB-Scheme, which certifies a product has successfully passed tests to show compliance with the requirements of the relevant IEC standard. The Scheme is intended to reduce obstacles to international trade by introducing an international safety standardisation. According to the type of the electrical device, different standards have to be satisfied. The EIT device under investigation as a safety minimum has to comply with IEC 60601-1 and ISO 14971.

Medical devices that are used in clinical trials or are commercially available have to adhere to IEC 60601-1 "Medical Electrical Equipment - Part 1: General requirements for basic safety and essential performance". The latest revision of the standard was completed in 2005. This standard is also valid for the in vivo use of Electrical Impedance Tomography, especially under the "Patient Auxiliary Current" clause that reflects the externally applied current to the patient. Applying current externally is actually at the core of EIT, however this has to be done within the boundaries of the standard. The defined maximum levels are depended on the frequency of the signal (Borsic & Paulsen, 2009):

1. Maximum 100μA for signals up to 1KHz
2. Increases linearly from 100μA - 10mA for signals from 1KHz - 100KHz
3. Maximum 10mA above 100KHz

Risk analysis is a requirement for any medical devices that are proposed to the MHRA – (Medicines and Healthcare products Regulatory Agency) for use in clinical trials. It is also a requirement for 60601 and CB Scheme and subsequently CE mark. CE marking is a mandatory conformity mark for products placed on the market in the European Economic Area (EEA). A full report of the Risk Analysis is provided in Appendix 9 based on the list of general hazards applicable to medical devices below:

- Energy Related Risk
- Biological Related Risk
- Environmental Related Risk
- Incorrect Output of Energy or Substances
- Operation Related Risk
- User Interface Misuse
- Functional Failure Risk

Following is a Risk Assessment for a combined EIM + Ultrasound device for breast cancer diagnosis. The system components will be described in the next chapters.

The analysis was compiled following guidelines of *ISO 14971– Application of Risk Management To Medical Devices* and with the support of Sussex Biomedical Research.

3.2 HAZARD, RISK AND ACCEPTABILITY ANALYSIS

Hazards may be classified by their severity on patient, user or third party. This risk analysis uses the following hazard classification:

Table 3.1 Hazard severity classification

Hazard: severity of consequence	**Rating**
Death or permanent injury	4
Serious injury	3
Minor discomfort	2
Irritation	1
None or Not applicable	0

For this risk analysis the following frequency classification is used:

Table 3.2 Frequency classification

Frequency of occurrence	**Rating**
Probable	4
Occasional	3
Possible	2
Remote	1
None or Not applicable	0

A Risk (= severity x frequency) Classification of four classes is used:

Table 3.3 Risk classification

Risk	**Classification**
8 – 16	Unacceptable
3 – 7	Low as reasonably practicable
1 – 3	Acceptable
0	Not applicable

Table 3.4 Risk reduction actions

Initial risk level	**Action to reduce risk**
Above 8	***Must*** be taken
Above 4	***Should*** be taken
1 – 3	***Should be considered***

Table 3.5 Risk after action

Risk After Action	Description
A	no identifiable risk
B	some residual risk, but likely to be of little consequence
C	despite everything a manufacturer can do, a user/patient could still be at risk
D	consider incorporating into Post Market Surveillance on a device-by-device basis
E	highest risk products where risk/benefit ratio is very low, for very critical patient situations

The 'Risk After Action' column is derived from a combination of views and logical assessments of mine, the supervisor and other senior biomedical staff.

Table 3.6 Patient risk analysis (extract*)

Hazard	Ref from Sect 1**	Severity	Freq	Risk	Action	RAA***	Notes
Patient Contact – Allergy	(c)	1	1	1	Materials in contact with patient are hypo-allergenic	B	Remote chance of allergy as with any material contact.
Patient Contact – Heat Burns	(d)	2	1	2	Temperature is constantly monitored both manually and by the system (operator is alerted if the value goes above 40°C).	B	The saline gets heated before the test in another compartment of the bed, and then is pumped to the patient interface, where it is not subject to further heating.
Patient Contact – Cross-Contamination	(h)	2	1	2	Instructions for Use (IFU) states patients with broken skin will not be tested. The system is disinfected after every patient.	B	IFU states not to be used on broken skin and patients diagnosed with MRSA. Cleaning agent used is 0.5% w/v Chlorhexidine spray
Patient Contact – Patient Leakage current	(b)	4	1	4	Use Medical Grade, isolated transformer. The device has been Certified with a Leakage Current test. Acquisition only happens when the system is in battery mode.	B	A universal non-negligible risk when using any device powered by mains electricity.

* The full table is in Appendix; **Section 1 Table is in Appendix; **RRA – Risk After Action

Table 3.7 Patient contacting materials

Material used	Location	Reasons for selection
$NaCl_{(aq)}$	Contact medium within Patient Interface	Electrically conductive liquid Controllable conductivity; low cost
Acrylic	Scanner head material	Mechanical stability; chemical resistance
Low-density Polyethylene (LDPE)	Holding plate between breast and scanner plate	Acoustic transparent material; safety
Faux Leather	Trolley covering	Patient comfort
Paper	Disposable cover (optional)	Low-cost; absorbency

3.3 QUALITATIVE AND QUANTITATIVE CHARACTERISTICS

The "identification of qualitative and quantitative characteristics which could impact safety" is a prerequisite and the referencing has to be compiled according to the standards mentioned.

Table 3.8 Qualitative and quantitative characteristics (extract*)

Ref *	Characteristic	Manufacturer's Response and Hazard Identification
a)	The intended use of the device	The device is intended for non-invasive imaging of the human breast within the environment of a dedicated imaging area
b)	Patient/other person contact of the device	The patient is not in direct contact with any active component of the device. A warm saline solution at body temperature is used as a medium of contact.
c)	Materials and components used in contact with device	The patient lies on the test bed in the prone position. A single-use NHS standard paper sheet covers the bed and prevents patient contact with the bed's upholstery. The patient's uncovered chest will touch the scanner part and one of the breasts will be placed inside the scanner aperture. The scanner is made of acrylic material.
d)	Energy delivery/extraction to/from patient	Electrical Impedance Tomography is a safe technique using micro-currents well below the thresholds deemed absolutely safe for humans under the terms of harmonised standard EN60601. The currents are not felt and cause no discomfort for the patient being imaged. The use of ultrasound energy is safe as it is commonly used within the clinical environment. To ensure compliance a CE-marked ultrasound system is utilised.

* The full table is in Appendix

3.4 DISINFECTANT AGENTS

The device will be classified as a multiple-use apparatus; therefore a cleaning and disinfection procedure after each patient scan is a requirement. The initial disinfectant agent of choice was a Sodium Hypochlorite solution that was pumped into the scanner and then was rinsed via a software-controlled automated process. The solution was very effective, however the process of washing and then rinsing would last between 5-7 minutes. The long-term effect of the solution would be too caustic on the device components: container, pump, pipes and the acrylic of the scanner. Also the solution requires preparation, dissolving tablets in water and then pumping into the agent container inside the bed.

Chlorhexidine is another NHS approved cleaning agent that could potentially be used for the device. Chlorhexidine does not require rinsing as it fully evaporates and can be administered manually with hand-wipes or bottle spray. This is the procedure

recommended for mammogram machines. This would mean that a disinfectant tank, pumping and rinsing are not required anymore. Before Chlorhexidine is accepted as the disinfectant of choice it has to be evaluated on its conductivity properties and also the long-term effects on components of the device.

The chosen disinfectant was ECOLAB – Hydrex® Pink - Chlorhexidine Gluconate 0.5% w/v in 70% v/v DEB, with contents of: Chlorhexidine Gluconate Solution 20% BP (Ph Eur) 2.5% v/v, Denatured Ethanol B 96%, Purified Water BP, Carmoisine (E122).

Conductivity of Chlorhexidine

Any residue after the cleaning cycle would affect the load resistance of the measurements; therefore the conductivity of the cleaning agent needs to be very low. The electrical conductivity of Chlorhexidine was measured using the standard calibrated equipment used for the saline. The conductivity measured at 23 degrees Celsius is 144.5 uS/cm (extremely low). As a reference saline at 0.5 mS/cm is used. The agent was poured in an open container and materials of the EIM+US scanner that will be in direct contact with it, were left for 72 hours, as shown in Figure 3.1.

Figure 3.1 Materials and components of the scanner submerged in Chlorexedine for 72 hours.

Results

The impedance measurements will not be affected by any Chlorhexidine 0.5% residue, due to its extremely low conductivity. After the 72 hour submerge test, the components that will be in contact with the cleaning agent do not show any deterioration signs at all (Figure 3.2), this applies to the: PTFE (piston seal); stainless steel (electrodes); LDPE (breast holding plate); transparent acrylic (scanner walls and plate).

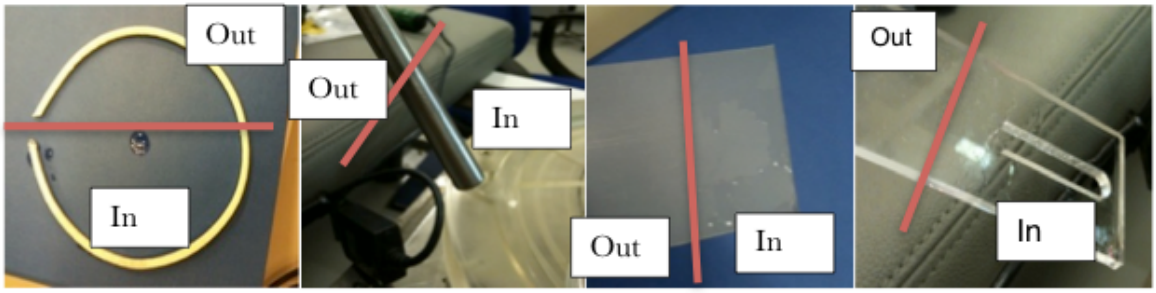

Figure 3.2 Scanner components that were half submerged in Chlorexedine for 72 hours and have not been affected. From left to right: PTFE (piston seal). stainless steel (electrodes); LDPE (breast holding plate); transparent acrylic (scanner walls and plate).

Some materials like nylon and silicon adhesive show discoloration as shown in Figure 3.3. Nylon components will not actually be in contact with the agent. Nylon was used for previous prototype scanners. The silicon residue on the ultrasound transducer is from previous plate-mating attempts. The dual component set resin now in use, as shown in the top part of the transducer has not been affected at all. Therefore it is concluded that Chlorhexidine 0.5% would be a suitable clinical cleaning agent for an EIM+Ultrasound medical device.

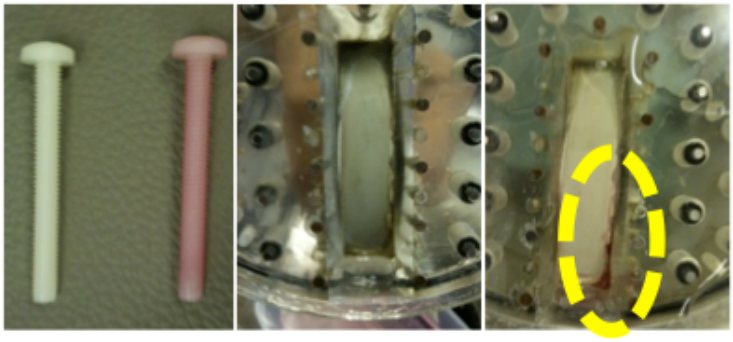

Figure 3.3 Discoloration from chlorexedine of nylon bolt (left); Ultrasound transducer glued to EIM plate with dual component resin (middle) and silicon addesive (right). Note, the resin has not been affected, the silicon addesive has.

3.5 Conclusion

The foregoing risk analysis has identified all potentially known risks in the manufacture, use and disposal of the Electrical Impedance based Sussex EIM+Ultrasound system for the purpose of clinical trial evaluation in identifying Breast Cancer in a non invasive manner. Chlorhexidine 0.5% would be a suitable clinical cleaning agent for the device. On the basis that the actions stated/proposed to mitigate the identified risks are followed, it is concluded that the device is safe to use and that the potential benefits of using the device outweigh any residual risks.

CHAPTER 4

- ELECTRICAL IMPEDANCE TOMOGRAPHY

4.1 INTRODUCTION

This chapter will introduce EIT (Electrical Impedance Tomography), its history, background theory and applications from other research groups and commercial companies. The Sussex EIT system will then be presented, from its beginnings as the De Montfort Mk1-Mk3 prototypes to the current evolution as the 'Sussex Mk4 EIM'. Detailed descriptions of the new architecture and selected sub-systems are given, concentrating on the new and flexible DAQ (Data Acquisition) approach. The chapter will conclude with a brief summary and the proposed changes based on the findings.

4.2 WHAT IS EIT?

Electrical Impedance Tomography (EIT) as we know it today was established in 1986 from a group of medical physicists and engineers in what is now known as 'The Sheffield Meeting' (Barber, 2000), (Bayford, 2006). This method, previously known as Applied Potential Tomography (APT) (Barber and Brown, 1984), reached a breakthrough in its potential use as a non-invasive imaging modality with the publication of the first images (Barber *et al*, 1983) and later the revolutionary 'Sheffield Mark 1 Clinical System' (Barber *et al*, 1987) for pulmonary functions. Metherall et al published the first 3D EIT chest images in 1996 employing a modified Sheffield system with multiple ring electrodes. Since then, many research groups worldwide have advanced the work on EIT on both hardware and algorithms, with the aim of perfecting it for practical clinical applications.

4.2.1 IMPEDANCE FUNDAMENTALS

EIT is an electrical imaging method where the acquisition builds on the principles of bioimpedance theory and measurements. Observations suggested that the electrical resistance of tissue decreased when the signal frequency was increased (Cole, 1940). This is depicted in Figure 4.1 (left). Based on this the circuit model on Figure 4.1 (right), was proposed by Fricke in 1925. Where R = Resistance of extracellular space; S = Resistance of intracellular space; C = Membrane capacitance.

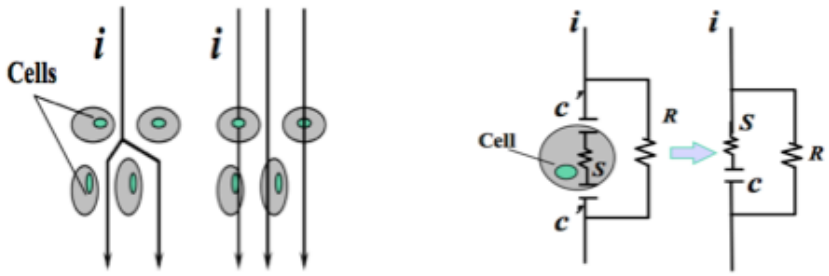

Figure 4.1 Electrical current dispersion in cells in low and high frequency (left); The equivalent circuit model (right).

Cole & Cole in 1941 published their now renowned Cole-Cole equation (4.1), which has become widely accepted to describe the dispersion in biological materials.

$$Z = R_\infty + \frac{(R_0 - R_\infty)}{1 + \left(\frac{jf}{F_r}\right)^{1-\alpha}} \tag{4.1}$$

Z = Impedance of the object (Ohms); R_∞= Resistance at low frequencies (to infinite, in Ohms); R_0= Resistance at high frequencies (to zero, in Ohms); j = complex number; f = injected signal frequency (in Hz); F_r = relaxation frequency (the frequency at which the dielectric loss factor reaches a maximum, in Hz); α = relaxation factor (the value of α is between 0 and 1, where 0 would represent an ideal resistor and 1 an ideal resistor and capacitor). Equation (4.1) can be represented as the graph in Figure 4.2. Biological tissue membrane acts as a dielectric at low frequencies. The graphs starts to dip at around 10kHz and full current penetration in the cells is achieved at around 1MHz. More plot examples of actual measurements of different 'tissue' type are given in Figure 4.5, where pre-cut cylinders of apple, cucumber and banana were measured. The plot response of each 'tissue' type is quite distinctive from the others and easily identifiable.

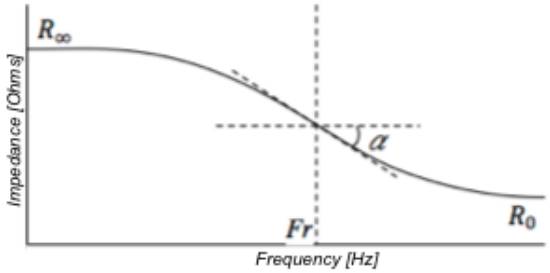

Figure 4.2 Impedance vs Frequency plot.

Based on this identification method, exists the possibility of identifying cancerous tissue based on it impedance signature. *In vitro* trials and data libraries have been provided by

the work of many scientists over the years. A review study on the resistivity of human tissue between 100Hz-10MHz was delivered by Faes et al, 1999; data and studies on breast tissue (Campbell et al, 1992), (Tunstall et al, 1997), (Surowiec et al, 1988), (Jossinet, 1998), (Chauveau et al, 1999), (Sha et al, 2002) and (Wang L. et al, 2008); prostate cancer data form Halter et al in 2009a; pancreas data (Wang W. et al, 2008), (Qiao et al, 2010) etc. In Table 4.1, are shown some of the results from the Surowiec et al study in 1988 on breast tissue with confirmed carcinomas.

Table 4.1 Conductivity values of *in vitro* breast tissue.

Breast Tissue	**Conductivity (mS/cm) @10kHz**	**Conductivity (mS/cm) @100kHz**	**Conductivity (mS/cm) @10MHz**
Tumour centre	3.98	4.28	7.24
Tumour surrounding tissue	1.62	1.70	2.70
Fat with tumour cells	0.65	0.67	1.05
Tissue away from tumour	0.28	0.31	0.37
Normal tissue	0.22	0.22	0.25

The measured *in vitro* values are not the same in all the studies. There are variations between the different studies, however there is a trend that clearly indicates that carcinomas exhibit a higher conductivity than healthy tissue and this is clearly confirmed at all frequencies. Assuming that all the technical challenges (electrode contact, DAS, ergonomics, image reconstruction etc.) can be engineered; a multi electrode impedance system has the potential to measure and identify the difference between cancerous, healthy and transitional tissue types.

4.2.2 Impedance Imaging

EIT is not a typical tomographic method (slice by slice reconstruction using an integration of multiple external viewpoints (Scott et al, 2005) as commonly performed on X-ray CT, 3D Ultrasound etc. (Kak & Stanley, 2001). The reason is that it is not possible to contain low frequency electrical currents on a single plane, ie. a slice. In EIT, an image of the conductivity of a closed volume is deduced from surface electrical measurements. (Boone et al, 1997), (Barber, 2000), Conductive electrodes are placed on or close to the skin, sometimes with the application of a contact medium, e.g. conductive gel or saline. Small alternating currents are applied to some of the electrodes, while the other electrodes are configured to measure the electrical potentials created (McAdams et

al, 1996), (Wang et al, 2007), (Ji et al 2009). Predefined and repetitive pattern combinations can be applied in order to offer maximum coverage and resolution of the tissue area under test. The effect of conductivity change is three dimensional not just in the projected path. This property while might seem to toughen the impedance tomography challenge can in fact be used to extract 3D impedance data information from a 2D EIT planar acquisition array (Sze et al, 2011). There are many 3D EIT systems (Vauhkonen et al,1999) (Hartov et al, 2000) (Xu et al, 2007) (Ye et al, 2006), but in essence they can be all arranged in two distinguishable groups; Systems with EIT ring electrodes and on plate electrodes (Lionheart, 2004). Both systems can use similar versions of image reconstruction algorithms, and the most notable ones are:

Back-projection - introduced for EIT by the Sheffield group (Barber et al, 1983). A very fast algorithm that uses a linear relationship based on the assumption of a small change in impedance and small change in boundary measurements.

Modified Newton-Raphson algorithm - known as a nonlinear least square estimation (Bayford, 2006). It solves inverse problem by iterative linearization of the nonlinear relationship between resistivity and the electrical measurement. Two sets of data are recorded, a reference or background and the object data. By removing the background from the object data, the information seems to outperform the back-projection method

Other software tools for aiding EIT reconstructions are:
GREIT (Graz consensus Reconstruction algorithm for Electrical Impedance Tomography) a collaborative project to develop a consensus linear reconstucution algorithm for lung EIT (Aldler et al, 2009).

EIDORS (Electrical Impedance Tomography and Diffuse Optical Tomography Reconstruction Software) an open source software suite for image reconstructions intended to facilitate collaboration in the research of these fields. (Polydorides & Lionheart, 2002)

4.3 PROMINENT EIT SYSTEMS

EIT is still considered a research imaging method, however over the years zealous academic institutions and commercial companies have ventured in producing commercial and/or investigative prototypes based on EIT. The initial use of EIT was

for pulmonary imaging and monitoring, however the need and methodologies for its use to identify breast cancer were also identified quite early on. The following are some recognized systems that in one way or another have influenced the progress of EIT as a medical technology.

Sheffield Mk1-Mk3A-Mk3.5 *(1987; 1989; 1990; 1993; 2000; 2001)* – Considered the classical ring electrode system with 8 or 16 electrodes (Wang et al, 1995), (Bayford, 2006). In 2001, Wilson et al. introduced a multifrequency successor to Mk3a. Pairs of electrodes can be controlled to be at any time, injecting current or measuring voltage. Different patterns have been applied to achieve the best special resolution. (Isaacson, 1986) (Brown et al 1987) (Webster, 1990) (Barber, 1990) Gisser et al, 1987) (Hua, 1987). Multiple rings can be placed in parallel (Metherall et al 1996), (Vauhkonen et al, 1999) or in a cone shape arrangement (Wang et al 1998) (Ye et al 2006), (Ybarra et al 2008) and effectively achieve a 3D scanning method. The system produced cross-sectional conductivity distributions of the forearm and the chest and introduced the first methods and algorithms for EIT (Barber & Seagar, 1987)

Dartmouth EIS *(2000; 2002; 2008)* – The Dartmouth design revives the traditional EIT method by employing circular ring electrodes (Hartov et al, 2000). The system uses 4 rings of 16 electrodes each with digital signal processing for all 64 channels. Significant is the high bandwidth of the DAS system with a frequency range of 10kHz-10MHz. Contact method was dry electrode with conductive gel. Osterman et al in 2000 published the first results, concluding that although they did produce absolute conductivity images they noticed artefacts from the electrode-skin contact. The system was upgraded with a better contact method and the conclusion was that scans with frequency >500kHz produced clearer images (Kerner et al, 2002). Halter et al, 2008 did just that by concentration on 2MHz-10MHz and did a blind study on tissue density identification. The results show a correlation with the tissue classification data.

T-SCAN™ *(1990; 2001)* – The first commercial EIT based device for the detection of breast cancer. (Assenheimer et al, 2001). After 10 years of the initial development of (Piperno and Moshitzky, 1990) in Israel, the device received FDA approval and was distributed by Siemens Medical. The system used a planar arrangement of electrodes and the clinical trials of Malich et al in 2000, report 'shadowing from the nipple'

therefore were unable to image behind the nipple. The reported penetration was 3-3.5cm.

Cherepenin BCDD (Cherepenin et al 2001). a.k.a MEIK(Campbell et al, 2007) and MEM (Trokhanova et al, 2008) – The Breast Cancer Detection Device, developed at the Institute of Radio-Engineering and Electronics of the Russian Academy of Science and commercialised by Technology Commercialization International Inc. (USA) (Cherepenin et al 2001). The system uses a planar electrode arrangement, on a handheld probe design. Using static EIT imaging, the manufacturer concluded in their initial trials that the device could distinguish difference in conductivity between cancer and normal tissue, however limitations were found when scanning dense breasts and in the nipple area (Cherepenin et al 2002). The device received CE marking and was tested in Italy, Czech Republic and Malaysia supervised by Campbell et al in 2007. Their conclusion was again there is a challenge with the saturation of high conductivity in the nipple but the device; rather than pure imaging could be used to monitor the whole breast e.g. fibrocystic changes. Trokhanova et al in 2008, looked at another approach using a version of the device. Their research was on the study of the mammary gland and the possibility of identification of mastopathy and any other non-cancerous lesions.

Rensselaer EIS a.k.a ACT4 EIT *(1987; 1994; 2007)* – This was the 4th generation EIT system from Rensselaer for breast cancer detection (Saulnier et al, 2007)(Kao et al, 2007) and was considered a big step from their previous high speed ACT3 EIT from Cook et al in 1994. The novelty of their system was the possibility to do a dual modality scan and register the electrode positioning with X-ray. The EIT electrodes were, as the authors describe them, radiolucent to X-ray (Kao et al 2007). This system also used a planar electrode arrangement and employed the optimal (parallel) current injection method advocated by Gisser et al in 1987 and then Cook et al in 1994. Kao et al published a preliminary patient study in 2008. They demonstrate that the system can distinguish abnormal lesions by presenting the images of two identified cases. However the authors declare that more studies are required and that the planar electrode arrangement suffers from penetration sensitivity.

Duke Conical Wet EIT *(2006; 2008)* – Researchers from Duke University have

developed an EIT breast scanner system with an interesting design. The patient lays in the prone position and the breast to be scanned in submerged in a plastic funnel-shaped bath with warm liquid. The liquid conductivity is similar to normal breast tissue. 128 electrodes are spaced on the cone's walls in 7 parallel 'rings', where the number of electrodes per ring is reduced according to the cones geometry. (Ye et al, 2006) (Ybarra et al, 2008). The papers show that the system is capable of 3D EIT and the results on phantom scanning and reconstructions were successful.

OTHER NOTEWORTHY COMMERCIAL DEVICES:

Zilico APX – An (EIS) Electrical Impedance Spectroscopy based device for diagnosing real-time cervical cancer and pre-cancerous conditions (Brown et al, 1998). The device aims to replace the Pap smear test by providing a safe, painless and accurate on the spot result. The device is expected to launch in the market in 2012.

Draeger PulmoVista®500 – Can be considered a commercially promising EIT system. The system is commercialised as a relatively low cost continuous respiratory monitoring system. The device has been developed and is commercialised by Draeger Medical AG with headquarters in Germany and with services in 50 countries. The method used is similar to the Sheffield thoracic ring electrode systems. (Hinz et al, 2003)

Karolinska Institute Skin EIT – A handheld, pen-like device with four concentric electrodes embedded in a ceramic plate. The outer rings function as drive electrodes and the diameter of the outermost electrode is 10mm (Aberg et al, 2004).

UCLH Mk2.5 Head EIT – A 32 electrode, high SNR, multifrequency EIT system for acute stroke imaging. The UCL research team claim that with their recent anatomical mesh model the system is sufficiently accurate to image severe acute stroke. (McEwan et al, 2006)

4.4 Electrical Impedance Mammography

EIM – Electrical Impedance Mammography is the use of EIT as a breast cancer imaging and diagnostic tool. Currently at the University of Sussex, an EIM research device is the forth functioning prototype, hence the name Sussex EIM Mk4. This prototype is based on the continuous research work of the group for more than 15 years.

4.4.1 Mk1-Mk3

Mk1 – Mk3 EIM systems and other minor variations of the main designs were developed by the group at De Monfort University, Leicester. Mk1 provided invaluable *in vitro* information (Tunstall et al, 1997) that was used for phantom data in EIM future generations. Table 4.2 shows the evolution and the Data Acquisition System specifications of the Mk1-Mk3 devices.

Table 4.2. Mk1-Mk3 DAS specifications.

Model	Mk1	Mk2	Mk3a/Mk3b
Frequency	Multi, Sig Gen	Multi, Sig Gen	16 freq, inboard fixed DSP
No of Electrodes	4	32	128, 85 in use
DAS	10-25 Frames/s	1 Frame/s	Up to 20 Frames/s depending on Freq no/ config
Image Type	Dynamic	Dynamic	Static (Dyn. option)
SNR	40dB	>46dB	>50dB

The design of the Mk2 system as shown in Figure 4.3 is quite unique. The system used 32 dry electrodes in a ring configuration embedded in a custom made bra (Wang et al, 2008). This layout only delivers a 2D EIT image. The method of scanning is straightforward, the patient wears the bra and the operator controls the scan from the PC. The scan is convenient, fast and painless therefore potentially finding use in primary care and does not require a qualified radiographer. This design was only suitable as a prototype. Considering the number of cup sizes and variations one would need to produce different bras for different women. Also the dry electrode contact produced a lot of artefacts, which reduced the repeatability of the scans.

Figure 4.3 The Mk2 EIM system a.k.a the electronic bra.

The Mk3 system in 2006, introduced the concept of the bed scanner. The breast is inserted a water filled bath, similar to the Duke Conical EIT system (Ye et al, 2008). However it goes one step further and introduces breast height adaptation. Figure 4.4 shows the 'bowl' design patient interface with the electrode arrangement and the controlled draining valve in the centre. The Mk3b system introduces a major breakthrough; the recessed electrode model on a flat patient interface plate.

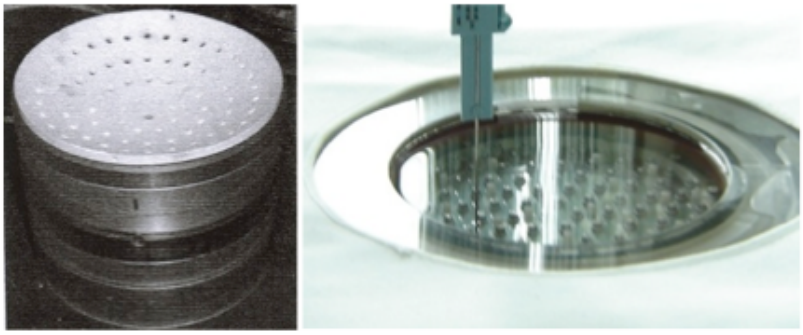

Figure 4.4 The concave Mk3a scanner plate (left); The flat Mk3b scanner plate filled with conductive liquid (right).

The system continues to use a warm bath and the plate is movable according to a predefined cup size arrangement. The electrodes are again fixed to the plate and are now recessed 2mm below the acrylic plate surface (Wang et al, 2007). This setup should ensure that there will not be a direct skin-electrode contact but a layer of conductive liquid will always assure a predefined conductivity path and value, therefore reducing the contact artefact. Having the electrodes at a known position and knowing the height of the movable plate, the reconstruction algorithm can now use a predefined accurate mesh therefore increasing the accuracy of impedance mapping. Figure 4.5 shows graphical and imaging results of organic tissue (fruit) scanned with the Mk3b system.

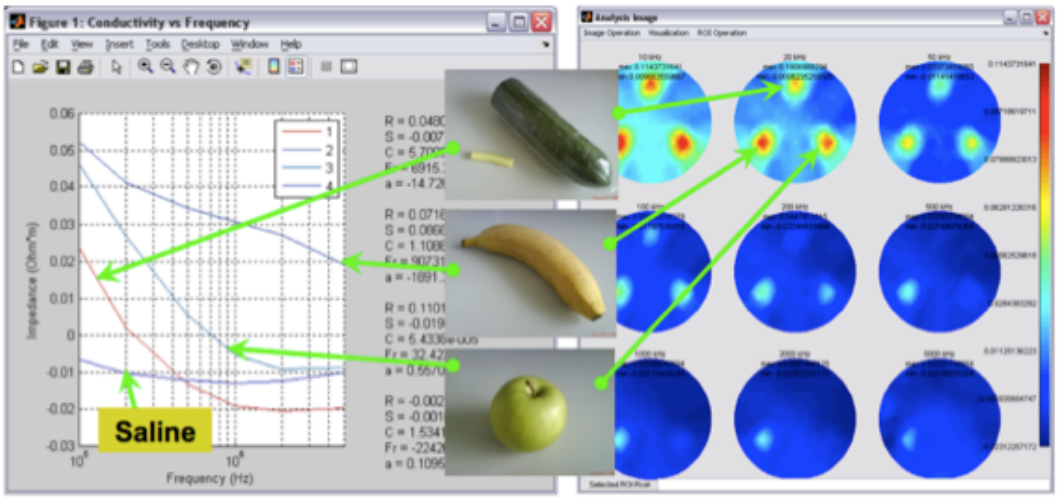

Figure 4.5 Graphical and imaging results of different 'organic tissue' types scanned and analysed using Mk3b.

4.4.2 Sussex EIM Mk4

The Sussex EIM Mk4 is the latest and most advanced EIT system. The system has leaped from a lab prototype to a full clinical trial device and has satisfied the MHRA clinical operational requirements to measure *in-vivo* impedance of breasts and study the feasibility of identifying cancers. Noteworthy main features are:

- A circular scanner with variable depth of plate to accommodate different cup sizes.
- Recessed electrodes to avoid contact impedance changes.
- PXI based acquisition and control system with custom software on laptop.
- A liquid system of tanks, pumps and valves to fill the scanner with fresh saline for every scan.
- A liquid warming systems so that the saline is at body temperature for the examination.
- A disinfecting, rinsing and waste disposal system for the used saline.
- Fixed planar electrode array to avoid errors caused by the geometry distortion of the electrode position.
- Dual power system; mains for general use and battery for patient scanning.
- Safety and emergency system with circuit breakers and manual override.
- Embedded controllers with control logic and status watchdogs.
- Cushioned bed with height adjustment for patient accessibility and comfort.

The software acts as a database, a scan control and all the way to producing a diagnostic report based on pre-learned parameters.

Clinical devices, before any *in vivo* tests are performed on humans, are required to be built and comply with health and safety requirements (e.g. IEC 60601-1-x). It is easier to achieve compliance if the individual parts of the device are already compliant with some recognised standards and/or certifications (e.g. CE marking or FDA approval). This is one of the main reasons of the new architecture set in place for the Mk4 systems and based on PXI chassis and modules. The rest of the section will describe the architecture, the components and the software that controls it.

4.4.2.1 PXI ARCHITECTURE

The Data Acquisition System (DAS) is based on a PXI (PCI eXtensions for Instrumentation) chassis with a number of dedicated PXI modules controlled by customer-written software. PXI is a modular instrumentation platform originally introduced in 1997 by National Instruments. PXI is promoted by the 54-member PXI Systems Alliance (PXISA) and has become an industry standard in computer-based instrumentation with over 1150 different modules, varying from data acquisition, signal generators to motor controllers and image grabbers. The modules are categorized in board series depending on their purpose (e.g. data acquisition, motion etc). Each board series has a product family categorized on the hardware capabilities of the modules (e.g. DAQ 12-bit, 14-bit) etc. Naturally the higher the hardware specification the more expensive the module is. For the purpose of this thesis the system will be using the product family (e.g. PXI-62XX) so that it complies with the purpose of maximum flexibility for an EIT system. Being based on CompactPCI, PXI offers all of the benefits of the PCI architecture including performance, industry adoption, COTS technology. Most PXI instrument modules are register-based products, which use software drivers hosted on a PC to configure them as useful instruments, taking advantage of the increasing power of PCs to improve hardware access and simplify embedded software in the modules. The use of this open architecture allows hardware to be reconfigured to provide new facilities and features that are difficult to emulate in comparable bench instruments. The wide variety of the off-the-shelf high specification modules allows to concentrate efforts on the unique features of the EIM system. Therefore a combination of custom and off the shelf hardware is used for the acquisition system.

The Sussex Mk4 system uses a quadrature method for impedance detection. The device uses a fully programmable planar array of 85 electrodes. The control method employed is such that any two electrodes apply current to the breast whilst any other two, similarly non-invasive, electrodes detect the developed potential difference under the control of proprietary software. The currents injected are provided by a signal source with available output frequencies that are continuous over a wide bandwidth. Table 4.3 shows the electronic specifications of the Mk4 system.

Table 4.3. Sussex Mk4 DAQ electronic specifications

Requirements:	
Bandwidth	100Hz – 10MHz
Peak-to-peak current	~0.01 - 1mA
Signal-to-Noise Ratio	>60dB (1kHz – 1MHz) >46dB (1MHz – 5MHz) > 46dB SNR (@1-5MHz)
Imaging Frame Rate	< 1 Frame / sec / Freq
Detection Method	Quadrature
Minimum electrodes	Up to 265 (85 active)
Calibration	Automatic, SW-based
Channel selection mode	Single End/Differential (Selectable)
Frequency selection	SW Programmable
Electrode selection	SW Programmable
ADC	Minimum 12-bit
Digital addressing protocol	32-bit
Data Storage	PC hard drive

Due to the fully programmable nature of the electrode selection, if the system is equipped with n – number of electrodes it is theoretically possible to select n*(n-1)*(n-2)*(n-3) electrode combinations. The system has 85 electrodes, therefore 85*84*83*82 = 48594840 electrode combinations. However only 1416 combinations are considered significant for the image reconstruction (Sze, 2012), due to their arrangement and distance from each other. The inject-acquire method is done in hexagonal clusters of electrodes, as shown in Figure 4.6. Where the red electrodes inject current and pairs of electrodes inside the cluster measure voltages in pairs.

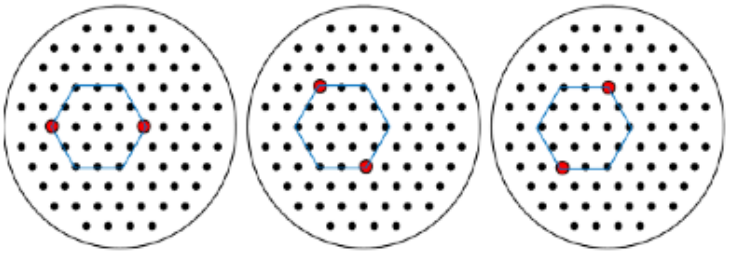

Figure 4.6 Depiction of the 85 electrodes and the hexagonal inject-acquire cluster that is performed 3 times at 60 degrees (Sze et al, 2011).

For each of the electrode combinations selected a number of user-programmable frequencies are injected sequentially. The setup uses 9 frequency selections: 10kHz, 20kHz, 50kHz, 100kHz, 200kHz, 500kHz, 1MHz, 2MHz and 5MHz. The acquired signals of all combination and frequencies are then fed into a multiplexer (part of the

board design). The output of the multiplexer is connected to the ADC of the PXI system. Figure 4.7 shows the block diagram of the electronics and the PXI connections.

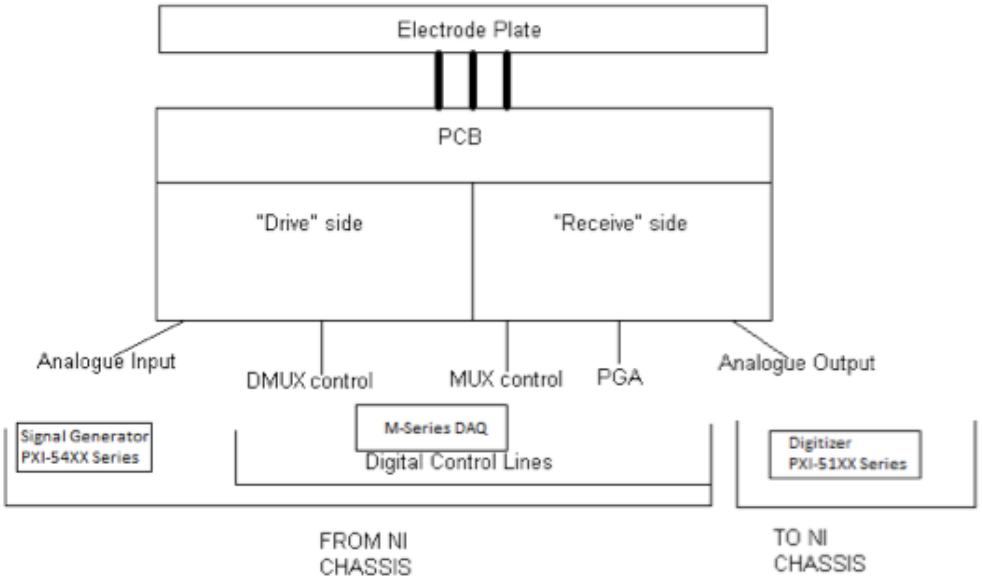

Figure 4.7. Sussex Mk4 EIM Data Acquisition block diagram.

A PXI-54XX series function generator is used to provide signals to a voltage-to-current convertor for application to the body. The exact electrode combination is selected via a PCI-62XX module. Each electrode can be either configured, using a 32-bit parallel port, for current injection or voltage measurements; but each electrode can only be configured for either differential current injection (I+ or I-) or voltage measurement (V+ or V-) at one time. Because of the high sample rates required to digitize the above signals, a high specification ADC board is used, PXI-5122, 100 MSamples/s at 14-Bit resolution. The acquired signal from the PXI module is streamed onto the hard drive. The acquired files are then recalled for analysis and image creation.

The created images are again stored onto the hard drive. The raw data file is left untouched and can be called again for post processing and analysis in order to calibrate any image algorithms.

The PXI platform for EIT and the first bench tests were performed in 2007, as a method to increase the flexibility of the DSP based Mk3. The successful setup was then ported to Mk4. Literature review shows that other research groups are also opting for flexible open module PXI based EIT systems, e.g Kourunen et al, 2009 from the University of Kuopio, Finland and Halter et al 2008 from Dartmouth College, USA.

4.4.2.2 CONTROL SOFTWARE

The controlling software is written in LabVIEW™ (Laboratory Virtual Instrumentation Engineering Workbench), a fast prototyping, graphical programming language based on data flow concepts, which provides excellent user interface development features. The PXI modules come equipped with drivers and an Application Programming Interface (API), which is called and controlled by LabVIEW™. This provides for a reduction in development time and cross-module integration compatibility with the software installed on a dedicated, high specification Microsoft Windows personal computer architecture.

The electrode injection and acquisition module works by:

- Sending the correct pin combination pattern using a digital waveform
- Sending analogue signals of 9 different frequencies to the EIM current injector pins.

The acquisition part will acquire the analogue voltage differences between the pin combinations and keep correct reference tags of the signals in order to reconstruct a correct image. Following is a text representation example on how the software controls and acquires the data from the electrodes:

- User selects a set of excitation frequencies to be used.
- User runs program:
    1. Electrode quad selected (drive combination1, receive combination1)
    2. Inject in series at all frequencies
    3. Receiving electrode pair changed (quad: drive combination1, receive combination2)
    4. Inject in series at all frequencies
    5. Repeat (3) and (4) for all receive pairs associated with the drive pair used (10-12 receive combinations per drive pair)
    6. Repeat the above five steps for all electrode quads defined for 85-electrode plate

4.5 MK4 INVESTIGATIONS

The Mk4 system has some notable improvements in its design, electronics and patient interface. The experiments using agar phantoms, doped at known conductivity values, to represent different tissue types, are very promising. However the purpose of the device is to be used for *in vivo* clinical scans, therefore a number of matters have to be addressed. Following are the identified matters and the proposed or implemented solutions.

4.5.1 ELECTRODE – TISSUE INTERFACE

The Mk4 patient interface plate, uses fixed recessed marine grade stainless steel electrodes embedded in an acrylic (very high impedance) plate. The electrodes are designed so that there is always a uniform layer of liquid conductor (i.e. saline) between the electrode and the patient's skin. Grimnes & Martinsen in 2008 and Qiao in 2011 in their studies have produced the reasons for a controlled electrode-tissue interface and a table with the most common methods (Table 4.4.)

Table 4.4 Electrode types, coupling methods and uses from different EIT systems (Qiao 2011)

Systems	Electrode numbers	Applications	Electrode materials	Electrode-skin interface	References
Sheffield MK1	16	Chest imaging	Ag/AgCl	Hydrogel	(Harris *et al.*, 1987)
Rensselaer ACT4	Up to 72	Breast imaging	Radiolucent electrode with gold surface	Direct contact	(Kao *et al.*, 2007)
Kyung Hee University EIT	16	Lung imaging	Ag/AgCl	Hydrogel	(Kuen *et al.*, 2009)
UCL MK	Up to 64	Head imaging	Ag/AgCl	Gel	(Yerworth *et al.*, 2002; 2003; McEwan *et al.*, 2006)
Dartmouth EIM	64	Breast imaging	Ag/AgCl	Gel	(Halter *et al.*, 2008a)
Moscow EIM	256	Breast imaging	Stainless steel	Wet gauze	(Cherepenin *et al.*, 2001)
Sussex EIM	85	Breast imaging	Stainless steel	Indirect contact made by saline	(Wang *et al.*, 2007; Huber *et al.*, 2010)

- Indirect contact between tissue and electrode reduces toxicity transfer from the metal. This is especially true for some types of metals.
- The use of contact medium provides a controlled metal-electrolyte interface.
- Pretreated tissue with aqueous or gel substance provides a better conductivity distribution on the surface of both the electrode and the tissue.

4.5.1.1 Saturation and Dead Channel Investigation

From the signal quality was noticed that some channels were maxed out (saturated channels) whilst some were actually returning low or no signal at all (dead channels). A transparent, water filled balloon was used to simulate and study the positioning of the breast on the EIM plate, as shown in Figure 4.8.

Figure 4.8. Water filled balloon testing; simulating a high impedance breast scan.

It was observed that the weight and the skin (of the balloon) were displacing the saline from the electrode pins therefore removing the contact medium to the object. Also displacement tests, pressing the pin area with fingers, returned the same results of saturated and dead channel.

Experiment - Acquire saline at different heights

The purpose of this experiment is to evaluate the impedance load created by the height of the saline on a predefined electrode pair, so that the conditions of saturation or dead channel can be created. Setup: Saline Conductivity ≈ 0.5mS/cm^2; Signal Gen. = 0.3V at 100Hz; Amplitude (sine) = 0.6V$_{pp}$; Drive$_+$ = Pin1; Drive$_-$ = Pin2; Receive$_+$ = Pin3; Receive$_-$ = Pin4. Table 4.5 and Figure 4.9 demonstrate the experimental results.

Table 4.5 Saline height – voltage relationship

Saline Height (mm)	$Vout_{pp}$ (mV)	Notes
31	340	
21	410	
11	560	
1	3900	1-2mm of saline left (Saturation)
0	29	No saline left on the pin groove (Dead Channel)

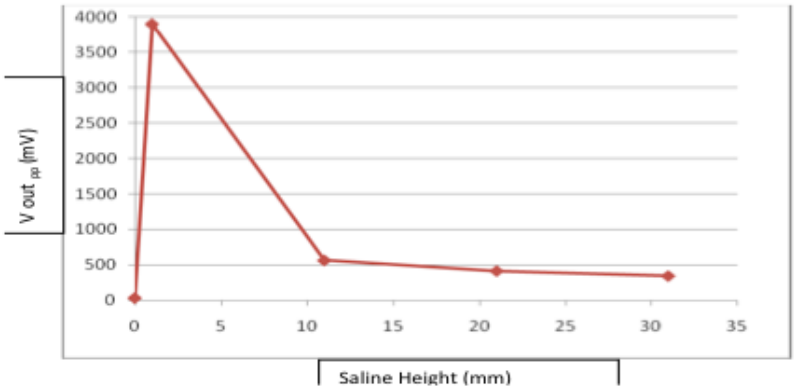

Figure 4.9 Saline height–voltage relationship.

Conclusions:

1. Modifying the injection values can eliminate saturation. The impedance of an object is constant (at set frequencies) therefore manipulating the V and I could create a list of compensation constants that could be used in the electrode combination list.

2. Tissue pressed on the pin displaces the saline from the groove but the tissue still doesn't touch the metal pin therefore a vacuum state is possibly created between the metal and the tissue. This returns the same result as when there is no saline in the scanner i.e. high impedance. Therefore a method to ensure that there is always a film of saline should solve the dead channel problem.

3. Tests where the scanner plate is not in direct contact show little or no dead channels.

4. Less saline returns higher voltage output (this makes sense because the height of saline represents parallel resistors). Therefore it is safe to conclude that background referencing should not be done as a default on cup size 'F' (current method) but every breast cup size acquisition should use the equivalent saline size.

5. If ultrasound (water-based) gel is applied to the pin grooves on a dry plate, and the path between the pins is shortened either by the fingers or gel itself, the signal returns proving once more that the absence of the contact medium causes dead channels.

Designs to eliminate dead channels

To answer the questions raised by the experiment above, a number of methods were proposed:

1. Grooves – Introduce channels between the electrodes, with the same dimensions as the pinhole, as shown in Figure 4.10 with the red lines, ensuring a liquid path between pins and between the tissue. An evolution of this design was to fully etch the acrylic plate with parallels and cross lines at 1-1.5 mm height, as shown in Figure 4.11 (left). This truly ensured a liquid-film between the plate and the tissue, as seen in Figure 4.11 (right).
2. Double plate – introduce a controlled height (few mm) and conductivity membrane (same value as saline) between pins and tissue. This can be done with:
    a. Conductive plastic - With or without holes where the pins are. The plastic can be 'cooked' to any conductivity value.
    b. A layer of agar - Single use agar cylinders of 0.5mS conductivity.
    c. Saline (water) saturated material - A layer of material that can be fully saturated in saline and fully release its air so that no bubbles can be placed between the plate and the breast. Possible solution: Sponge, cloth, multi perforated solid material, etc. Note: single use or disinfectable material is required for health and safety
3. Washing up liquid - Adding some washing up liquid to the saline should act as a surfactant and eliminate the 'vacuum'. This was tested and was concluded as not viable as kept introducing soap bubbles.
4. Chlorhexidine treatment - cleaning the plate with Chlorhexidine before a scan did reduce the air bubbles trapped in the pinholes and/or grooves, but not the vacuum issue.

In the next section the impedance response of some of the solutions above were tested and compared. The reason is that any variation in the plate or any additions to it should not affect or interfere with the reference (background) impedance measurements.

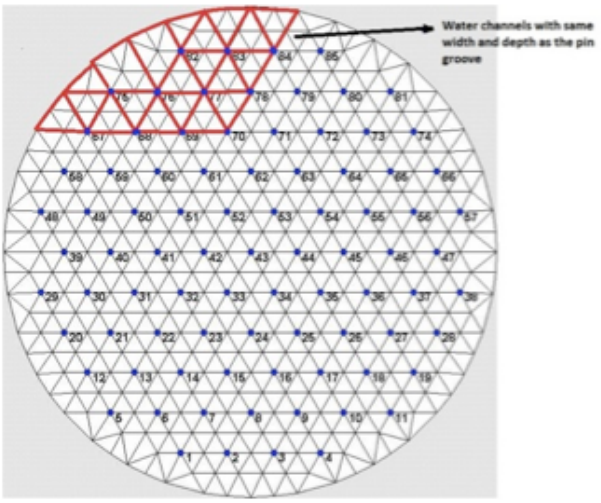

Figure 4.10 Schematic of the electrode plate and the pins. Red lines are depictions of the grooved channels creating a constant saline path between the electrodes.

Figure 4.11 Grooved and etched plate ensuring a liquid pathway at all times (left); Photograph demonstrating the constant liquid film on the plate (right).

4.5.1.2 Experimental Solutions

An investigation on the actual pin combination confirmed that if one electrode is blocked and is 'driving' it will create a saturated return in the electrodes around it. When this particular blocked electrode becomes a 'receiver' will return a low signal or no signal at all.

Various experiments were done to reduce or eliminate the medium (saline) displacement from the pins. The basis of the experiment was to change the surfactant value of the acrylic plate or create a constant thin layer of medium (saline) between the pins and the object.

Medical cotton-based gauze, when fully saturated in saline proved successful in creating a constant layer of conductive medium. Because the gauze fully saturates with saline, its response is almost transparent to the electrical field. This is a very important issue because if the gauze was to introduce a higher impedance load it would mask the

impedance of the object aimed to scan, and if it introduces a shunt, it would reduce the electrical field around the object.

The practical use of gauze shows that if not placed correctly the gauze will move and negate its purpose of creating a constant layer. Improvements to the gauze positioning were introduced by means of an acrylic ring that keeps the gauze constantly tight and in a perfect unfoldable layer.

These developments were hand in hand with another method that could ensure the constant saline layer; the grooved plate. Different designs of the grooved plated were tested until a 'ridged' design returned the best repeatability and a signal quality similar to the gauze. Figure 4.12 shows the three types of feasible solutions added to the patient interface plate: loose gauze, gauze taught over acrylic ring and ridged-grooved plate.

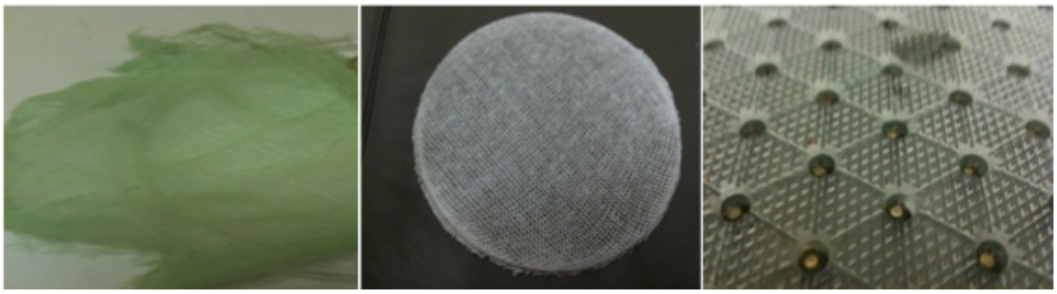

Figure 4.12. Picture of loose gauze (left); Cotton gauze taught over acrylic ring (middle); Ridged and grooved plate (right).

Saline Comparison Table and Observations

Following is a comparison of the introduced impedance of the three designs and the original reference acquisition. The reference (a.k.a background) acquisitions were done at cup size F with warm saline at 35 degrees centigrade. The acquisition frequency was 50kHz. Figure 4.13 shows the original plate filled with saline and the signal response.

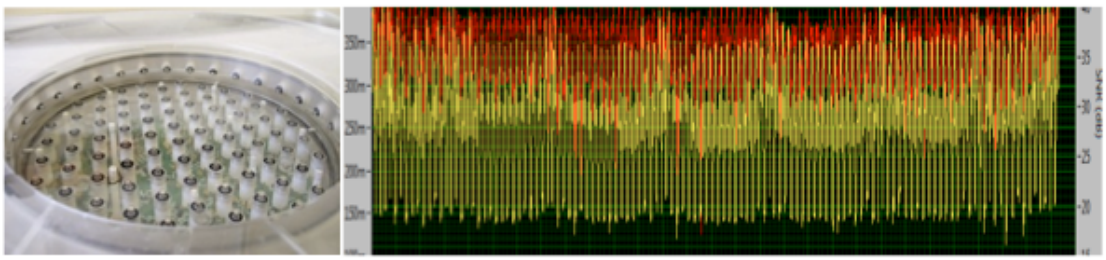

Figure 4.13. Picture of original plate (left); Signal return of original plate (right).

Table 4.6 presents the results, showing the maximum-minimum Amplitudes, SNRs and relative Impedances measured for each method.

Table 4.6 Table of value comparison between reference saline scans

	Original	Gauze	Ring Gauze	Ridges
$\mathbf{A_{max}}$	400 mV	400 mV	490 mV	500 mV
$\mathbf{A_{min}}$	140 mV	150 mV	190 mV	200 mV
$\mathbf{SNR_{max}}$	41 dB	41 dB	43 dB	44 dB
$\mathbf{SNR_{min}}$	32 dB	32 dB	35 dB	35 dB
$\mathbf{Z_{max\ (relative)}}$	0.2735	0.2785	0.3616	0.3652
$\mathbf{Z_{min\ (relative)}}$	0.2355	0.2397	0.2882	0.3052

From the results is deduced that:

Plain gauze is the method with values closest to the original EIM plate (i.e. least interference).

Ring gauze and ridges are very close in data value to each other but is observed that ridges return a 2D image more faithful to the original plate. A possible explanation is the break in impedance uniformity with the introduction of the acrylic ring (with a high impedance value) around the gauze (saturated with same impedance as saline). A test done with simply the ring without any gauze returned the same values and image of ring-gauze, hence confirming this.

Amplitude and SNR have increased for ring and ridges.

Difference of A_{max} and A_{min} has also increased for ring and ridges

Signal Response under Load

Once the possible solutions for the saturated-dead channel issue were identified and their response tested on reference scans, the next step was to establish their performance under impedance load (i.e. simulation of a breast scan) and how a human breast lies on the EIM plate and its relationship with saturated and dead channels. The tests were performed using the balloon phantom as shown on Figure 4.14. There were 3 different setups for the scanner plate:

1. Standard EIM plate
2. Gauze on top of the EIM plate
3. Wide groove plate

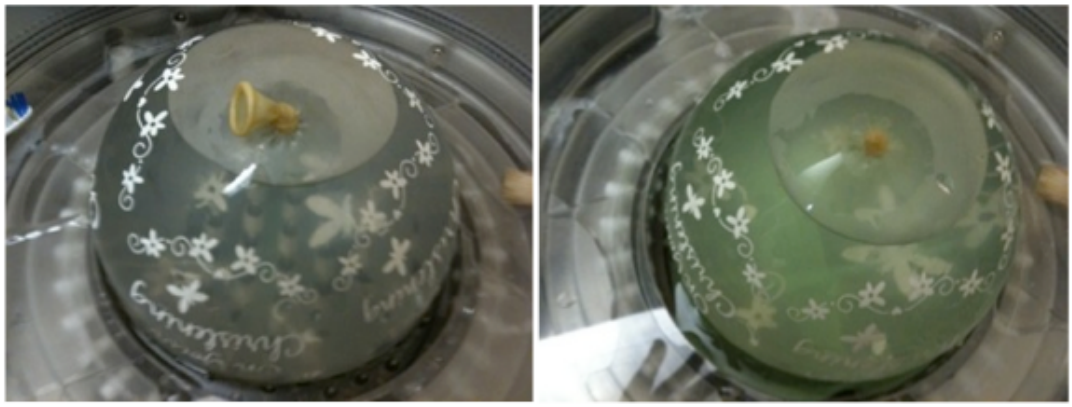

Figure 4.14 Water balloon on EIM plate (left); Balloon on EIM plate with gauze in between (right).

Conclusion: On the standard EIM plate shown in Figure 4.15 (left), the balloon's skin and weight displaces the water fully and small air bubbles can be seen under the skin. This is visible through the transparent balloon in Figure 4.14 (left). The air bubbles insulate the pins. From the data graph in Figure 4.16, dead channels and saturations are observed and the 2D image has been corrupted. Gauze fixes dead channels but there are a few saturations. Results are shown in Figure 4.17. The grooved plate returns a perfect signal and image, shown in Figure 4.18.

Latter experiments with gauze uniformly stretched by an acrylic ring as shown in Figure 4.12 (middle) did in effect return the same signal quality as the grooved plate. Therefore both solutions are acceptable. Gauze on its own is inconsistent and keeps moving inside the plate when the breast (balloon) is being positioned, this explains the mixed results in Figure 4.17.

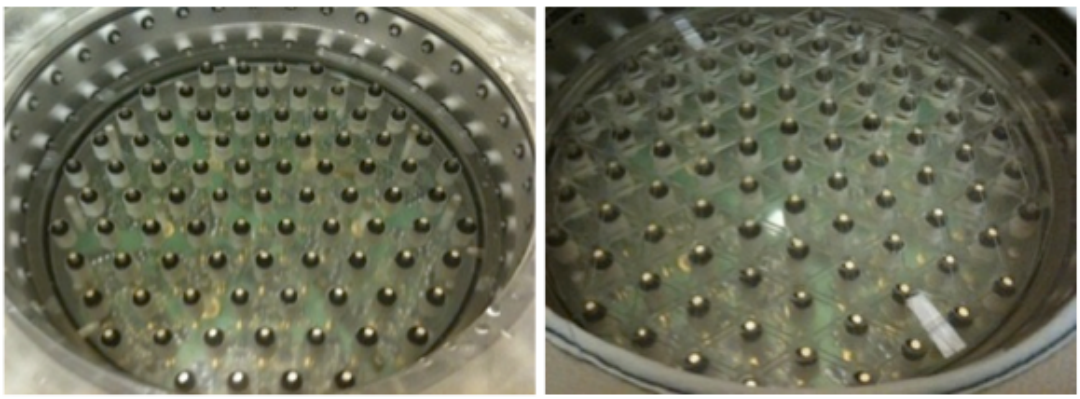

Figure 4.15 Original EIM plate (left); EIM plate with grooved plate on top (right).

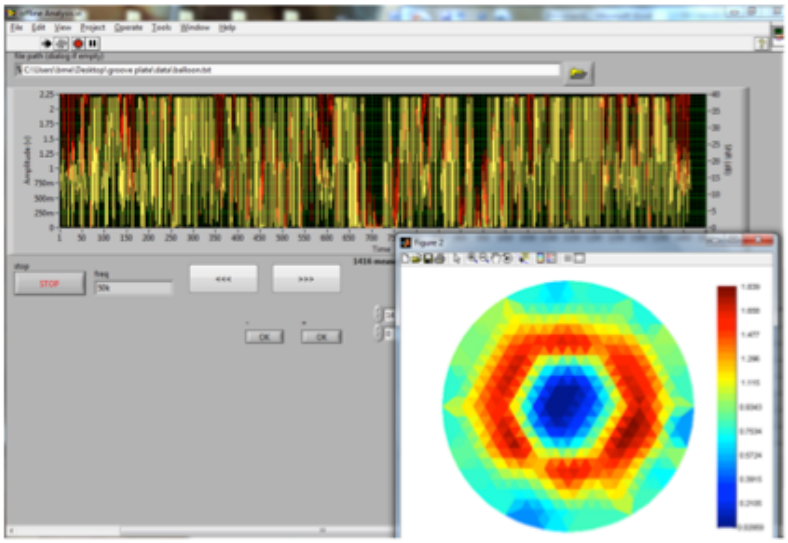

Figure 4.16 Acquisition of balloon on original EIM plate. Note the saturated signals in the graph.

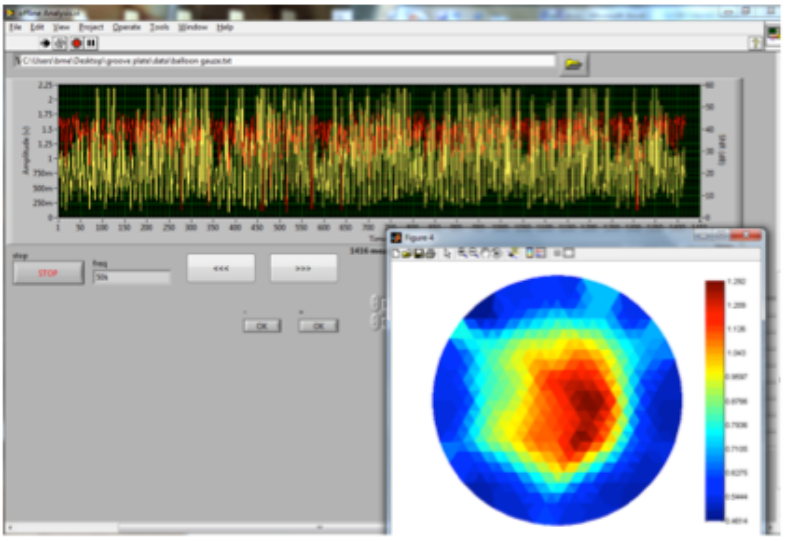

Figure 4.17 Acquisition of balloon on gauze. No dead channels and less saturations.

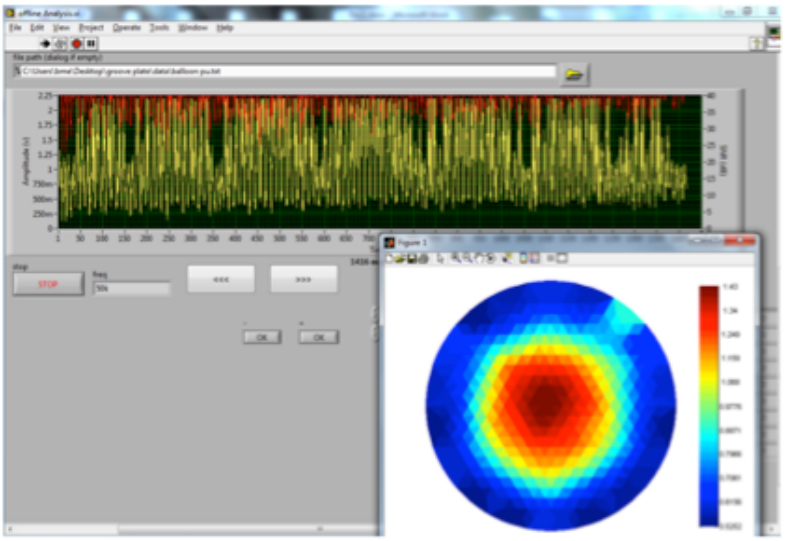

Figure 4.18 Acquisition of balloon on grooved plate. The signal and the image are almost perfect.

NB: The balloon phantoms were made of latex and were filled with water for shape, consistency and how they sit on the scanner plate. Therefore their impedance response is high, uniform and fully masked by the latex. Tissue mimic phantoms are made from doped agar (more on this in the next session). However agar sets, and up to certain extend hardens, like 'cream caramel' or 'panna cotta', therefore no shape distortion information or localised pressure on electrodes is identified.

Natural condoms made of sheep intestine offer some of the properties missing. They allow electrical permittivity but keep liquids separate. So initial experiments were performed with a natural condom filled with saline (conductivity of healthy tissue) and a 1cm^3 agar block (doped with the conductivity of a cancer). These can be seen in Figure 4.19. Note the green agar cube inside.

The experiments were promising but the balloon needed to be bigger in order to exert some pressure on the electrode pins. So a material with similar properties and volume of a breast would be the answer. It must also be clarified that if this new phantom was left for extended periods of time inside the saline tank, osmosis did take place, as confirmed by the conductivity measurement of the liquids.

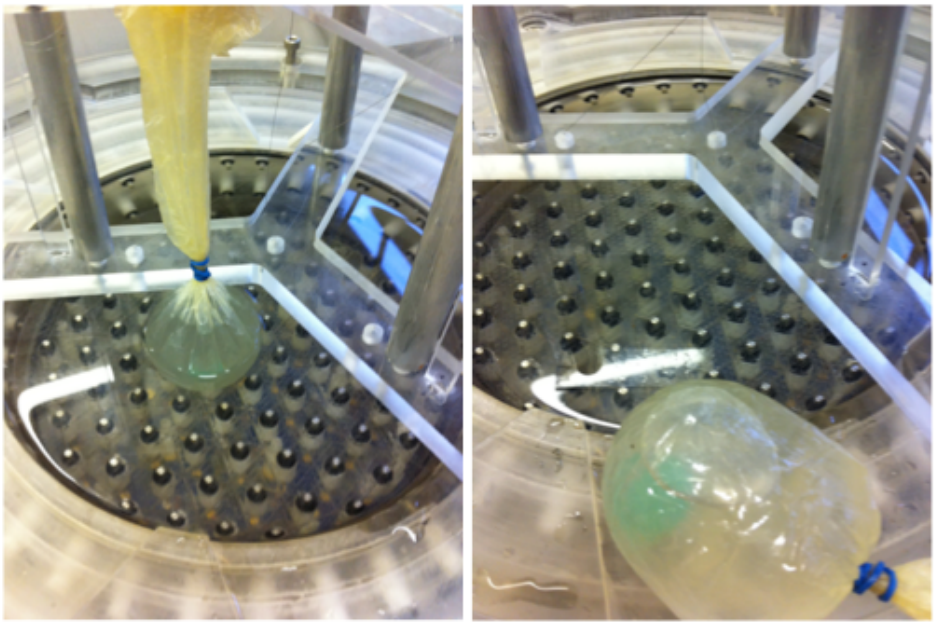

Figure 4.19 Natural condom phantom filled with saline and agar cube with cancer conductivity.

4.5.2 MK4 DAS PERFORMANCE TESTING

Following is the analysis and the results of the DAS (Data Acquisition System) of the Sussex Mk4 EIM. The tests were done using the gold plated Version 3 electrode plate electronics. The system was evaluated using agar phantoms at known conductivities to simulate various impedance loadings. Data was collected using: multiple frequencies; multiple saline conductivities; doped agar phantom simulating breast tissues using two differing "background" conductivities, with values from fat, stroma and carcinoma, as shown in Figure 4.20

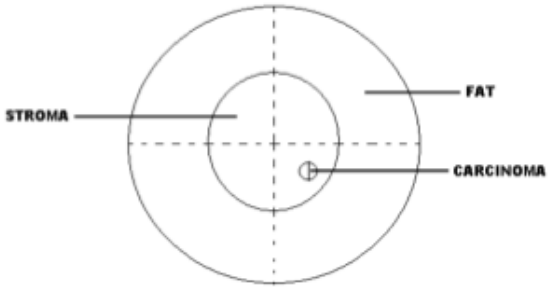

Figure 4.20 Schematic diagram of the agar phantom highlighting fat, stroma and carcinoma tissues.

The aim of the experiments were to evaluate magnitude (Figure 4.21), phase (Figure 4.22) and SNR (Figure 4.23) responses at different frequencies; evaluate signal response at different loading levels; evaluate phantom response using differing background conductivities. The graphs on the left are the responses of the system when acquiring only saline at a filling height of 4.5cm. The saline conductivity was 0.5mS/cm at low, 0.7mS/cm at medium and 1.7mS/cm at high conductivity levels. These values were chosen because they correlate with the bioimpedance values of fat, stroma and carcinoma (Wang L. et al, 2008). The tests were repeated using low and medium conductivity saline and a submerged agar phantom. The results are shown on the graphs on the right for comparative load reasons. The outer diameter of the phantom was approximately 16cm and the height 4.5cm.

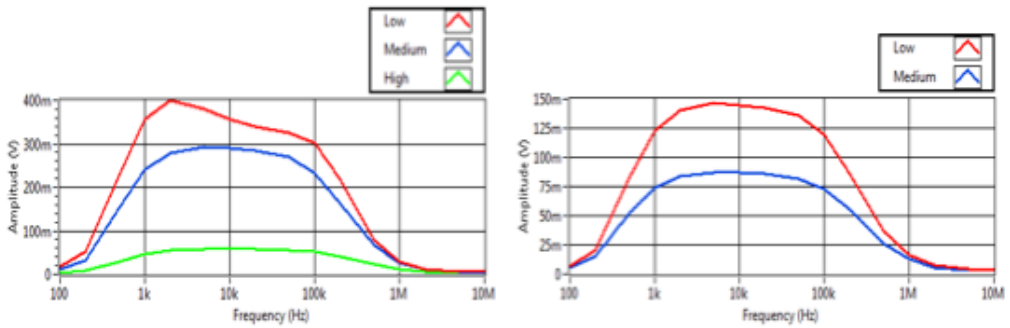

Figure 4.21 Amplitude response over the frequency range of Mk4 DAS; only saline at 0.5mS/cm, 0.7mS/cm and1.7mS/cm (left); Agar phantom in saline at 0.5mS/cm and 0.7mS/cm (right).

Each saline line represents the average value of 10 repetitive tests. The phantom tests were not repeated at high conductivity saline values. The conductivity of the phantom and the saline were too close to each other for the current system to make a distinction.

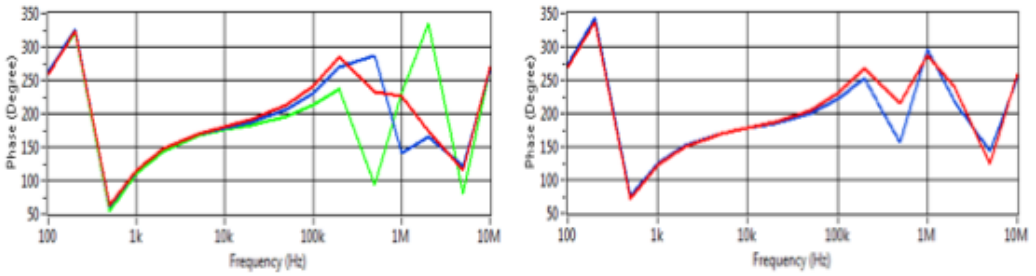

Figure 4.22 Phase response over the frequency range of Mk4 DAS; Saline at 0.5mS/cm, 0.7mS/cm and 1.7mS/cm (left); Agar phantom in saline at 0.5mS/cm and 0.7mS/cm (right).

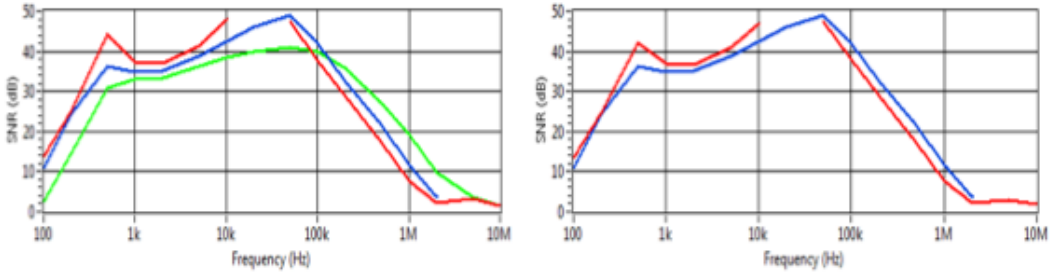

Figure 4.23 SNR response over the frequency range of Mk4 DAS; Saline at 0.5mS/cm, 0.7mS/cm and 1.7mS/cm (left); Agar phantom in saline at 0.5mS/cm and 0.7mS/cm (right).

4.5.3 Signal Calibration

There are currently two image reconstruction algorithms for the Mk4 system and these are described more in depth in G. Sze PhD Thesis (2012). Impedance imaging is created by mapping the magnitude difference between electrode pairs and parametric imaging by using information by both magnitude and phase differences (Sze, 2012), (Sze et al, 2011). The signal source is controlled by the NI PXI-5406 signal generator and a voltage of known amplitude, frequency and phase is passed to the voltage-current converter, which is then directed to the drive electrodes. The current source has been manufactured to keep the same attributes of phase and frequency as the signal source. Injecting the current in a bath of saline should not produce a phase shift in the received signal and also the frequency should be the same. However a magnitude change is expected. An example of a 'Signal In – Signal out' for an electrode pair is given in

Figure 4.24. There is no phase and frequency shift and the output is faithful to the original signal, however fluctuations in the signal itself are noticed (the red signal). These are caused by internal noise and/or external interference.

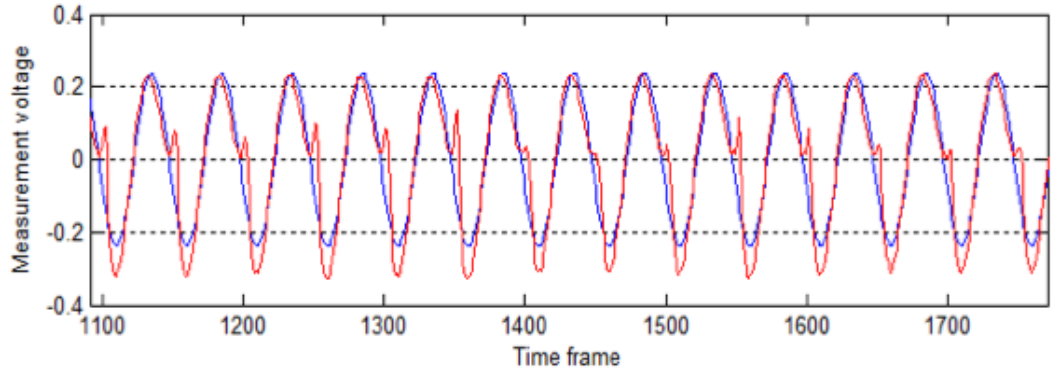

Figure 4.24 Signals measured from an electrode pair in Mk4 system, with the injected signal blue and the measured signal in red. Note the noise levels. Ideally it should be a pure sine wave.

This section presents an initial assessment of filtering and calibration effects to the return signal before image reconstruction. An agar phantom breast model has been engineered using materials simulating known bio-impedance properties of fat, stroma tissues (Wang et al, 2001). A carcinoma section has been introduced in the phantom at 6 o'clock position. The phantom is shown in Figure 4.25.

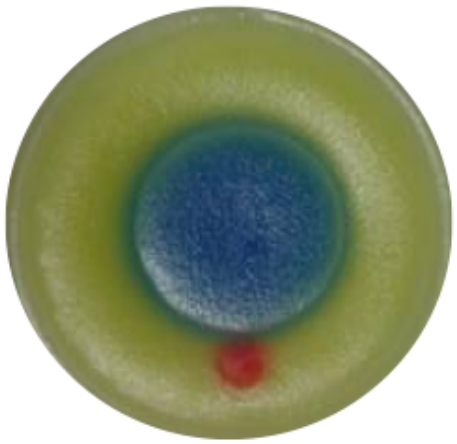

Figure 4.25 Agar phantom breast model doped at different conductivity levels in sections, for simulating fat (yellow), stroma (blue) and carcinoma tissues (red).

Frequencies of 500 kHz and 1000 kHz of three layers have been chosen for comparing reconstructed data with and without calibration as shown in Figure 4.26. Conductivity distortion on the un-calibrated reconstructed data is easily observed. This has been

greatly reduced in the calibrated reconstructed data. Of the two frequencies, calibration performed after data reconstruction at 500 kHz restores the greater spatial information of the carcinoma. Furthermore generally greater distortion is observed in the ventral layer closer to the electrode array (closer to the point of contact) as shown in the last row of Figure 4.26.

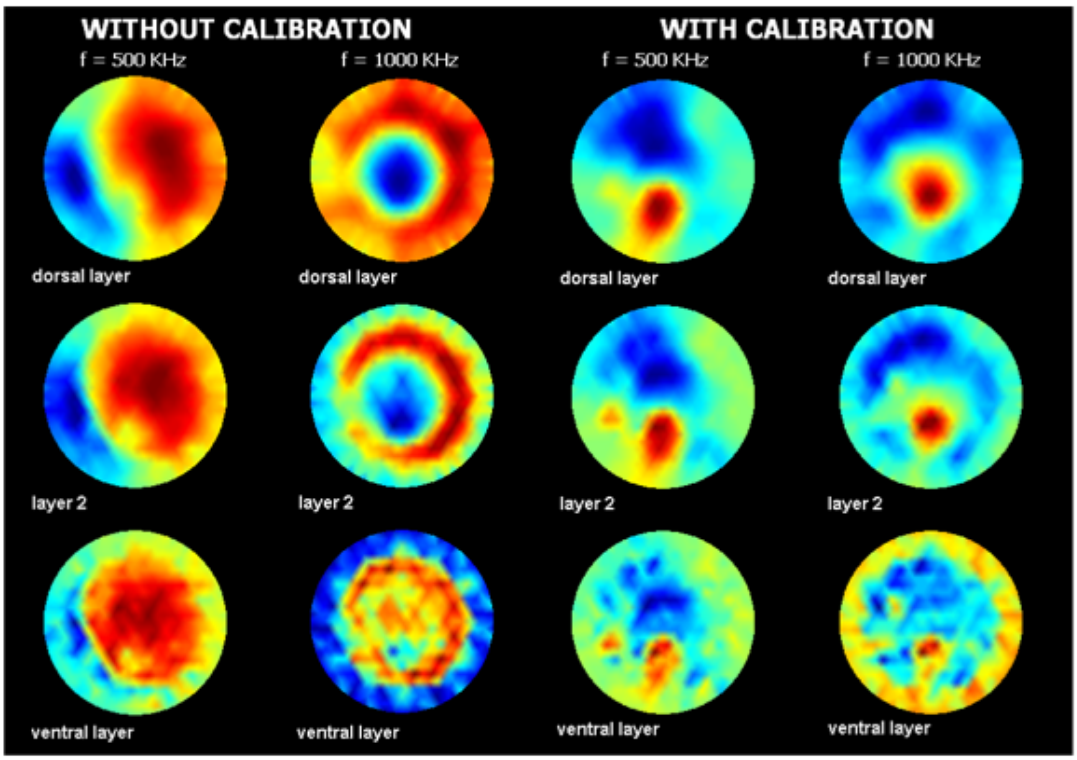

Figure 4.26 Phantom data reconstructed with and without calibration at 500 kHz and 1000 kHz.

Conclusion: The effect of signal quality before reconstruction does make a big difference to the quality of the image. Filtering is the first step, however it is important not to manipulate the amplitude of the returned signal, as impedance mapping relies on it. Phase shifting due to filtering should also be measured and taken into account in parametric imaging. The effect of distortion arising from close proximity to the electrode array can be minimized by reconstructing data of variable thicknesses - thin slices (closer to the ventral layer can be ignored) to thick slices (closer to the dorsal layer).

4.5.4 Fast Method for Artefact Detection

The effects of the patient-electrode interface have been covered extensively in the literature, as they have been shown to affect adversely the accuracy and repeatability of the image reconstruction algorithms, especially ones based on absolute imaging (Hua et al, 1993), (Boone et al, 1996), (Kolehmainen et al, 1997), (Nissinen et al, 2009). To circumvent the inherent variability of the contact impedance, the Sussex EIM system employs a 'wet' electrode system (Wang et al, 2007) which allows indirect contact between the skin and electrodes, via a liquid contact medium, assisting in the reduction of artefacts and increasing the repeatability of EIM measurements. However, it was shown that this method requires very careful design to avoid unexpected artefacts due to load positioning, such as suction vacuums, bubbles or any debris that might have been introduced into the scanner. A fast method for the detection of such artefacts, which can be put to use before data capture and/or *in vivo* scans, warning the operator of their presence, so that the problem can be rectified and therefore preserving the quality of the data, has been proposed (Beqo et al, 2011). An extension of this method can also be applied for the better localisation of breast boundaries as it comes into contact with the electrode plate.

In the Mk4 system, the 85 electrodes can provide thousand of potential drive-receive combinations. 1416 of them have been deemed to provide enough information while at the same time keep the scan time at acceptable levels. A standard acquisition can take from 30 seconds to 5 minutes depending on the frequency range and sample rate selected. However this is still a long time for a pre-scan test. Following is scan method with a 'scan to results' time of 1-4 seconds.

Through the principle of reciprocity, bubbles, objects or skin contact can be mapped on individual electrodes by looking at the signal response generated during normal measurements, and when the drive-receive pairs have been swapped.

In Figure 4.27 are presented three different types of combination patterns that can scan the plate quickly and identify affected pins. To increase resolution, scans can be done at +/- 120-degree angles in the same sweep method (see orange lines in Figure 4.27/a) and then the acquired signals can be merged.

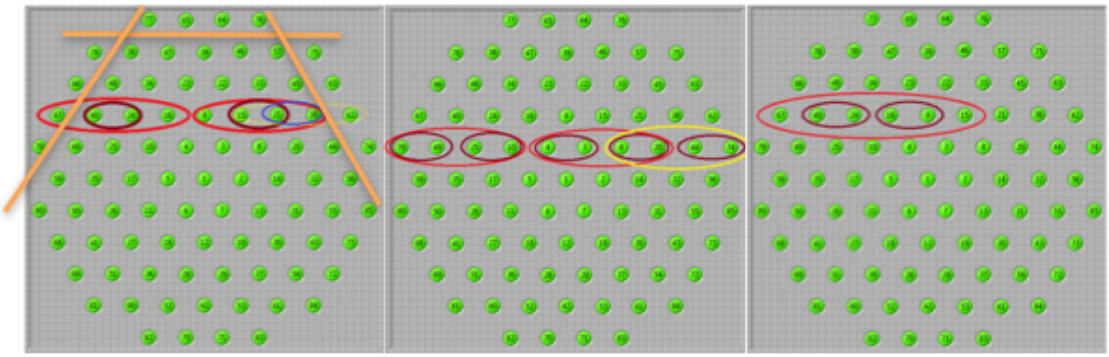

Figure 4.27 Electrode plate and three fast scan combination patterns.

Using this scan pattern, a flat response was expected if only saline was present in the system. This was confirmed by the experiment and the result shown in Figure 4.29 (left). To test this hypothesis, an air bubble (seen as high impedance by system) was artificially introduced on top of pin-1 with a syringe as demonstrated in Figure 4.28.

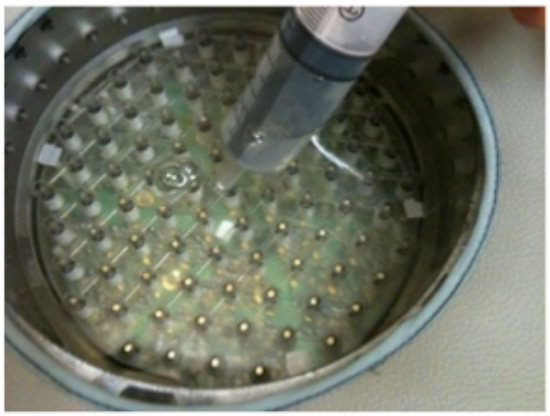

Figure 4.28 Scanner filled with saline; Indroducing an air bubble on top of pin-1.

The acquisition was done at low frequencies. Spike responses were identified on combination 25 (positive) and 26 (negative) as shown in Figure 4.29 (right). Pins 25 and 26 are reciprocal drive-receive combinations to each other.

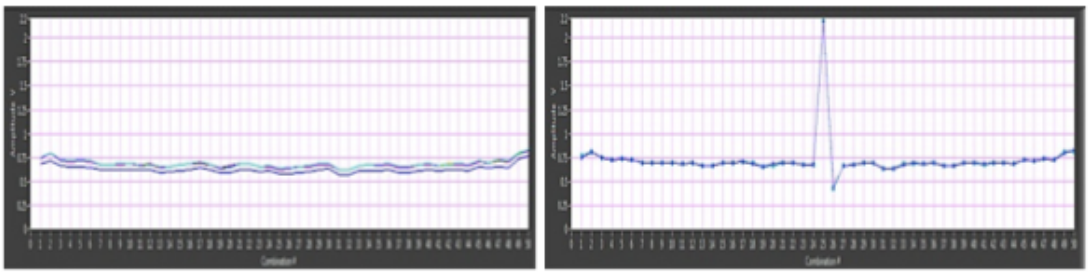

Figure 4.29 Flat response of saline acquisition in a clean plate (left); Spike response identifying air bubble on pin-1 (right).

The magnitude of the signal can be used to identify how covered the pin is (i.e. how big the air bubble is) and/or map if/where the breast is laying/touching.

4.5.5 Real-Time Breast Boundary Definition

In the Sussex Mk4, the scanner head plate moves up-down to accommodate different cup sizes by slightly compressing the breast and holding it steady. One of the clinical challenges here is to make sure that the plate and the breast have made good contact and there is not too much or too little contact, also that there is no fold in the breast. A standard acquisition followed by image reconstruction can take a couple of minutes; therefore there is no fast indicative method to notify the operator that the breast is not positioned correctly before the scan.

By using the fast electrode combination in Figure 4.27, the 1416 combinations have been reduced to 50, where all the pins alternate into drives and receives using the same distance in every combination. The scan is done at low frequencies. Because there is no reconstruction involved the mapping is instant. See Figure 4.30 for a mapping example. A party balloon was filled with water and was placed inside the scanner full of saline. The software 'Acquire-Map' was in continuous mode, at a mapping speed (refresh rate) of 4 seconds from acquisition to pin coverage mapping. The balloon was moved around the scanner to see how the map signature corresponded to the new position. This proved the validity of the method and its potential use.

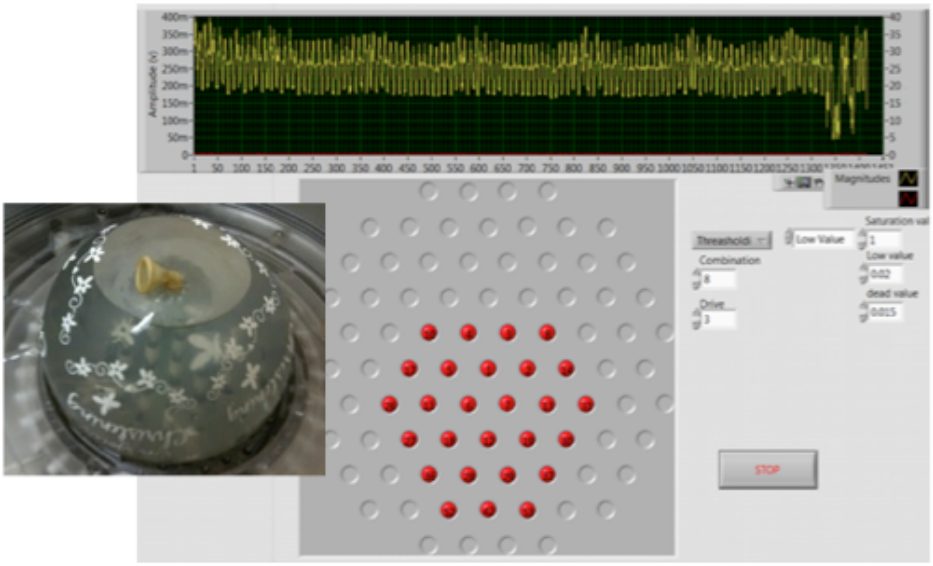

Figure 4.30 Water filled balloon simulating positionings of the breast in the scanner and the fast acqusition software identifying the 'covered' electrodes. The latency is between 1-4 seconds.

4.6 CONCLUSION

This chapter introduced EIT, its theory and its major applications. It explains how this can be used for detecting breast cancer and the work done so far.

The chapter presented a new concept in system architecture, with the use of an instrumentation industry based PXI platform. This adds flexibility and faster prototyping in comparison to standard DSP custom based systems. The system achieved the required specifications. The use of a PXI-based set-up proved successful in building a working system in record time. The module swapping capability has proved vital in the calibration process. Due to the modular nature of the PXI system future improvements will not require major modifications. Based upon this experience it is concluded that a PXI system would be very beneficial to the further study of EIT.

A number of investigations on the performance and problem solving methods for the Mk4 system were also presented:

The addition of ringed-gauze or grooved plate to ensure the presence of liquid coupling between electrode-tissue and removal of dead and saturated channels.

Fast sweep electrode combination pattern acquisition to ensure that no air bubbles or debris are present on the electrodes. The next stage of this method is the ability to dynamically map the breast position on the plate before a full scan takes place. This dynamic scan method can help in patient positioning and reduce nipple folds that could inherently compromise the acquired raw data and the reconstruction that follows.

Mk4 DAS performance tests with saline and phantom load, and comparison of image quality between raw and calibrated data.

CHAPTER 5

- ULTRASOUND IMAGING

5.1. INTRODUCTION

Sonography, also referred to as Ultrasound imaging is a widely used medical imaging and diagnostic technique. Ultrasound imaging is non-invasive, non-ionizing and is effective in imaging soft body tissue. Subcutaneous body structures such as muscles, tendons, breasts etc. are normally scanned at high frequencies (7-18MHz), which provide high axial and lateral resolution. Internal organs are scanned at lower frequencies (1-6MHz), which results in a lower axial and lateral resolution but greater penetration (Udupa & Herman, 1999). The transducer is placed directly on, and moved over the patient by a trained professional. This introduces a subjective factor during a scan, which may affect any subsequent diagnoses. By sweeping the transducer on the patient a 2D image representation of a slice into the body is created. Acquiring and collating a series of 2D images can generate 3D images. To introduce consistency, the 3D scanning process can be mechanized and automated. Ultrasound is gaining momentum and acceptance for breast cancer detection (Kolb et al, 2002), especially for patients with dense breasts. However it is still considered an adjunct to x-ray mammography due to its imaging being depended on the operator and limited diagnostic 'power' (Stavros et al, 1995). This section will expand on the ultrasound investigations that were done as part of this research.

5.2. ULTRASOUND IMAGING PROPERTIES

The propagation of ultrasound in tissue is depended on the tissue characteristics and variations. This is expressed mathematically in equation 5.1:

$$Z_a = \rho V \tag{5.1}$$

Where Z_a is the acoustic impedance, ρ is the material density and V the acoustic velocity. While there are two types of ultrasound imagining setups; transmittive – where the tissue is between the transmitter and the receiver, similar to x-ray; and reflective – where the transmitter and the receiver are on the same transducer; reflective systems are by far the most common setups in medical. The reflected energy R_a is governed by the equation 5.2 in relation to the acoustic impedance between tissue layers.

$$R_a = \left[\frac{Z_2 - Z_1}{Z_2 + Z_1}\right]^2 \tag{5.2}$$

In turn the speed of sound (V) through a material is depended on the properties of the material [material density (ρ) and elasticity constant (c)] and not on the amplitude of the propagating wave. This is expressed by equation 5.3:

$$V = \sqrt{\frac{c}{\rho}} \tag{5.3}$$

A major portion of energy is absorbed or scattered and never makes it back to the receiver. This is called acoustic attenuation and defined by equation 5.4. Where A is the conclusive amplitude of the propagating wave with reference amplitude A_0 and frequency (f) travelling a distance (l) with attenuation coefficient α=0.5 dB/MHz/cm.

$$A = A_0 e^{-\alpha(f)l} \tag{5.4}$$

Spatial resolution – The wavelength of the sound in the tissue determines the ultrasound image spatial resolution. Expanding on reflective imaging the equation 5.5 explains this relationship:

$$\theta = 0.5\lambda \tag{5.5}$$

Where θ is the resolution and λ is the wavelength.

$$\lambda = \frac{v}{f} \tag{5.6}$$

Knowing the relationship between speed, wavelength and frequency, as shown in equation 5.6, then ultrasound image resolution can be expressed in relation to frequency as in equation 5.7:

$$\theta = 0.5\frac{v}{f} \tag{5.7}$$

Most of the research was done with an auto-variable 3-7MHz transducer. According to the equation 5.7 and to the manufacturers specifications this would translate into a resolution of: 0.45 - 1.1mm.

Image contrast – Ultrasound images are presented in 8-bit or 16-bit grayscale (Dreyer et al, 2006). The transition intensity between dark and light grey pixel areas represents the level of contrast. The acoustic properties of the tissue and more precisely the acoustic impedance (density x speed of sound) difference between the adjoining tissue types and/or other materials (e.g. bone) determines the visual contrast in the image (Bushberg et al, 2002).

5.3. 3D Ultrasound Systems and Methods

'Standard' handheld probe ultrasound is common for breast visualization and needle guidance FNA and core biopsy (Kopans, 1999). However holding and operating the transducer is very subjective and requires skilled clinical personnel. Automating the acquisition process and adding more complete information from the 3D data could benefit cancer screening a lot more. The following companies are pursuing automated 3D Ultrasound based scanners and claim that their results prove that Ultrasound needs to be in 3D and removed from the subjectivity of the operator for better performance.

- Siemens has collaborated with U-Systems and have commercialised 'Somo-V'. This is a multiple-slice vertical-layers real 3D 'Automated Breast Ultrasound' (ABU) scanner with the patient lying on the supine position. The system offers high-resolution coronal images, which are not achievable on 2D Ultrasound. The transducer is a high frequency 14 MHz automated ultra-broadband device giving slides of 15cm x 17cm x 5cm. This automated sliding transducer can achieve high repeatability because of the stabilising membrane between it and the breast.

- Techniscan Svara™ WBU™ – Takes a different approach, the patient lie in the prone position with one breast inserted in a warm water bath. The breast is suspended in the water and the ultrasound sensor does not exert any force or compression. The ultrasound sensor is split into sending and receiving units, not like the convention 2 in 1 transducers. The units rotate around the breast, collecting 2D transmissive images (through the breast) that are converted into DICOM images and then rendered in 3D. According to the manufacturer, the company has received over $4 million in funding and is going through 510(k). Section 510(k) of the Food, Drug and Cosmetic Act in the USA, requires medical device manufacturers to notify FDA (Food and Drug Administration of the U.S. Department of Health and Human Services) of their intent to market a medical device. This is similar to the MHRA procedure in the UK.

- Delphinus Ultrasound SoftVue 3D – A tomographic system with transmit-receive frame comparison. The patient lies in the prone position with one breast inserted in a water bath. The system employs rings of ultrasound sensors and fuses reflective

and transmitive data. The manufacturer claims 1 minute scan time and identification of 5mm lesions.

- SonoCiné – Acquires and stores multiple frames done by hand in a 'brush' up-down method while the patient lies in the supine position. The system identifies the location of the transducer and creates a 'panoramic view' collage of the 2D images. The manufacturer's statements are very positive after multicenter trials of more than 6,400 examinations and have produced an interesting size identification chart shown in Figure 5.1.

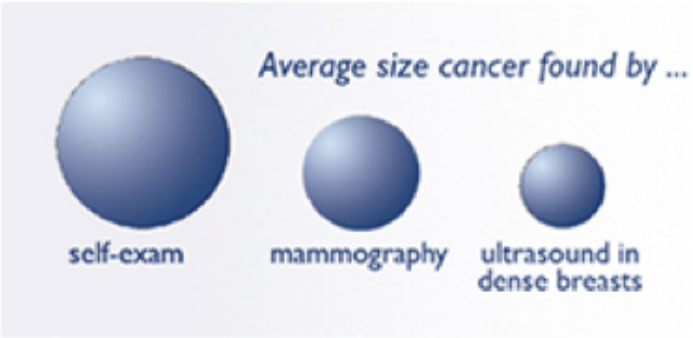

Figure 5.1. 100% scale of cancer size identification from various methods as claimed by SonoCiné® 3D Breast Ultrasound.

5.4. CUSTOM 3D ULTRASOUND SCANNER DESIGNS

It is accepted that Ultrasound imaging is well established in the clinical environment (Udupa & Herman, 1999). Almost all big international medical equipment companies (GE, Siemens, Philips, Toshiba, etc.) manufacture them. The purpose of the investigation is to explore how can Ultrasound and EIM be adapted to work together and complement each other. The basis of the investigation starts with the design, mechanics and the layout of the EIM device. Figure 5.2 shows a depiction of this basis. In its simplest terms there are; an outer cylinder capable of holding saline; an inner cylinder with the ability to move up and down; an electrode plate with predefined electrode location and diameter size 18cm. The fixed mesh EIM algorithm necessitates these conditions so the 3D ultrasound method has to work with or around them.

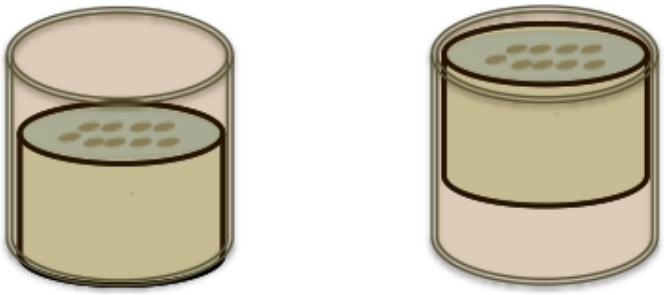

Figure 5.2 Depiction of the Mk4 scanner head showing the inner cylinder at its lowest point on the left and at its highest point on the right.

At this stage it makes no sense to reinvent the wheel and produce a custom ultrasound machine, which in essence would have to infringe on the Intellectual Property of others. Therefore the decision was made investigate how to adapt a commercially available ultrasound machine and transducer to work in symbiosis with the already established Mk3-Mk4 EIM design. The requirement of the ultrasound imaging is to achieve 3D visualisation. There are two methods by which one can achieve this, either by having fixed multiple sensors around the object or by single sensor tomography (Herman, 2009).

Method one is very desirable as this would remove the need for any mechanical movement; rotation, translation etc. However similar systems are semi-custom and expensive. Singular 3D transducers, with internal motorised fanning effect are reasonably cheap and are great candidates, but one: their field of view is quite small, meaning they cannot visualise the whole breast and two: the manufacturers do not allow the sharing of their control software for the 'fan', meaning that the frame information and position would be very hard to establish.

Method two is essentially more feasible as far as purchasing and adapting a Commercial Off The Shelf (COTS) medical imaging ultrasound unit and transducer. The difficulty here lies in the design and the mechanical integration for a full 360-degree tomography while at the same time having a reference frame that can be fed to the tomographic software.

The chosen method was number 2 and with guidance from Diagnostic Sonar Ltd, the ultrasound device selected was a standalone Medison SonoAce 9900. The device is a good all-round mid-range system and offers many imaging and diagnostic features, including breast cancer imaging. The device is compatible with a range of ultrasound

transducers. As a rule of thumb categorised by the industry; low frequency transducers for deeper penetration and high frequency transducers for higher resolution imaging. (Baert, A. L., 2008) (Bushberg et al, 2002). The ultrasound components used in the research are (Figure 5.3):

- Ultrasound device: Medison SonoAce 9900
- Transducer1: Medison C3-7IM Convex (curvilinear); 3-7MHz
- Transducer2: Medison L5-12IR, Linear; 5-12MHz

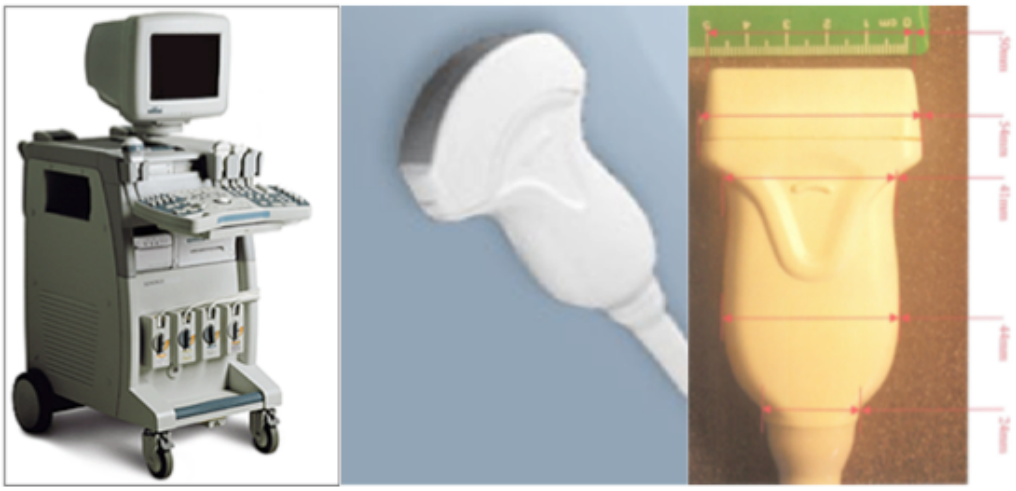

Figure 5.3 Medison SonoAce 9900 (left); Transducer C3-7IM Convex (middle); Transducer2: L5-12IR Linear (right).

The next sections will expand on the designs and prototypes of the 3D ultrasound machines achieved. There are two major designs; tomography from the sidewall of the outer cylinder or on the electrode baseplate.

5.4.1. V1 Scanner

The investigation started with a feasibility study on achieving 360 degrees rotational tomography with the ultrasonic transducer on the outer wall (Figure 5.4). For these reasons, the base plate offered no height adjustments; therefore the outer wall could be of a fixed height as well. The outer cylinder (wall) can rotate 360 degrees via a motor driven mechanism, as seen in Figure 5.6 (left). The ultrasound transducer was placed on an aperture of the sidewall. A hemispherical housing was produced for the transducer so that angle and field of view adjustments could be done to the transducer as shown in Figure 5.6 (right). The transducer performs a full rotational scan, therefore its penetration depth should be at least equal to the radius of the scanner plate, which is

18/2=9cm. Field of view ray depictions shown in Figure 5.5. Only the convex transducer C3-7IM, in Figure 5.3 (middle), offers that range, so a trade off between penetration and resolution was accepted in this case.

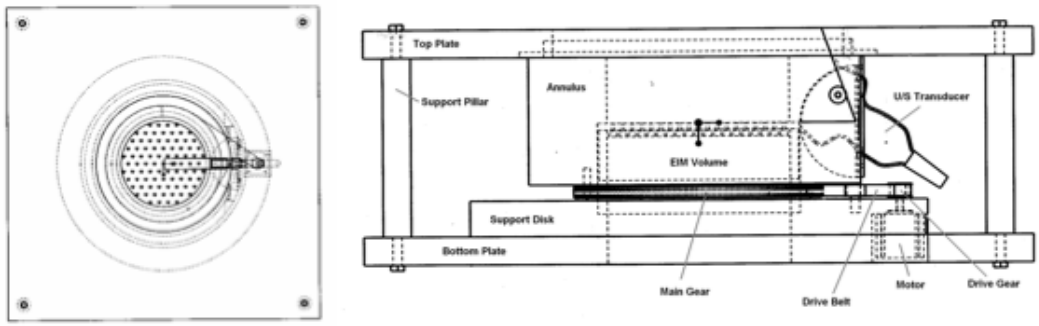

Figure 5.4 Top and side view of the V1 scanner.

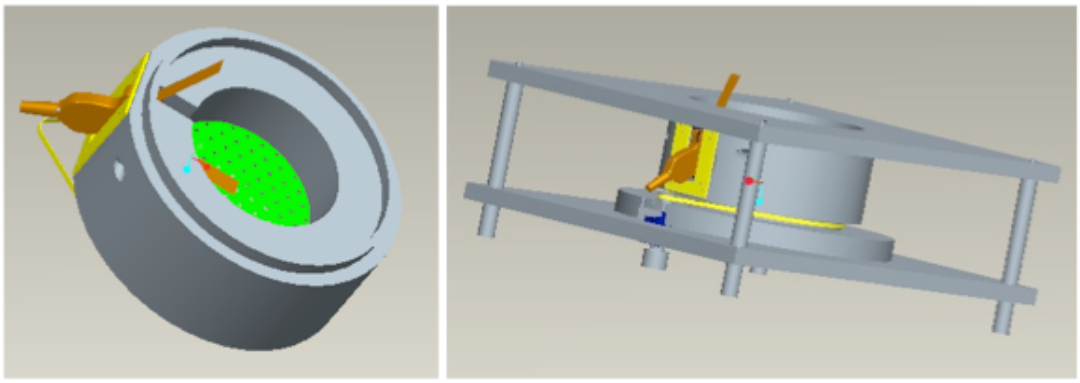

Figure 5.5 CAD modellings of the V1 scanner .

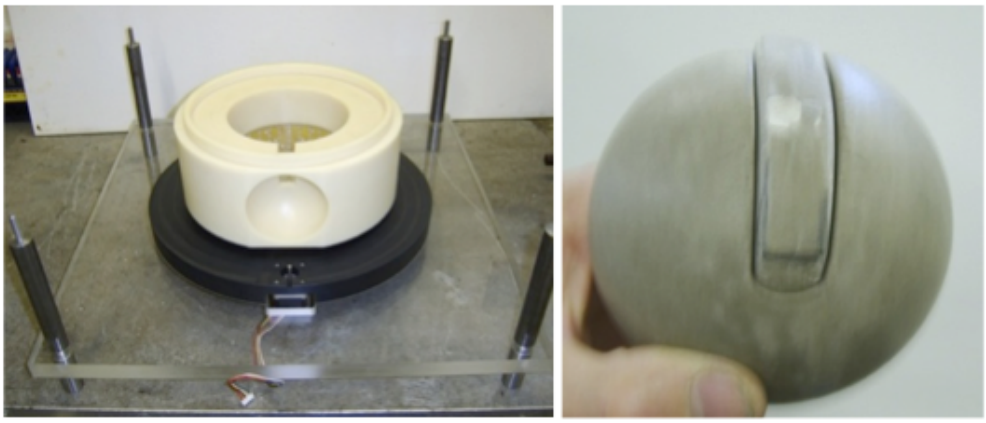

Figure 5.6 V1 scanner prototype and components (left); hemispherical housing for the ultrasound transducer that fits in the side apperture of V1(right).

3D scans were successfully performed and the prototype proved its purpose. It should be mentioned though that there were issues. The outer cylinder needed to be free to rotate but at the same time hold water/saline inside the chamber. So many types of sealants were tried and tested; from rubber, latex, Teflon etc for both the walls and the ultrasound housing. Rotation mechanism variations; belt driven, gear driven, higher torque motors etc.

5.4.2. V2 SCANNER

The V2 scanner was an evolution to the V1 scanner with the main feature to add breast cup size adjustment (i.e. up-down movement to the electrode plate). EIM needed to have a variable depth to accommodate different breast sizes. This however introduced a problem of 'shadowing' for the ultrasound transducer when the EIM plate was to high up and a problem of Field of View (FOV) visualising the lower part of the breast when the plate was too low. Figure 5.7 demonstrates the FOV adjustments of the ultrasound.

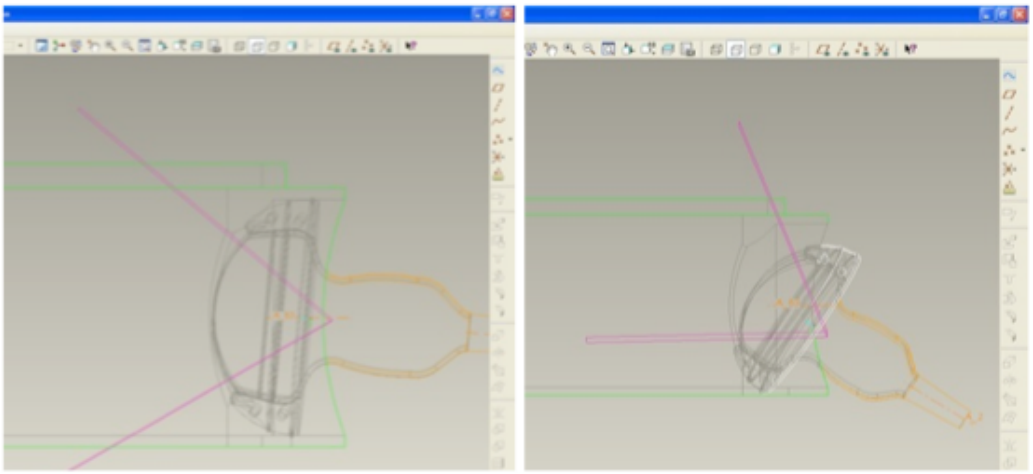

Figure 5.7 CAD modellings of the ultrasound FOV (Field of View) adjustments for the V2 scanner.

The C3-7IM transducer has 128 channels/sensors along its head. According to the manufacturer the device will produce a better image when the least amount of shadowing is employed on the transducer (i.e. full 128 active channels). A full up-down movement of the plate and a full FOV adjustment of the ultrasound introduced even more engineering challenges for manufacturing a water-sealed scanner with the above scanning characteristics. A separate working prototype to the specification was not manufactured, however adaptations were done to the V1 scanner:

- EIM height adjustment testing was achieved by stacking plates on top of the base.
- A fixed ultrasound transparent membrane cylindrical wall was placed between the chamber (breast holding area) and the ultrasound transducer holding rotating wall. This also introduced a safety parameter to the breast scan, as there are no rotational parts touching the breast. The coupling between the transducer and the ultrasound transparent plate was done manually with gel.
- The rotational wall was now not a subject to free flowing water; hence adjustments to the ultrasound FOV could be mechanised and were a lot easier.
- Ball bearings were introduced under the rotating wall to speed the scan.

5.4.3. V3 SCANNER

This was a revolutionary design because the ultrasound scanning was not to be done from the sidewall anymore but from the base plate. The EIM scans were already done from the base plate, therefore the merger of the images would be with less geometric distortion. As a fast proof of concept method to achieve horizontal ultrasound scanning a rig, named V3a, was designed and manufactured as shown in Figure 5.8. The idea was to test 360 degree horizontal scanning and 3D radial reconstruction, and then make the decision to fully manufacture V2 or change path and pursue the V3 design. The tests used the water-sealed chamber of the V1/V2 scanner and V3a was positioned above the chamber. As far as scanning and reconstruction is concerned, there is no difference if the plate is above or below the object. A scanner with a plate below would be more challenging to produce and keep the water tight as was seen in V1/V2. So scanning from above offered a fast solution. An ultrasound transducer was fixed perpendicular to the V3a plate. The transducer holding clamps are visible on the white plate in Figure 5.8 (right). The V3a plate, drive shaft and motor height (submersion in water) could be adjusted by the guide rails in the V3a body; red unit in Figure 5.8 (left).

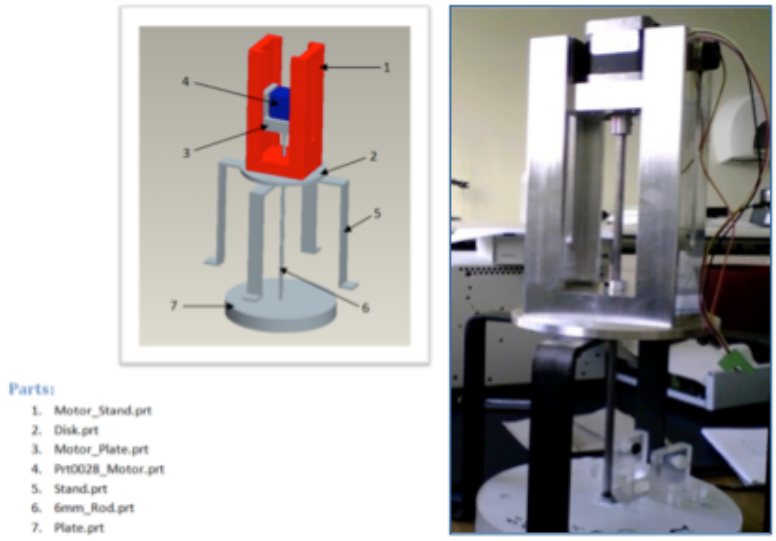

Figure 5.8 V3a CAD design and components (left); Manufactured V3a ready for testing (right).

The scans with V3a proved successful. The maximum penetration distance required now was the highest depth the EIM plate could go = 5cm (i.e cup size G, explained in Chapter 2.3). This opened the path for using linear transducers with better imaging at higher resolution. Work started on the next prototype based on V3 methodology. Figure 5.9 shows the evolution of the baseplate into a fully integrated EIM + ultrasound plate.

Figure 5.9 Baseplate of V3a showing the gap for the ultrasound transducer (left);
Evolution of the base plate for V3b with electrodes and transducer in position (right).

V3 designs (aka Pizza slice) 'forced' a gap in the EIM plate and 4 electrodes had to give way to the ultrasound transducer. Figure 5.10 shows the measurements and the adaptations required on the electrode plate and the PCB in order to accommodate any of the ultrasound transducers. The linear transducer was 5.5cm wide and the convex one was 8cm. in both case scenarios for a better water seal, 4 electrodes had to be removed. Chapter 6 will cover the scanning methods and how the missing electrode issue was solved.

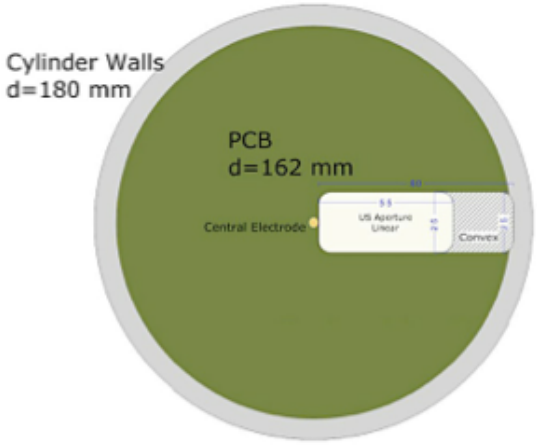

Figure 5.10 Depiction of the comparison of EIM PCB electrode plate d=162mm; electrode breast plate reaching the scanner inner walls=180mm; a linear (high frequency) ultrasound transducer 55mm x 25mm; a curvilinear/convex (low frequency) ultrasound transducer 80mm x 25mm.

The ultrasound transducer had a bulky body and a thick cable. These dimensions had to be accounted for and accommodated inside the inner cylinder of the EIM scanner, as shown in Figure 5.11.

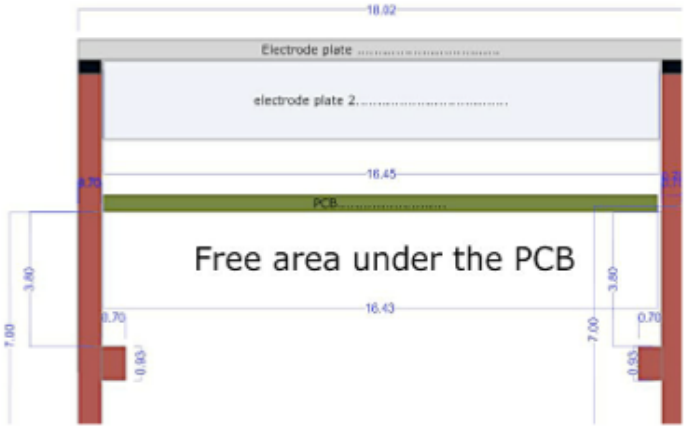

Figure 5.11 Dimensions of the EIM inner cilinder where the scanner plate and electrodes are positioned.

Scanner V3b was designed and manufactured successfully as shown in Figure 5.12.

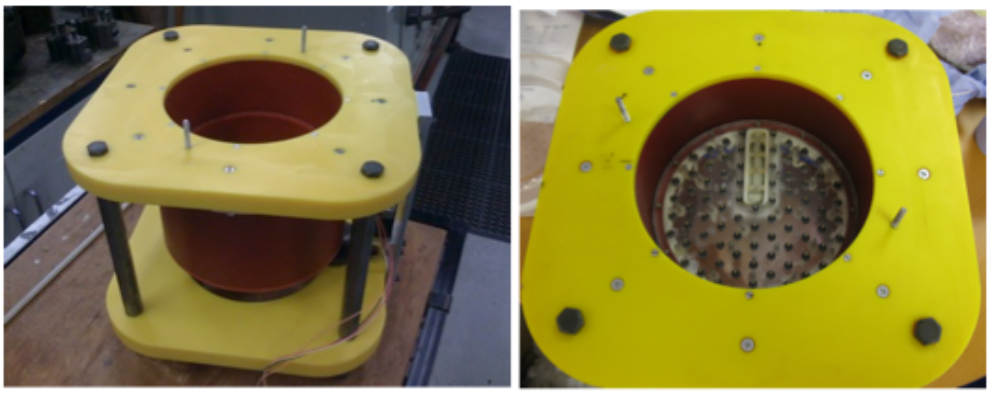

Figure 5.12 Side view of V3b scanner (left); Top view of V3b showing the plate with the transducer (right).

5.5. PERFORMANCE TESTS

The fixed ultrasound transducer scans need to be tested so that their performance can be regarded as matching the quality of a 'normal' skin contact ultrasound scan. To do this, a industry certified breast phantom was scanned in a V3 scanner version using the 'on the base' ultrasound setup. This phantom uses Zerdine® tissue mimicking material (Figure 5.13) and has been randomly doped with solid masses in white and cystic masses in black. Two test were performed: one, where the transducer was touching the phantom and the purpose was to identify the lesion masses specified by the manufacturer; and the second was to see if there is any degradation in detection quality when the transducer is away from the phantom.

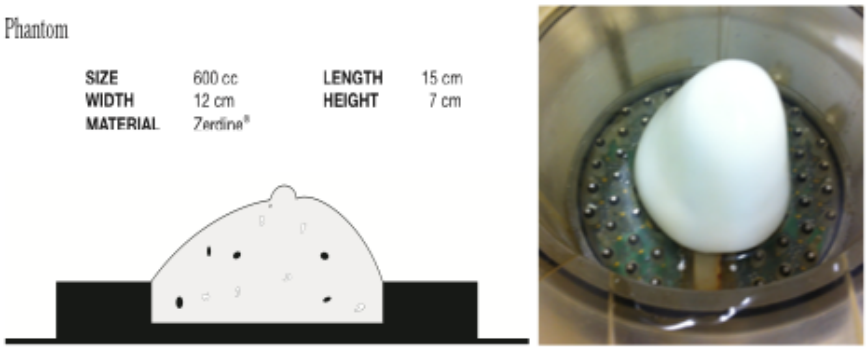

Figure 5.13. Depiction of the Zerdine® breast phantom and its specifications (left); Breast phantom inside the scanner head, showing the ultrasound transducer and the EIM electrodes underneath (right).

5.5.1 DETECTED FEATURE SIZES

The phantom was dropped inside the scanner head full of water and hand positioned until the features were made visible. The features are about 2.3cm apart (Figure 5.14). The dense/solid mass in white measures 0.54cm and the cystic mass in black is 0.3cm. The measurements were done using the metric ruler option of the ultrasound machine.

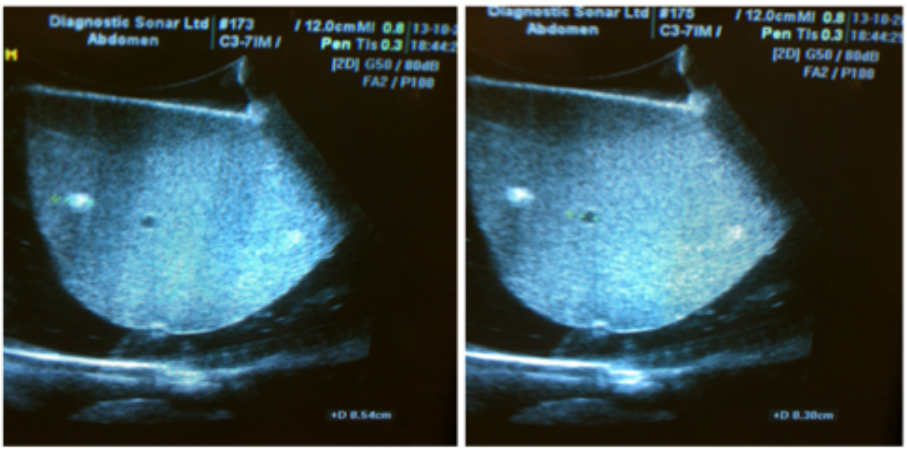

Figure 5.14 Solid masses (white) Ø=0.54cm and cystic masses (black) Ø=0.3cm as measured by the ultrasound ruler feature. Values shown on the bottom right corner of the images.

5.5.2 Imaging Distance Test

The Zerdine® phantom was held above the ultrasound transducer at different heights ,as shown in Figure 5.15 (left). The dense and cystic masses are visible and in the frame as shown in Figure 5.15 (right). The curved white line at the top of the image is the transducer; the white horizontal line is the breast holding plate.

The phantom shape and the two masses are quite distinguishable in the middle of the image. Also the thumb, the palm and the index finger, that are holding the phantom, show quite clearly in the image. Both the dense and the cystic mass show up clearly at a distance of 9.6cm from the transducer in Figure 5.16. Even though the phantom has been moved 4.59cm away from the plate the image has not degraded.

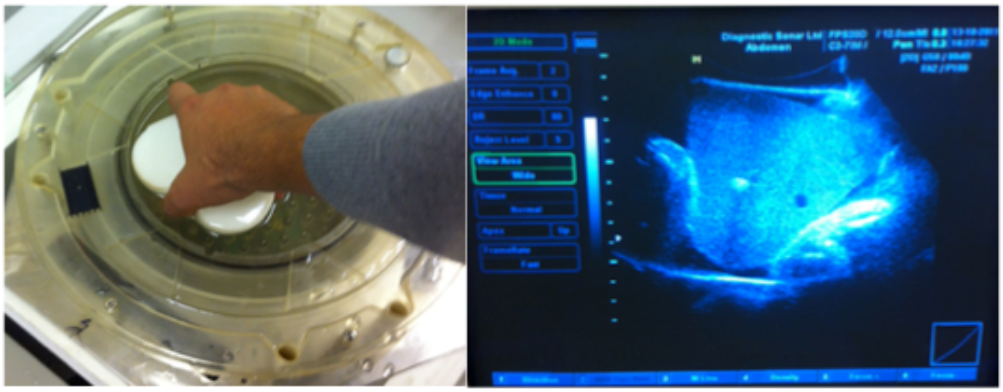

Figure 5.15. Holding the phantom in a filled scanner ready for testing (left); Screenshot of the ultrasound monitor, clearly showing the fingers holding the phantom, and the solid/cystic masses inside the phantom (right).

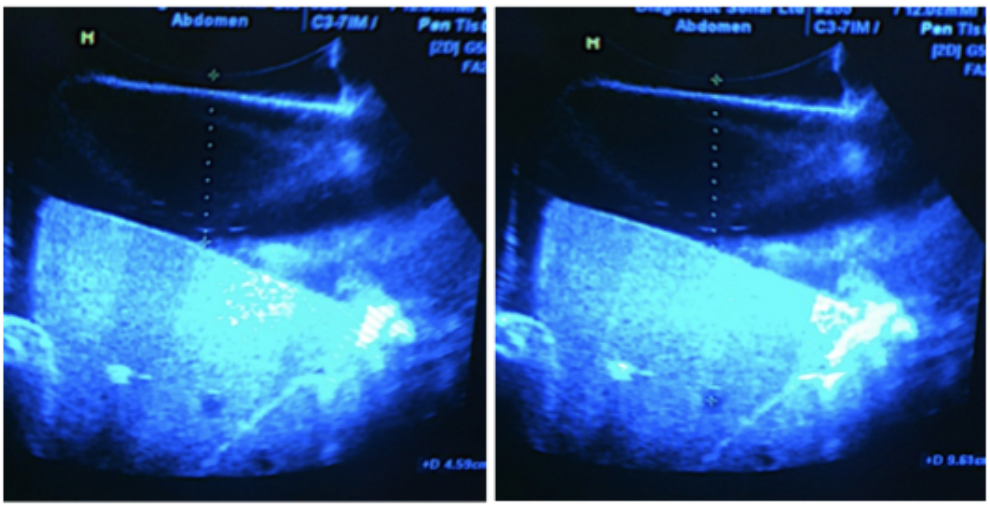

Figure 5.16 Phantom visualised clearly at 4.59cm away from transducer (left);
Cystic mass identified at 9.6cm away from the transducer (right).

5.5.3 PRECLINICAL EVALUATIONS

The 3D ultrasound adaptation and the multimodality scanner variations of the research will eventually go through a clinical trial. However before that stage is reached the ultrasound module has to satisfy the requirements of a preclinical evaluation. This section will expand on some of the issues and the proposed setups that could expedite the transition between a lab prototype to a clinical device.

5.5.3.1 ULTRASOUND MACHINE

The ultrasound device used for this research was 'Medison SonoAce 9900' shown in Figure 5.17 (left). This was a very capable and a good all-round machine. However it was a big and heavy machine, measuring 1.6m in height. The ultrasound device market has evolved quite rapidly and devices like Zonare in Figure 5.17 (right) offer the same power and features as a standalone ultrasound with the benefit of a small form factor. Zonare is as big as a laptop. Figure 5.17 (left) demonstrates a rough comparison of the form factor between the two devices. A small ultrasound unit can be adapted easier and even incorporated as an OEM unit in the trolley of the clinical device in investigation.

Figure 5.17 Sonoace 9900 and Zonare laptop size comparison(left); Zonare scan engine laptop, zoomed in (right).

5.5.3.2 ULTRASOUND SCAN SETTINGS

Ultrasound machines are manufactured to cover a range of scanning methods and on different parts of the body. They use different types of transducers to maximize results on the scans. Therefore they offer the flexibility of settings selection depending on the scanning method. Information gathered from consultations with Dr Gary Rubin (Consultant Radiologist at NHS Park Centre Clinic For Breast Care), with ultrasound device sales representative and from literature concludes that the scan settings on the

device are subjective from the operator. For safety reasons, ultrasound devices boot up at low power settings (Stavros, 2004) and they offer preconfigured scanning modes for a particular body part. The operator will either scan with those settings or tweak them subjectively for a better image. Following is a list example of settings for breast scanning:

- Transducer: L14-5w
- Centre frequency:12MHz
- Dynamic Range: 65
- Grey map:3
- Persistence:3
- Gain:70
- Edge enhancement:2
- Output:100%
- Mechanical index: 1.2
- Thermal index (soft tissue): 0.2
- Depth:3.5 cm
- Frame (shutter) rate: 13Hz

Manual setting changes would add an extra step and subjectivity to the 3D scans under investigation. So the options are either predefined settings or auto-adaptive settings. The auto-adaptive settings in turn are two; either rely on the manufacturers algorithm or where possible, under licence, the manufacturers allow programmatic control via (e.g. RS232, GPIB or USB) connections to their devices, so a feedback loop with settings auto-corrections can be set in place. The Zonare laptop ultrasound under investigation previously offers proprietary auto-optimization for both power and gain levels. The manufacturer claims that the device auto-sets the levels and optimizes focus based on algorithms that use speed of sound estimation in the tissue it is scanning.

Figure 5.18 demonstrates the autofocus results on a urethane phantom ($c \approx 1455$ m/s).

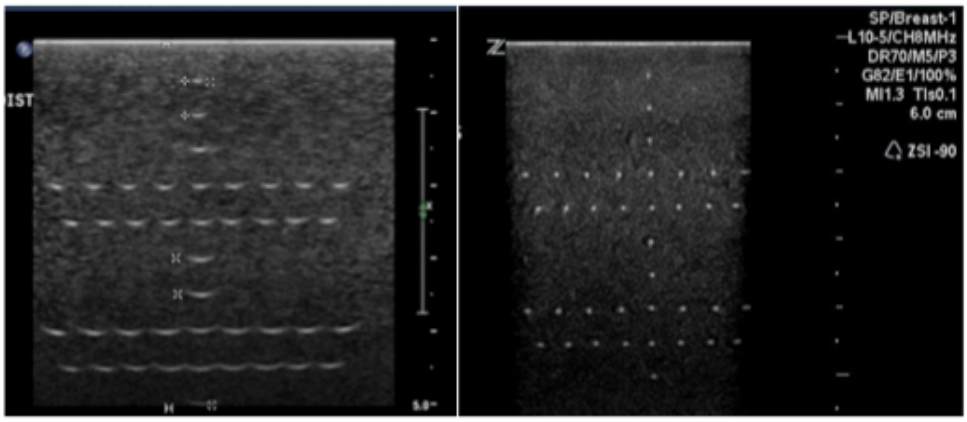

Figure 5.18 Comparative pictures of a urethane phantom, $c \approx 1455$ m/s;
High performance conventional scanner (left); Zonare ZST auto-correction (right).

5.5.3.3 IMAGE DIGITISATION ERROR

The video feed from the stand-alone ultrasound scanner is a standard analogue VGA that is connected to a frame-grabber and digitized (pixelated) for storage and data manipulation on the PC. The cable from the ultrasound machine to the computer frame-grabber might become loose, not connected properly or the contact might not be ideal. All of the above will translate in loss of analogue signal and further on in a digitization of bad quality.

By using the grey scale difference between the pixels that will always be at their lowest or highest value (e.g. letters and characters on the monitor *vs* their background, see Figure 5.19), the software can determine that no image anti-aliasing has happened. This will ensure that the contrast between the pixels in the scan is the correct one and no information has been lost or covered from the digitisation.

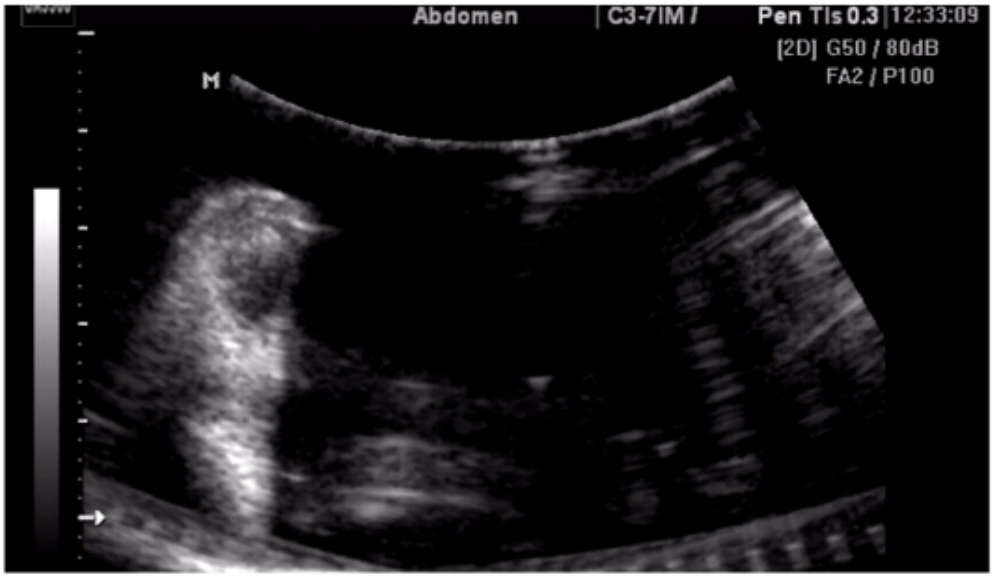

Figure 5.19 Fixed pixels in the header of the image will always have the same value. If that value is corrupt that would indicate an overall image digitisation error and the ultrasound pixels might not be reliable.

5.5.3.4 OBJECT LOCATION REPEATABILITY STUDY

One of the conditions of the MHRA approval for clinical trials is to metrically prove the repeatability of the device. Following are some proposed tests that could satisfy that requirement.

Test conditions: scanner filled with saline at an F-cup; an object of known size (preferably 1-2cm^3) located such that the bottom surface is 30mm above the electrode

plate at a position 50% of the distance between centre and periphery at the 3 o'clock position.

1. Repeatability could be validated by doing 360 degree scans continuously (x5)

    a. Split frames by their tagged number (e.g. Scan1 Frame56 = S_1F_{56})

    b. Image filter frames

    c. Extract pixel matrix of object in each frame

    d. Standard deviation of each of object coordinates between same tag frames of each acquisition. (e.g. comparing S_1F_{56} *vs* S_2F_{56} *vs* S_3F_{56}..... *vs* S_nF_{56})

2. Repeat test with same object in different scanning positions but keeping the same distance from the center point of the scanner (x_0,y_0)

    a. Extracted matching frames on each scan

    b. Standard deviation of each matching frame

(Experiment 2 should return the same results as Experiment 1 but the comparison will be more complex and will be between scans and frames of different tags. This will prove the repeatability of the object identification and localization even further.)

3. Repeat tests 1 and 2 with objects of different size and position

4. Repeat test with object randomly positioned in the scanner

    a. Boundary detect the object

    b. Extract frames where object is visible

    c. Match frames of different scans by the amount of boundary

    d. Standard deviation of the matching frames

(Experiment 4 would demonstrate the robustness of the edge detections algorithm and its repeatability).

5.6. CONCLUSION

This chapter introduced ultrasound as a medical imaging modality. The theory and the properties of ultrasound were explained in preparation for selecting the best setup for breast scanning. The trade off is between resolution and penetration. The higher the ultrasonic frequency, the higher the resolution and the lower the penetration range. The research also focused on the current prototype or ready to enter the market, new 3D ultrasound scanners for breast cancer detection. All of the above information was then transferred to achieve the best 3D scanner for this research but always bearing in mind the specifications and limitations set by the EIM system.

The designs were based on a cylindrical water tank with a diameter of 180cm. The breast is to be submerged in the tank and a 360-degree scan of the breast will be done by mechanically rotating the ultrasound transducer. There were two major designs; the transducer scanning from the sidewall of the tank; or scanning underneath the tank's base. The best method chosen via experiments, image quality and ease of manufacturing, was scanning from the base. The evolutions of these scanners are called V3a, V3b, V3c and V3d (which is the final version fulfilling all the specifications).

The ultrasound transducer that fulfilled the 3D scanning criteria was Medison C3-7IM Convex (curvilinear), 3-7MHz. Performance tests of the scanner using the above transducer proved very satisfactory, be that in small feature detection and on penetration testing. The results were certified by industry standard ultrasound phantoms.

This chapter also expanded on the preclinical evaluation research done on the 3D ultrasound scanner, in preparation for the finalised version going through the scrutiny of the MHRA.

The prototypes and the software proved satisfactory that the current design of the 3D ultrasound breast scanner offering the required imaging capabilities and the features required for the next step of this project – merging it with 3D EIM.

CHAPTER 6

- COMBINING EIM WITH ULTRASOUND

6.1 INTRODUCTION

Multi-modal imaging is the creation of a single image set by the use of multiple imaging modalities. It is hoped that through the use of two distinct imaging modes additional information, that is not available from either modality in isolation, will be made available for diagnostic and detective purposes. This section describes how a totally configurable system was achieved combining current EIT technology for breast cancer detection to the 3D Ultrasound scanner prototype. This was done with a quick turn-around in development time using off-the-shelf hardware and a 3U PXI Chassis. The architecture of Mk4 chassis was left open for the additional PXI modules required for ultrasound acquisition and control. Figure 6.1 shows the complete setup of the PXI modules and the control diagram.

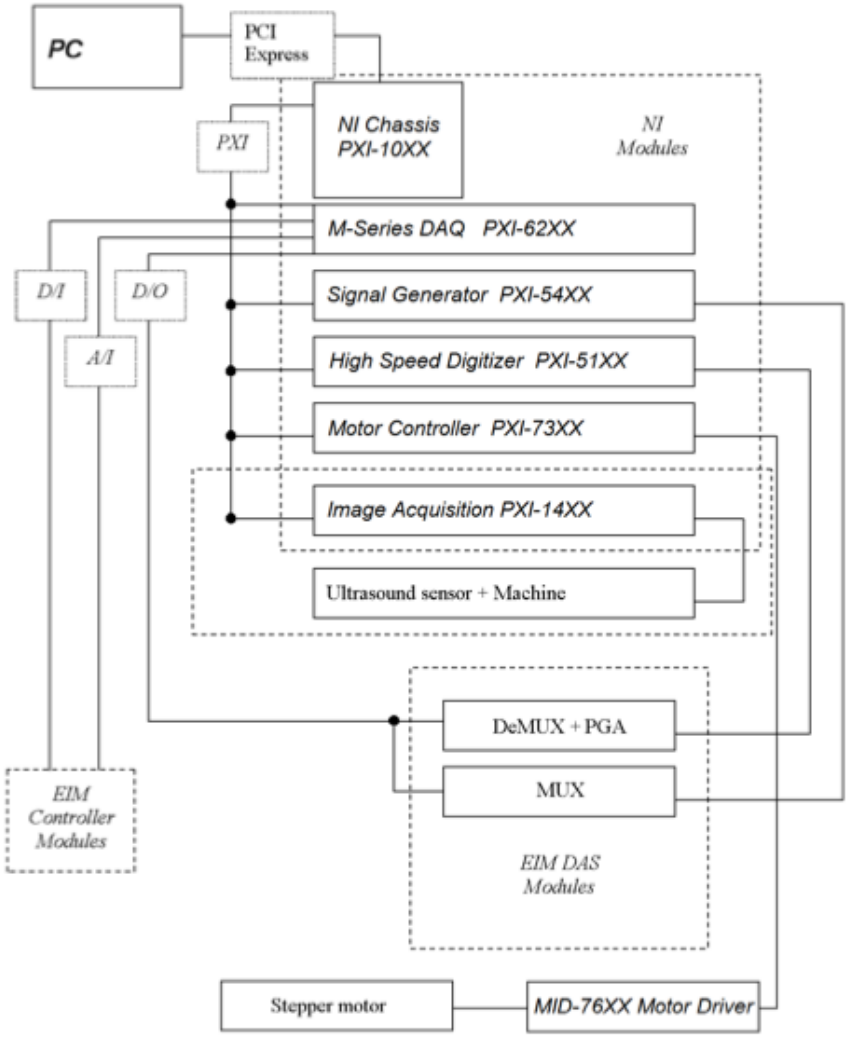

Figure 6.1 System control and acquisition systems for combining EIM and Ultrasound.

From the Medison ultrasound device (Chapter 5) 2D slices are captured as images via the video-out port available on the system (CCIR TV format 25Hz frame rate). Video capturing is done using a PXI-14XX analogue frame grabber. The movement of the transducer, permitting a 3D scan, is achieved by using a motion controller PXI-73XX connected to a MID-76XX drive unit to power the stepper motors (Figure 6.1).

6.2 SCANNERS AND CHALLENGES

6.2.1 SCANNER DESIGN VARIATIONS

There are two major design variations in order to achieve dual modality in EIM and Ultrasound:

1. Ultrasound from the side wall (EIM plate intact)
2. Ultrasound from underneath (embedded on the EIM plate)

6.2.1.1 ULTRASOUND ON THE SIDE

The EIM plate stays intact while the Ultrasound transducer rotates around the outer perimeter in 360 degrees, similar to a CAT scan. Figure 6.2 shows a Computer Aided Design (CAD) of this type of scanner and its assembled components in different colour codes. Note: the ultrasound transducer on the side of the scanner with an enhanced depiction of the acoustic field of view angles.

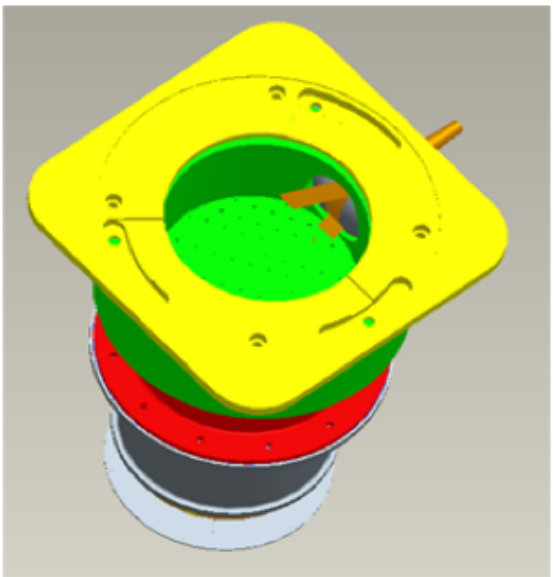

Figure 6.2 Dual scanner with Ultrasound on the side with depicted rays of the acoustic path.

This kind of setup favours the EIM scan because it does not disturb it. However the ultrasound scan would suffer from major shadowing on the small cup sizes, when the

EIM plate is further up. Also water sealing the scanner while at the same time allowing 360 rotational freedom proved to be a challenge in itself.

Imaging wise ultrasound scanning from the side introduces a 90mm penetration requirement for the ultrasound beam, as this is the radius of the scanner. Also the geometrical distortion of the 3D reconstruction has to be taken into account.

6.2.1.2 ULTRASOUND ON THE BASE

The EIM base plate has been modified to accommodate the ultrasound transducer. The aperture has caused the removal of 3-4 EIM electrodes, therefore creating a 'blind' zone (Figure 6.3). To overcome this, two methods could be used.

1. Bridge electrodes above the ultrasound transducer – this method introduces minor shadowing on the ultrasound image and due to the wiring method some noise on the signal of the 4 EIM electrodes. However this method is fast and does not interfere with the EIM reconstruction. See Figure 6.3 (right).
2. Completely remove the electrodes and scan EIM 3 times at 60-degree angle and overlap images – ultrasound imaging will be clear. The EIM plate will have to do 3 scans in order to cover the 'blind spot'. This introduces position errors and will make the EIM scan 3 times longer. Also modifications are required on the EIM reconstruction.

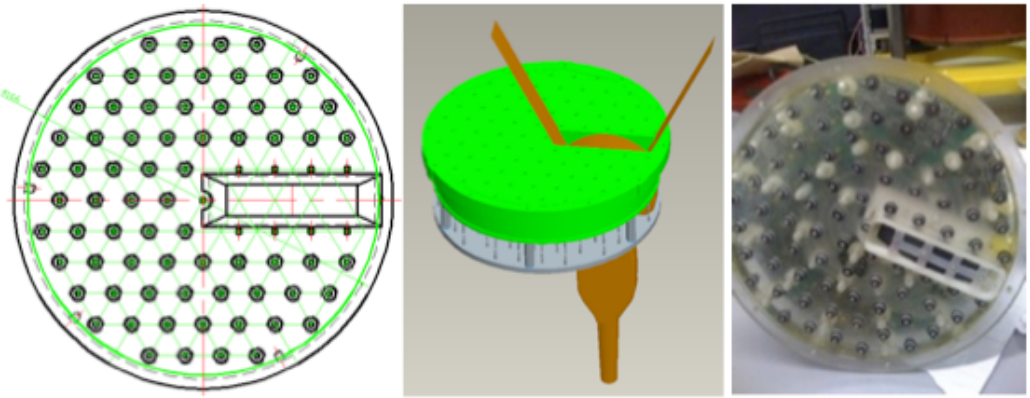

Figure 6.3. Breast plate with apperture ready for the ultrasound transducer (left); CAD of the plate assembly (middle); Assembled plate with electronics, electrodes, ultrasound and electrode bridge above it (right).

In the current setup, by placing the ultrasound transducer on the base plate a new problem arises. The viewing window of the ultrasound cannot 'see' the central zone when it is rotated 360 degrees, creating a blind cone for the ultrasound imaging, as seen

from the CADs images in Figure 6.4. The diameter of the cone's base is around 10mm and the height between 20-40mm depending on the transducer type (i.e. beam angle). This problem can be solved by shifting the ultrasound transducer more towards the center and 'bridging' the central EIM electrode. The EIM central electrode was deemed too valuable to the reconstruction to be removed and the 3 scan superposition could not recover it, so it was left intact.

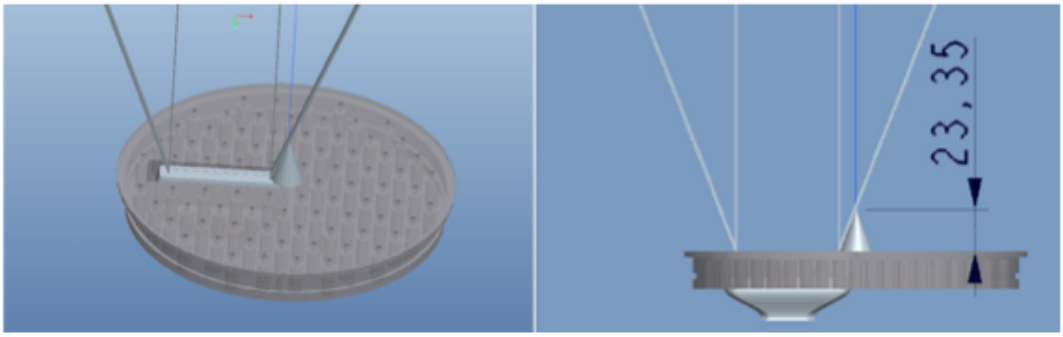

Figure 6.4. CAD of the base plate and the ultrasound beam window, showing the blind area cone in the centre.

6.2.1.3 INTERCHANGEABLE DRUM DESIGN

Full exchangeable single modality scanners that scan an object (breast) held in fixed plate position (blue plate shown in Figure 6.5). The design uses the principle of a revolver and bullet, where the common unit is the chamber and different types of modalities can be inserted one after the other. Figure 6.5 shows an event reel of the process. The EIM and the ultrasound unit would be completely independent from each other, therefore there would be no conflict in each others acquisition or reconstruction. However, there are great mechanical challenges to produce this interchangeable, water holding design.

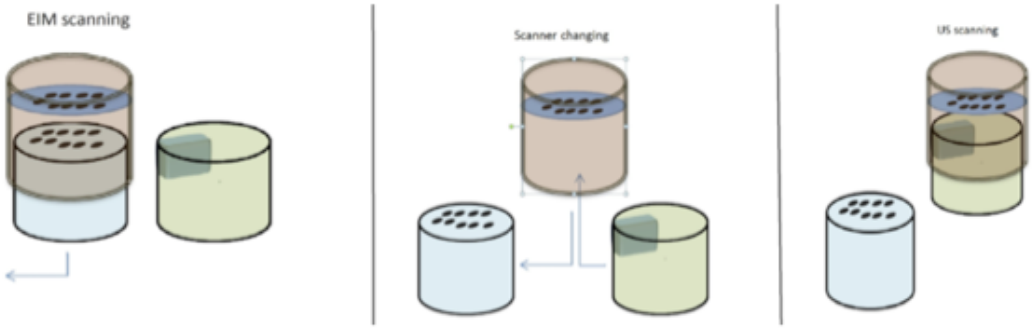

Figure 6.5 Interchangeable drum design.

6.2.2 Winning Design Implementation

Scanner V3b, shown in Figure 6.6 (left) is a full-featured dual modality scanner with horizontal rotation of 360 degrees but only one fixed vertical position. Figure 6.7 shows the components of V3b in CAD and physical form. Because the base plate is now rotating this introduces a hazard for the objects to be scanned therefore a fixed plate (in the XY plane) to hold the objects (breasts) had to be introduced. The material of the plate had to be ultrasound transparent and also needed holes in accordance with the EIM electrode pin coordinates. Figure 6.6 (right) shows V3b scanning an image distortion measurement phantom using a fixed holding plate underneath.

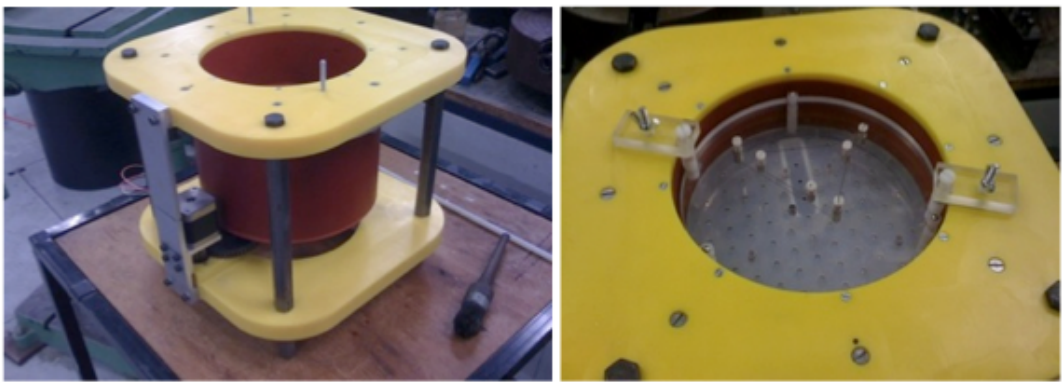

Figure 6.6 Dual modality scanner V3b (left); V3b with an image distortion measurement phantom (right).

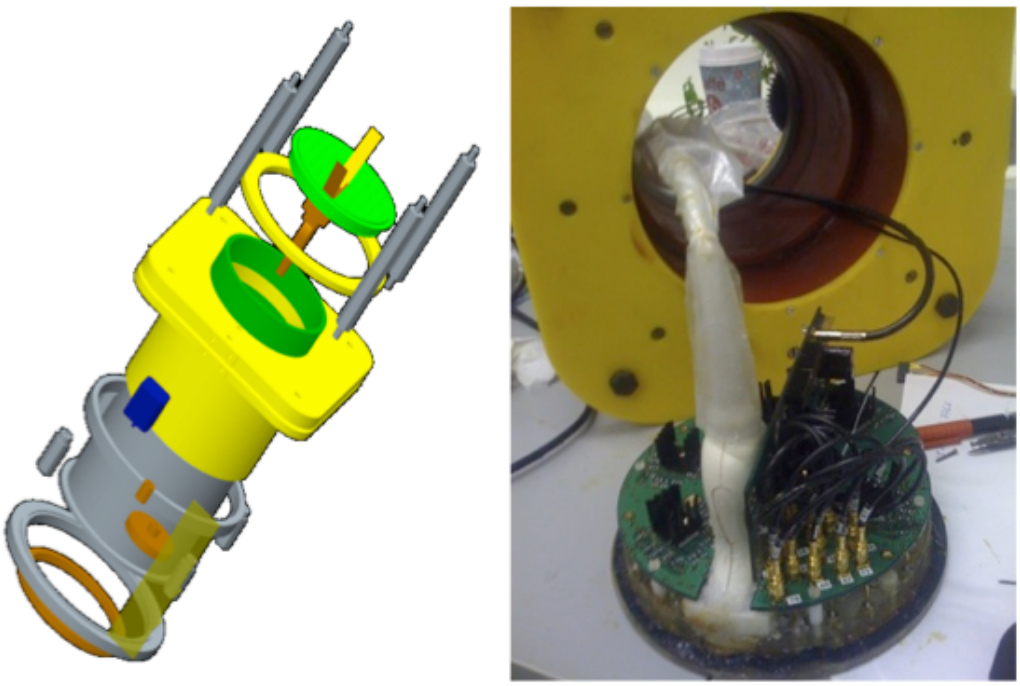

Figure 6.7 Exploded CAD assembly of V3b scanner (left); Disassembled V3b showing electronics and ultrasound (right).

V3c scanner, shown in Figure 6.8, introduced cup size up-down vertical adjustment. The practicalities of a seal that can hold water but at the same time allow vertical and rotational freedom forced some limitations on the design. The scanner could go up and down on all cup sizes but could only do 240 degrees rotation. The up-down and rotation motors and gears were positioned inside the inner cylinder.

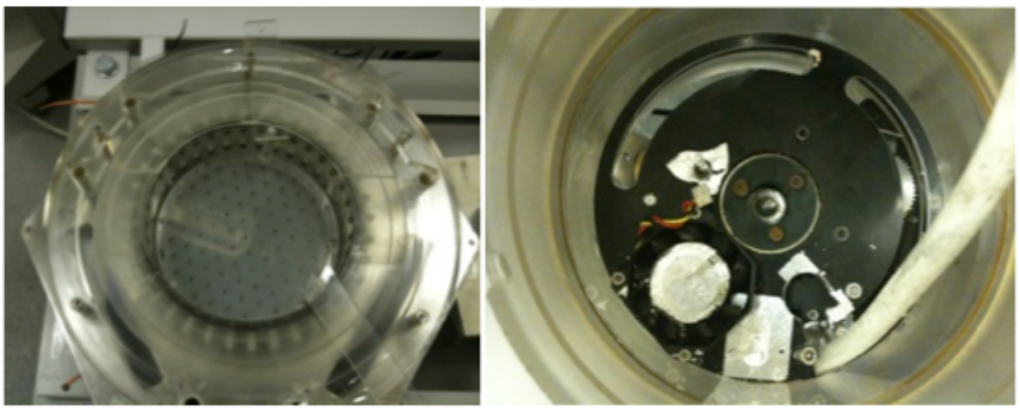

Figure 6.8 V3c scanner ready for testing (left); V3c with the plate removed showing the mechanism (right).

V3d scanner (Figure 6.10) - the final and most successful design; the scanner fulfils the specification. Up-down on all cup sizes and 361-degree rotation. The scanner design is an evolution of the V3b design, where the motors are positions outside of the inner cylinder. This allows the inner cylinder to be free from any clutter for the electronics and the ultrasound transducer cable can move freely and not get tangled.

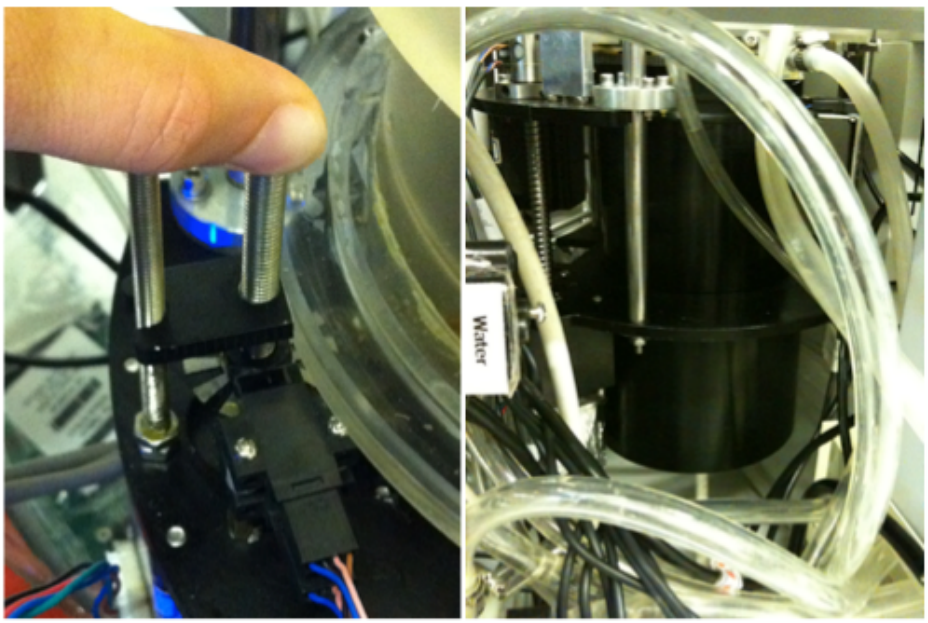

Figure 6.9 V3d scanner photographs showing rotation counting optical sensor (left) and up-down movement shaft (right).

6.2.3 The Breast Plate

With the rotation of the inner scanner plate a safety and also engineering problem has been introduced. If the breast lies on the plate and the plate rotates, at certain situation so will the breast. Therefore distorting the physical shape of the breast and potentially causing discomfort to the patient. The introduction of a breast-plate was deemed necessary. The plate has to follow the inner cylinder in the up-down movement and does not rotate. This is done via guide channels in the outer cylinder. Figure 6.10 shows a prototype breast-plate before guide channels were opened in the inner walls of the outer cylinder. Hence the plate is fixed from above and is used for testing at a single height.

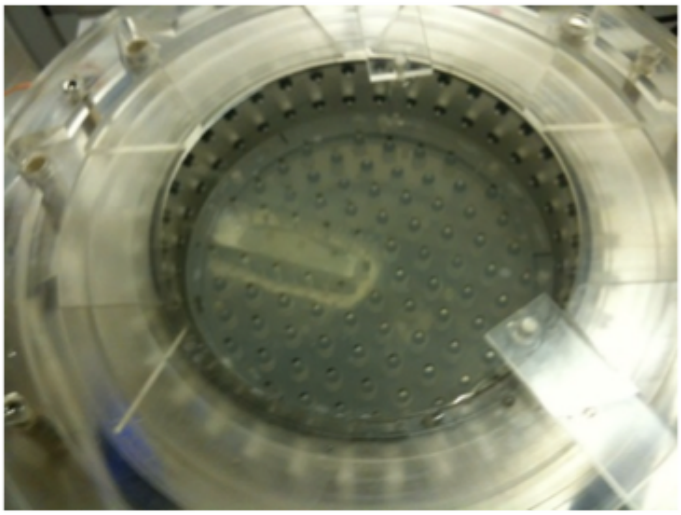

Figure 6.10. Combined scanner filled with water and with LDPE prototype breast plate, held from above.

The properties of the 'breast holding plate' are required to be:

1. Rigid, so that the breast is held firmly during the scan and no motion artefact is transferred from the rotating scanner plate underneath.
2. 'Transparent' or minimally blocking to ultrasound waves.
3. Ideally 'transparent' to electrical fields or at least a machinable material of high impedance where holes can be drilled in order to direct the electrical field from the electrodes to the breast tissue.
4. Due to its prolonged liquid submersion, the material must be water resistant and not change its volumetric properties (e.g. swell or distort)
5. Disinfectable and corrosion resistant for multiple patient scanning or low in cost in order to manufacture single use, disposable plates for each patient scan.

A number of materials that satisfy requirements 1-5 were identified and prepared for testing.

1. LDPE (Low Density Polyethylene)
    a. 1.2 mm thick – in sheet format
    b. bendable but can be kept rigid from a circular drum type design
    c. machine workable and drillable for holes
    d. high electrical impedance

2. Polyimide P1-M (Black) at 4 mm thick
    a. 4 mm thick – in sheet format
    b. rigid and non bendable
    c. fragile and brittle if made any thinner
    d. machine workable but quite brittle for holes
    e. high electrical impedance

3. Polyimide P1-E (Orange)
    a. 7 mm thick – in sheet format
    b. rigid and non bendable
    c. fragile and brittle if made any thinner
    d. machine workable but quite brittle for holes
    e. high electrical impedance

4. Polyimide PK-E (Beige)
    a. 3 mm thick – in sheet format
    b. rigid and non bendable
    c. bends if exposed to heat
    d. fragile and brittle if made any thinner
    e. workable but quite brittle for holes
    f. high electrical impedance

A photograph of the acoustic transparent materials tested is shown in Figure 6.11.

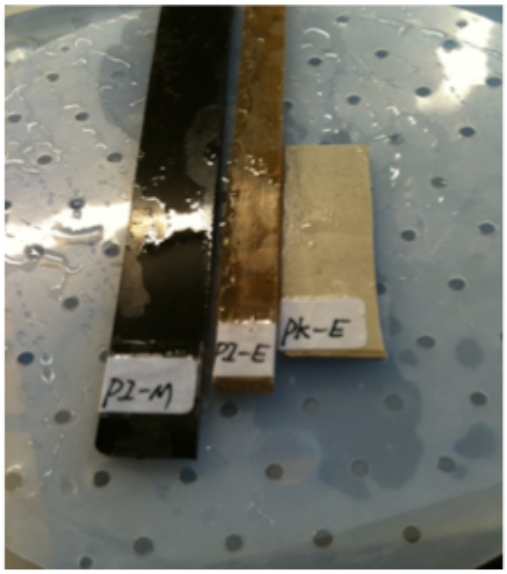

Figure 6.11 Ultrasound transparent materials for acoustic transparecy testing.

Experiment Setup:

- Ultrasound device: Medison SonoAce 9900
- Transducer: Medison C3-7IM Convex Probe (3MHz~7MHz / 78°/ 50mm)
- Combined EIM and Ultrasound planar scanner

The scanner was filled up with water, making sure that there were no debris or air bubbles. The ultrasound device was switched on and connected to the image capture hardware. The first scan was done with no plates in front of the ultrasound transducer. A hand was moved in and out of the transducer field of view and the image frames were recorded for post evaluation. In the following setups the 4 plates were placed above the transducer at a distance of 3 mm. Figure 6.12 shows the frame capture of just water.

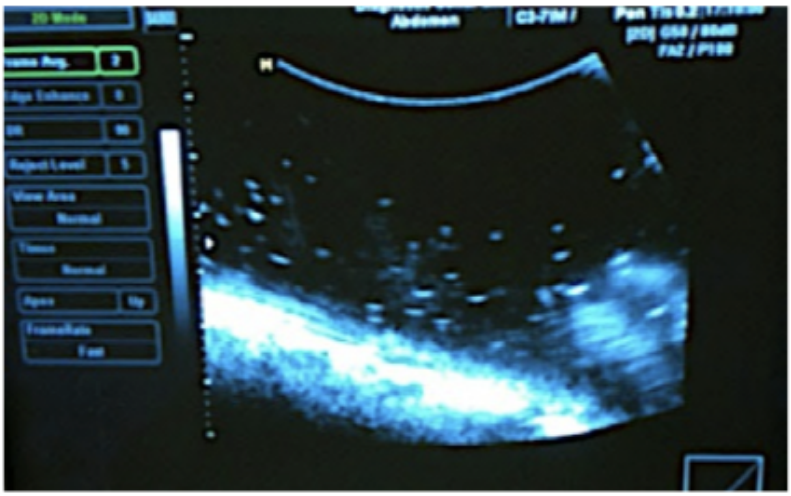

Figure 6.12 Reference image with no plate above the transducer.

The hand is placed about 40 mm above the transducer. The scan is vertically reversed in the image hence the hand is shown below the transducer arch. There is nothing in the water therefore the image background is black with some impurity speckles.

Figure 6.13 (left) is the scan of LDPE (1.2mm thick). The layer of LDPE can be seen in the image and some fingers below it. The material shows good acoustic transparency properties with no reflections (reverberations) in the image. Figure 6.13 (right) is material P1-M (black); rows of reflections can be seen from this material. The material is not fully acoustically occlusive but the image is noisy.

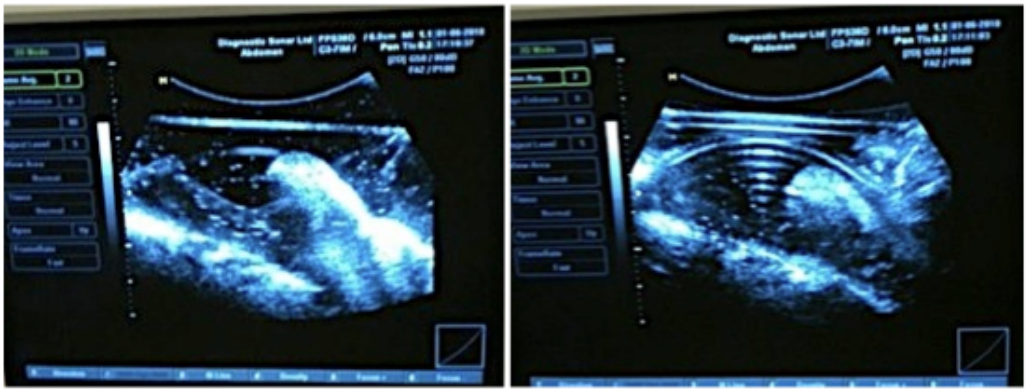

Figure 6.13 Ultasound imaging with support plates above the transducer:
LDPE (Low Density Polyethylene) (left); P1-M (right).

Both P1-E and PK-E introduce reverberations to the ultrasound image, therefore they are not suitable (Figure 6.14). As expected the thinner material, PK-E (beige) has a better overall image, but the other materials seem to have better contrast. So in thinner layers their response might be better, however they are quite brittle to be machined, so unsuitable. So far LDPE remains the best transparent material but it is not rigid. Holding it like a drum skin on a rigid acrylic ring solves the problem. Design sketches of this method are shown in Figure 6.15.

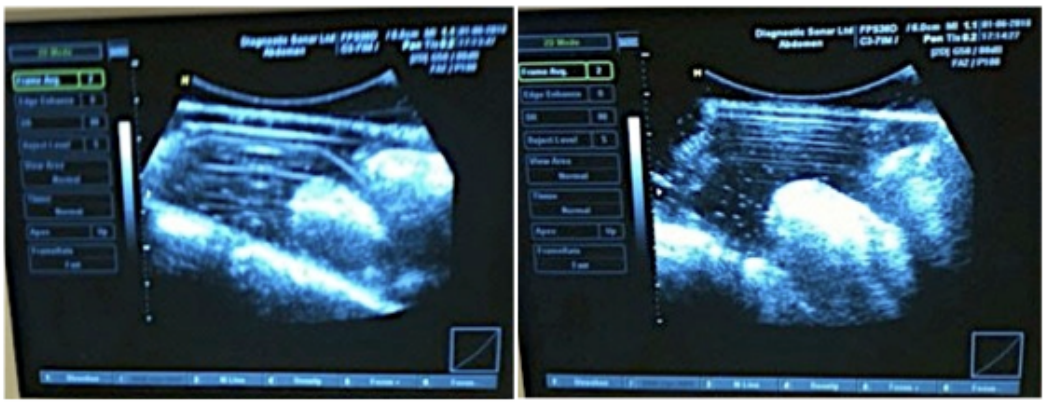

Figure 6.14 Ultasound imaging with support plates above the transducer: P1-E (left); PK-E (right).

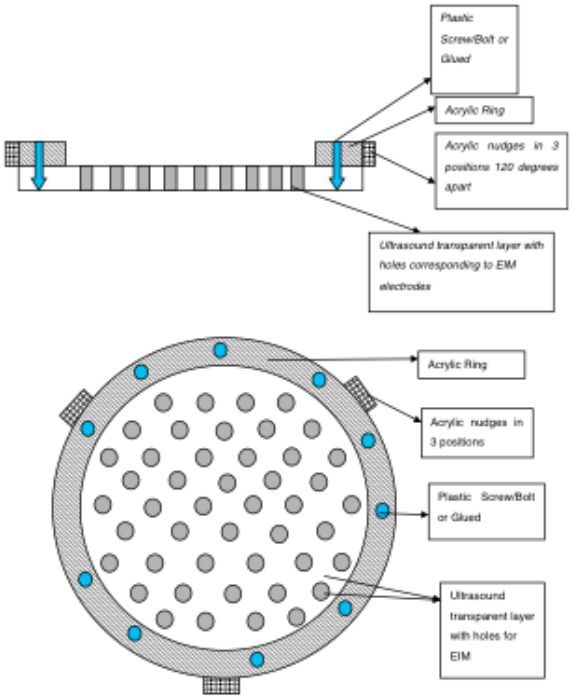

Figure 6.15 The design of the breast plate using LDPE held by acrylic ring.

The introduction of a ring holder in the design opens new possibilities for the use of non-rigid materials that are suitable electrically and acoustically transparent. Saturated cotton or gauze was proven to be acoustically transparent and it turned out to be electrically transparent as well. So it looked like the solution, offering the best signal responses, low cost for single use and hygiene, and can be sold as a consumable. However because pure cotton is stretchable it would sometime stretch and fold when the ultrasound rotation was in motion. The substitute was found to be a 50-50 mix of cotton and polyester, offering full saturation and all the properties of cotton but held in shape and non-stretch due to the polyester. Figure 6.16 (left) shows cotton gauze held by an acrylic ring and the 'stretch marks' are visible. The 50-50 cotton-polyester gauze in Figure 6.16 (right) does not show any signs of stretching and the pattern is intact.

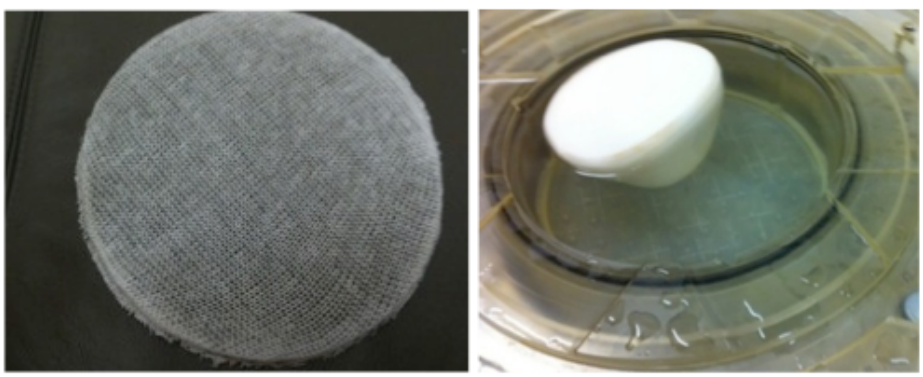

Figure 6.16 Breast plate with ring holding stretched cotton cloth. Note the uneven stretching in the weave pattern (left); Ring holding 50-50 cotton polyester non stretch material during a scan. The weave pattern is intact (right).

6.3 SOFTWARE AND VISUALISATION

In the Chapter 4, it was described that the acquired data is saved on the PC for post processing, visualisation and analysis. Figure 6.17 shows the data flow diagram of how the data is acquired and the steps it goes through until it is displayed in 3D form either in test software or with the option to be converted to DICOM.

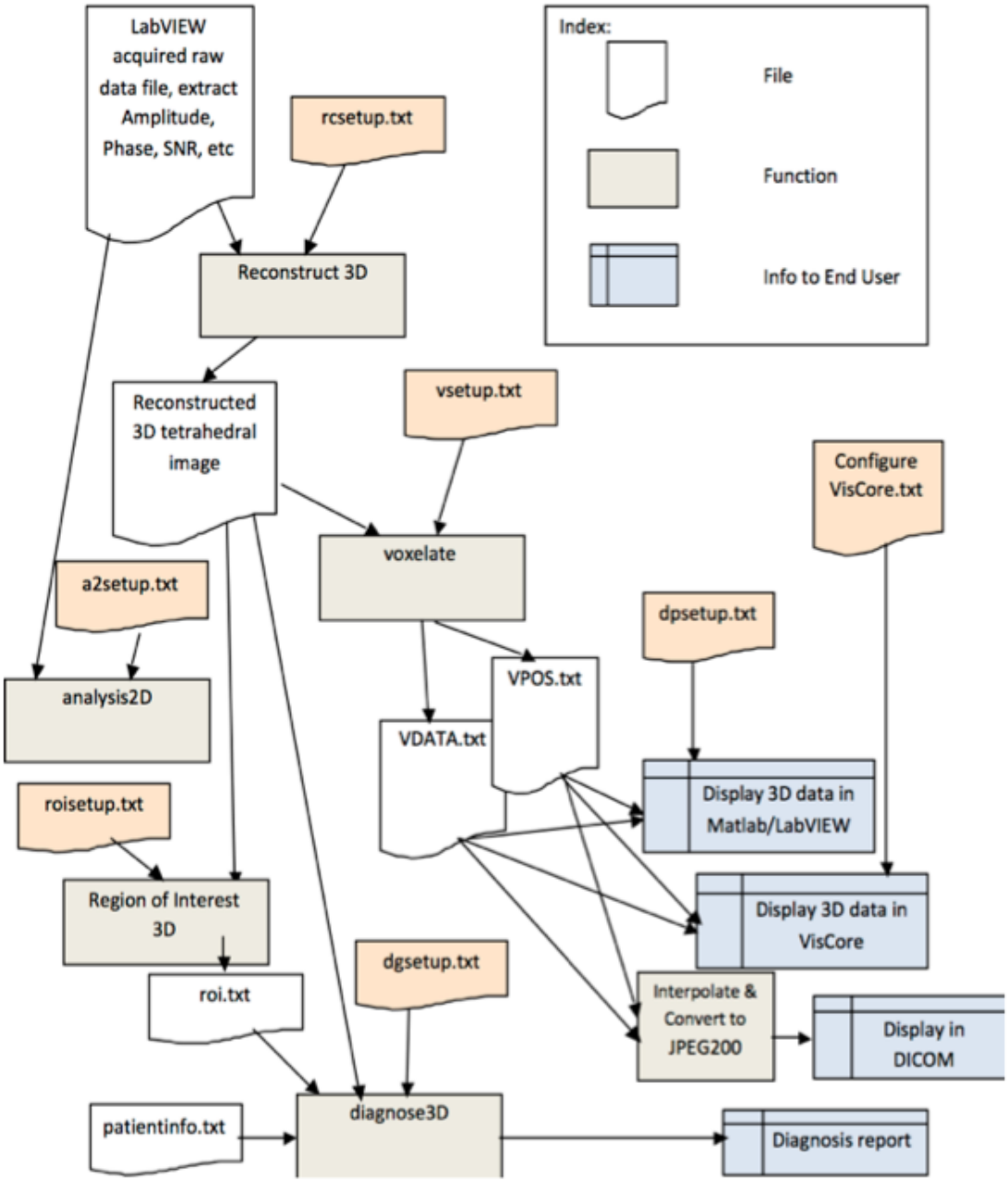

Figure 6.17 Reconstruction-visualisation software data flow diagram.

The EIM data is expressed in voxels and is composed of two files VPOS.txt (voxel position) and VDATA.txt (voxel data value).

VPOS.txt (voxel position) - The file represents a (n x 3) matrix where the columns hold the coordinate values in the X-Y-Z axes.

VDATA.txt (voxel data value) - The file represents a (n x m) matrix, where the value in column n corresponds to the same location in VPOS and is the pixel value for that coordinate set. In the matrix, $m \geq 1$ and represents data values for one or more frequency scans.

The Ultrasound system is based around a B-Mode transducer that transmits sound waves and creates images from reflections of 'body slices' in the XY Cartesian plan with Y=0. The current transducer gives a scanning window of 5.5cm in the X-axis and up to 9cm in the Z-axis. In order to achieve full 3 dimensional coverage the transducer is mechanically rotated. The Z-coordinates are kept constant and correlated to breast cup size while the transducer line of vision creates sweeps with one set of (x_0,y_0) coordinates fixed to the x=y=0 and (x_1,y_1) are relative to the angle of rotation.

The ultrasound machine outputs the data in composite analogue video feed. The image is grabbed, digitised and stored in 640x480 pixels frames. The angle range and speed is selectable but 360 frames, one at each rotational angle was deemed suitable. This creates a cylinder of pixels where the radius=640 and the height is 480.

Co-location - EIM uses voxelation in its final 3D display form; therefore the coordinate tags of each voxel are available. Ultrasound images have pixel tagging in their 2D frames. EIM produces low resolution imaging therefore a low number of voxel mappings. Ultrasound resolution is higher, though scalable at the 2D frame level for a balance between resolution and real time image processing and ROI filtering. Due to the resolution incompatibility between the modalities a calibration method ensures co-location. The calibrations are based on the known parameters: Cup size; Scanner cylinder diameter; Ultrasound field of vision diameter; 0 angular coordinates = 12 o'clock in EIM; EIM electrode distance. Some co-located dual modality images will be demonstrated in the next section.

6.4 Dual Modality Imaging

6.4.1 Plastic Phantom on EIT Missing 4 Electrodes

The introduction of the ultrasound transducer to the EIM plate meant that 4 EIM electrodes are missing, blanking about 1/12 of the image. Therefore 3 scans needed to be merged to recover the missing area. The plastic phantom in Figure 6.18 (left) was positioned at about 7 o'clock and was scanned 3 times. The scans were done at: 'home' position 0^0 (Figure 6.18); position 120^0 (Figure 6.19) and position 240^0 (Figure 6.20).

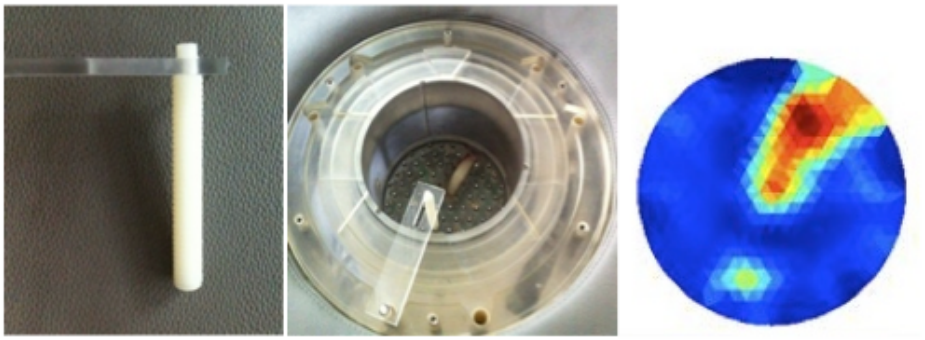

Figure 6.18 The rod plastic phatom (left); The EIM+US scanner in the 'home' position with the phantom at 7 o'clock (middle); The 2D EIM reconstruction, showing the rod at 7 o'clock and the missing electrodes at 1 o'clock (right).

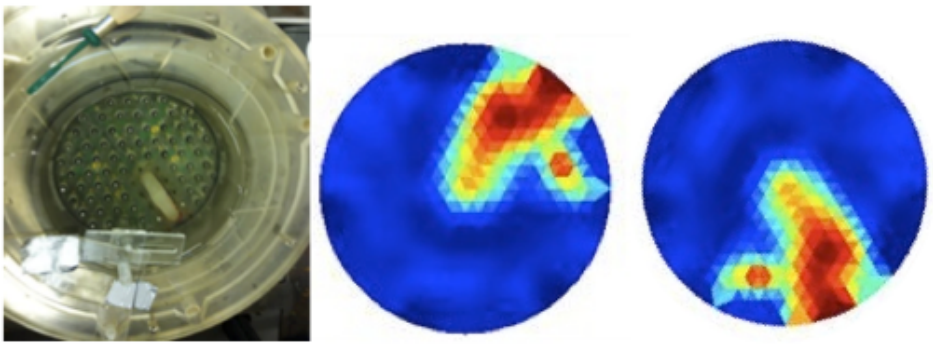

Figure 6.19 The EIM+US scanner in the '120 degree' position with the phantom at 7 o'clock (left); The 2D EIM reconstruction as the algorithm sees it (middle); The adjusted reconstruction, with rod at 7 o'clock (right).

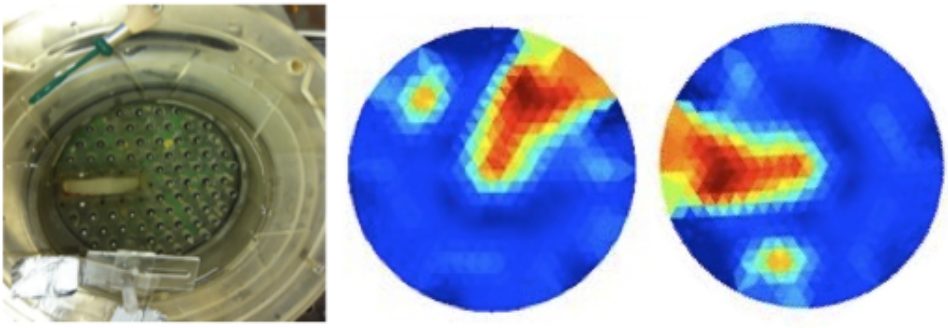

Figure 6.20 The EIM+US scanner in the '240 degree' position with the phantom at 7 o'clock (left); The 2D EIM reconstruction as the algorithm sees it (middle); The adjusted reconstruction, with rod at 7 o'clock (right).

The data of the 3 scans was merged to create a final data set equivalent to a single scan and suitable for 2D/3D reconstruction. The merger indicated the correct size and position of the phantom and eliminated the 'dead' zone of the ultrasound transducer. The results are shown in Figure 6.21.

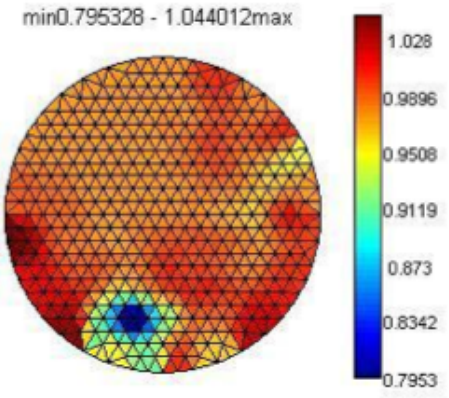

Figure 6.21 EIM data merger of the 3 scans, completely recovering the missing electrode area.

Without removing the rod phantom, a 360-degree ultrasound scan was performed. The data was reconstructed in 3D and is displayed in Figure 6.22 (left). The EIM data was also reconstructed in 3D and both data was merged as shown in Figure 6.22 (right).

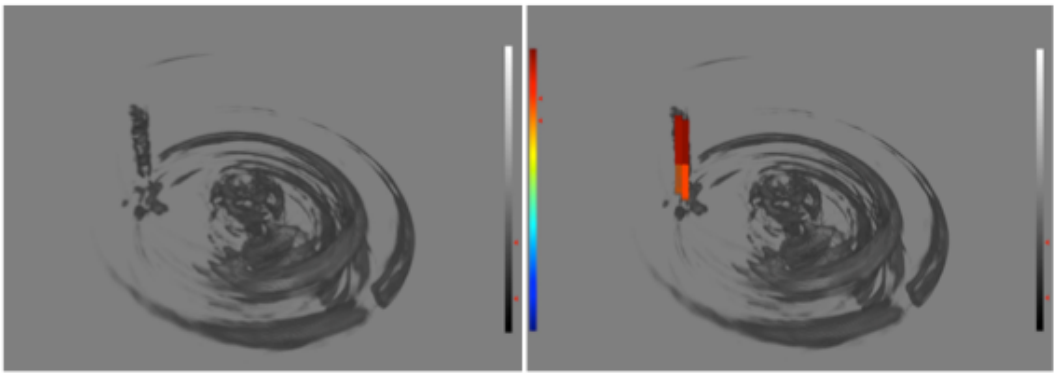

Figure 6.22. 3D reconstructions of the rod phantom; Ultrasound only (left); Merged ultrasound and EIT (right)
(Note: the image has been rotated to enhance viewing angle, hence not appearing at 7 o'clock).

Another solution to overcome the missing electrodes is by placing a 'bridge' above the ultrasound transducer as shown in Figure 6.23. This solution only requires a single EIM scan and uses the predefined reconstruction algorithm. However manufacturing the 'bridge' proved challenging, there is a higher noise level on those 4 channels than the average, and the 'bridge' is not mechanically steady. The shadowing on the ultrasound imaging is negligible. All in all, 'the bridge' looks like the best solution as the channels noise and structure rigidity issues can be resolved in manufacturing.

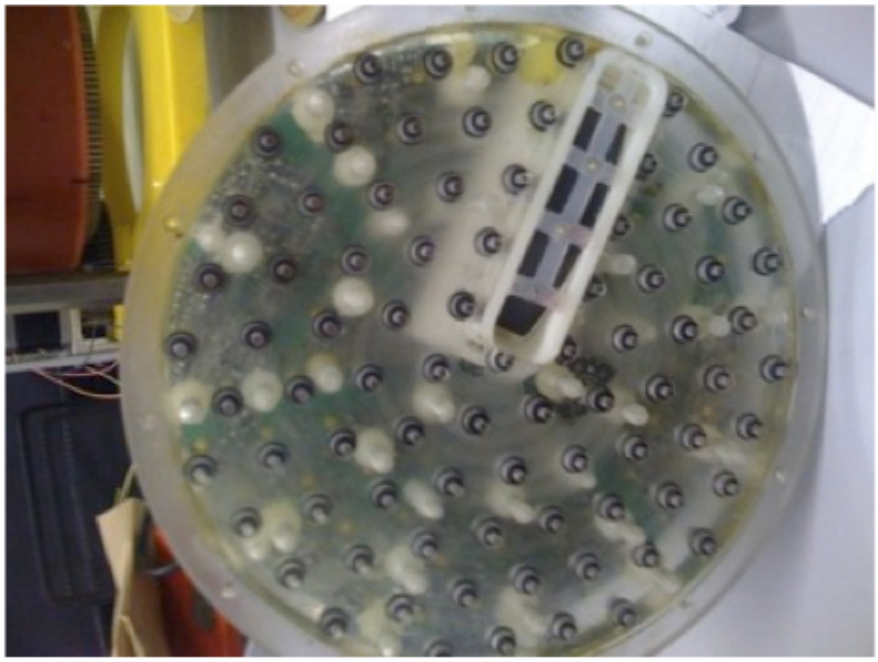

Figure 6.23 Bridge electrodes on the EIM plate above the ultrasound transducer.

6.4.2 Metal & Plastic Phantom

More phantoms were scanned in dual modality, shown in Figure 6.24 (left) and the results are shown in Figure 6.24 (right). The rod at 9 o'clock is metal, and the one at 6 o'clock is plastic. The purpose was to test the ability of conductivity (material) distinction in EIM and the boundary information in ultrasound. The EIM image shows the metal in blue and the plastic in red. Noticeable are also the small plastic rods doted around.

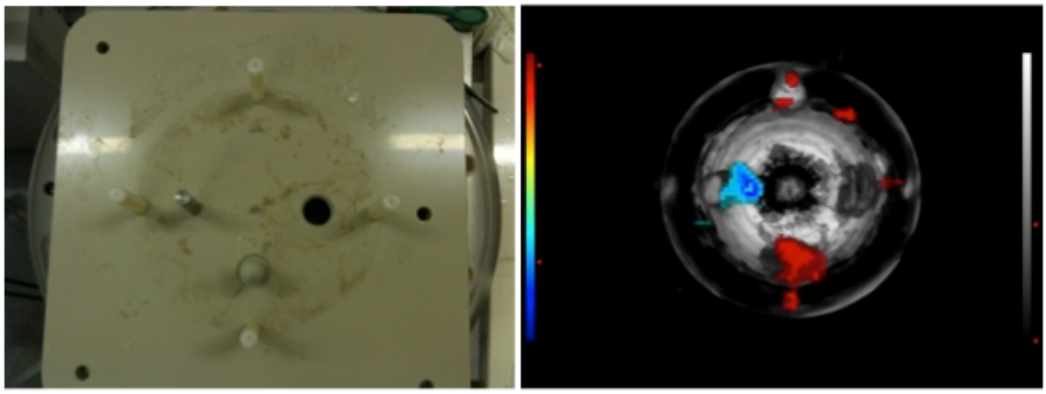

Figure 6.24 Dual modality phantom with a metal rod (Ø=5mm, length 50mm) at 9 o'clock and a plastic rod (Ø=10mm, length 50mm) at 6 o'clock (left); Merged dual modality imaging of the phantom, ultrasound in grayscale and Impedance mapping in colour (right). Note the impedance distinction on metal and platic in the blue, red colours.

6.4.3 In Vivo Scans

The previous tests were done with the combined dual modality scanner; one scan after the other. During this time the EIM electronic plate of the original Sussex Mk4 system was improved with a multi-layer PCB, separating the digital and the analogue power lines. This simple solution improved the raw data SNR from 35dB up to 45dB. In addition the acquisition sample rate was increased from 20-30 samples per cycle (depending on frequency) to 60 samples per cycle. This also increased the SNR of the returned sine wave from 45dB up to 60dB (depending on frequency). In essence this method can also be applied to the combined scanner and increase the SNR from 35dB to 50-55dB. To add to the improvements, the reconstruction algorithm and imaging were equipped with interpolation features for better visualisation. All of the improvements mentioned were tested *in vivo* with the scan of a hand in the Mk4 system (Figure 6.25). Using reference points, the hand was then also scanned with the modified scanner but only in ultrasound mode. The two scans were then registered using the above reference points. The method and the results of these scans are shown further down in this section. Since the EIM electronic plate of the combined scanner is in essence the same PCB used in Mk4 (the 4 pins for the bridge electrodes are tracked around the ultrasound gap and can be wired when needed), all of the improvements in hardware and software of Mk4 can be transferred to the combined scanner. The tests prove the feasibility of the device and its ability to distinguish human tissue and bones in both EIM and ultrasound.

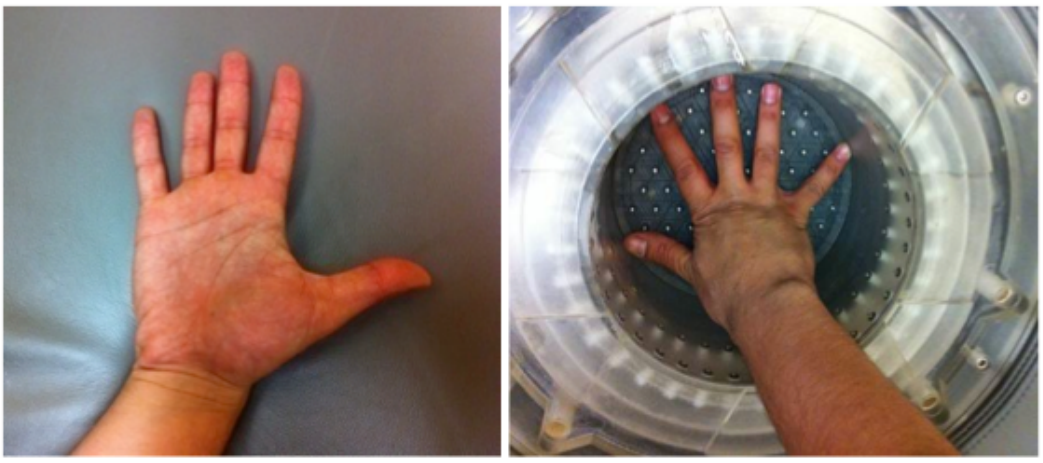

Figure 6.25 Photograph of the hand and position method that was scanned in EIT Mk4 and then ultrasound modalities.

The EIM reconstruction provides functional images based upon a tetrahedral finite element mesh, which is fundamentally based upon the location of the electrodes within

the planar array. The 2D and 3D meshes of the EIM reconstruction are shown in Figure 6.26. In addition to the geometrically corrected image provided by the EIM, the data is also associated with 'meta-information' that assists with the co-registration of the ultrasound data. This is due to the fixed geometry of the plate and scanner reference points which in turn translates to fixed known voxel coordinates in (x,y,z) .

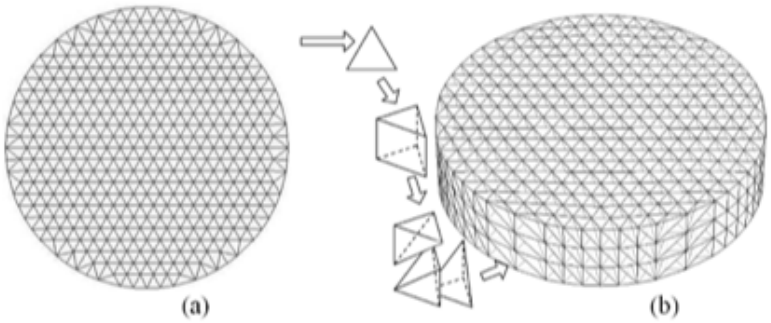

Figure 6.26 2D mesh with triangular elements (a); Multiple layers of tetrahedral elements as a 3D mesh (b).

Figure 6.27 shows the reconstruction of a hand scanned with the current Mk4 EIM system and reconstructed in both two and three dimensions using the mesh given in Figure 6.26. To enhance visualisation, the images can be filtered, thresholded and rotated using the mouse. The hand was scanned in the Mk4 systems and not on the modified dual modality scanner due to the new and improved SNR, therefore the EIM image quality is higher and of course there are no issues with the missing 4 electrodes.

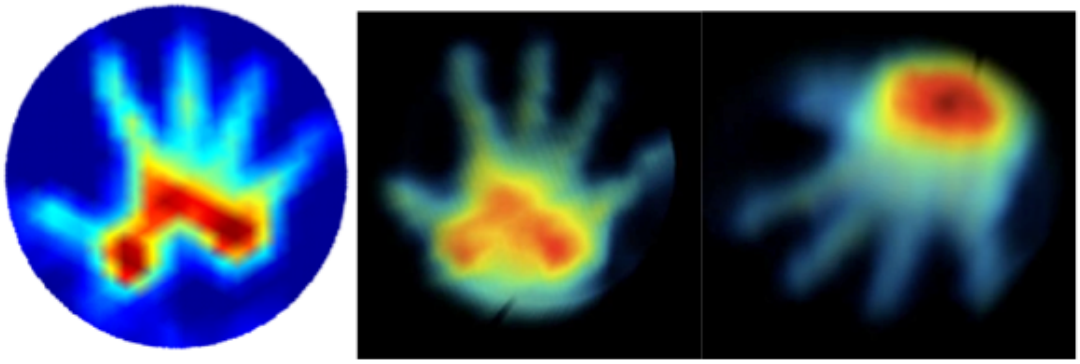

Figure 6.27 EIT 2D reconstruction of a hand scan (left); 3D reconstructions showing palm (middle) and back/wrist (right).

In addition the hand was scanned in ultrasound mode in the dual modality scanner, making sure that the position and reference points were kept for co-location. Two dimensional slices are captured as images (Figure 6.28) via the video-out port available on standard medical ultrasound system in CCIR TV format (25Hz frame rate). The angle subtended by the ultrasound 'beam' is specific to the transducer used. Three

dimensionality is achieved by mechanically rotating the transducer about the central axis of the imaged cylindrical volume with individual images captured at a number of distinct angles (Figure 6.29). The image data is supported by a range of meta-information, which include: radial slice angle; penetration range; number of pixels; number of frames etc.

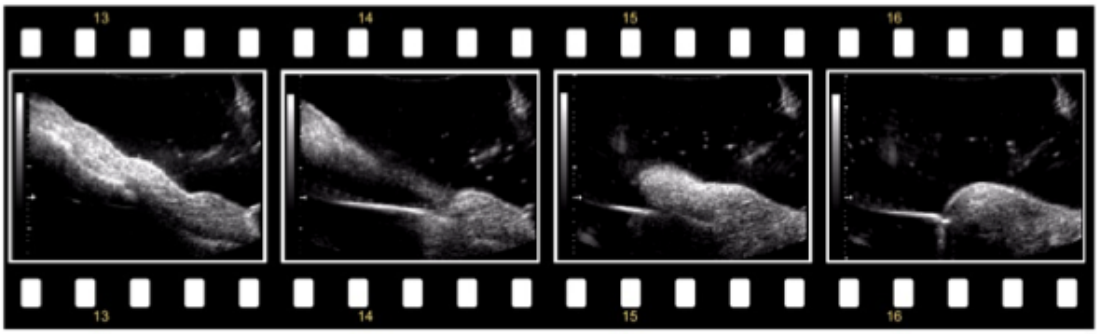

Figure 6.28 Ultrasound consecutive frames saved in AVI format, depectited in film frame arrangement.

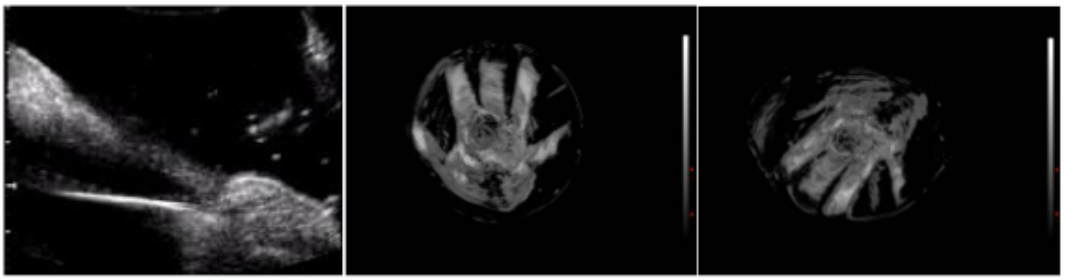

Figure 6.29 Ultrasound vertical radial slice (left); Ultrasound 3D reconstructions of the hand scan with palm view (middle) and back/wrist view (right).

Note - the reconstruction is a vertical mirror of the original object; hence the thumb is showing on the left side in the reconstructions. Figure 6.30 shows the EIM and Ultrasound 3D merged data rotated in two viewing positions; frontal showing the palm and posterior showing the back of the hand and wrist. The data merger is quite faithful on both modalities, and in the 3D EIM Mk4 image, the high impedance of the bone in the wrist and palm is quite distinguishable.

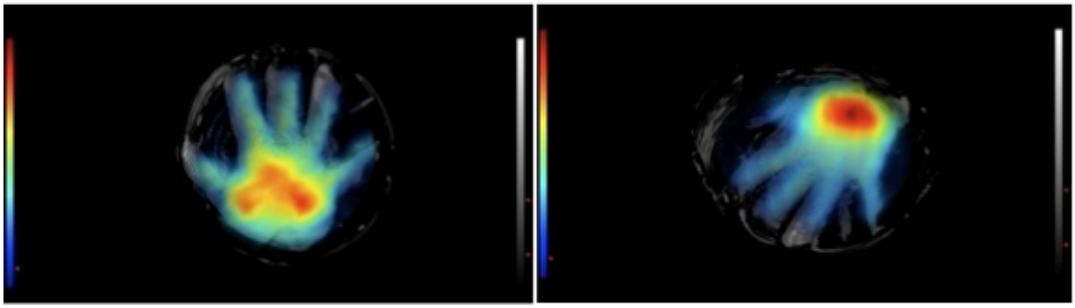

Figure 6.30 Image merger of 3D ultrasound and EIM scans; palm view (left); back/wrist view (right).

6.5 DICOM

DICOM (Digital Imaging and Communications in Medicine) is the standard for handling, storing, printing, and transmitting information in medical imaging. Therefore it was deemed important to port the EIM and Ultrasound images to this format and test them with one of most complete DICOM Viewers – OsiriX. A commercial version of the software has recently received FDA approval, proving the power of this software and the verifiable proof of concept for this research. DICOM data object contains the image data (that can be in multiple frames) and also file tags or attributes such as: ID, name, conditions, date etc. The image data is stored in compressed data format according to the JPEG or JPEG2000 standard (Kak & Slaney, 2001).

The EIM Mk4 data is saved in voxel (volumetric pixel) form. This form is analogous to bitmap pixel arrangement therefore the information of position and pixel value is available. Custom software was writen to convert the voxel-position into a 3D numerical matrix and the voxel data to 8-bit grayscale value. The position data was arranged using matching metrics with the ultrasound array so that superpositioning is available. The software then converts the ultrasound and EIM Mk4 data in the DICOM compatible visualisation format of JPEG2000. The files were opened and tested in the DICOM package OsiriX as shown in Figure 6.31, where on the left is shown the merged EIM and Ultrasound data and on the right is shown the EIM Mk4 data on its own.

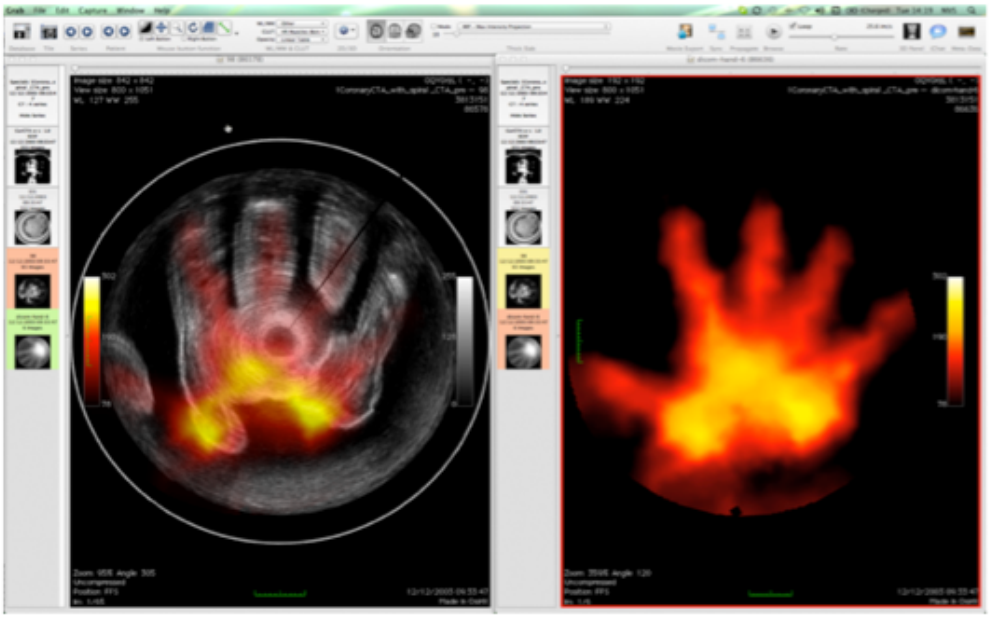

Figure 6.31 DIACOM image merger, visualisation and threasholding of ultrasound and EIM scans (left); EIM only data (right).

The original EIM and ultrasound data have been shown in Figure 6.32 to demonstrate the faithfulness of the DICOM converted images in Figure 6.31.

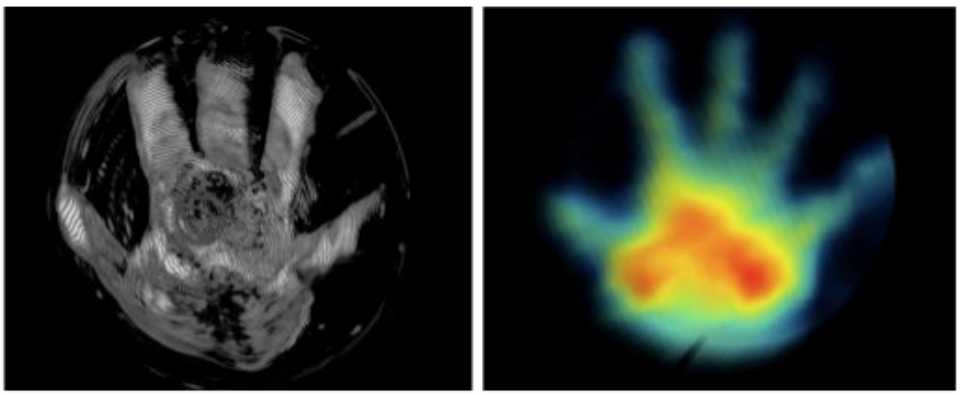

Figure 6.32 3D reconstructions using the old test software; Ultrasound (left) and EIM (right).

Figure 6.33 shows the EIM Mk4 data in DICOM in a rotated 3D view. The rotation, segmentation and thresholding features are fully compatible.

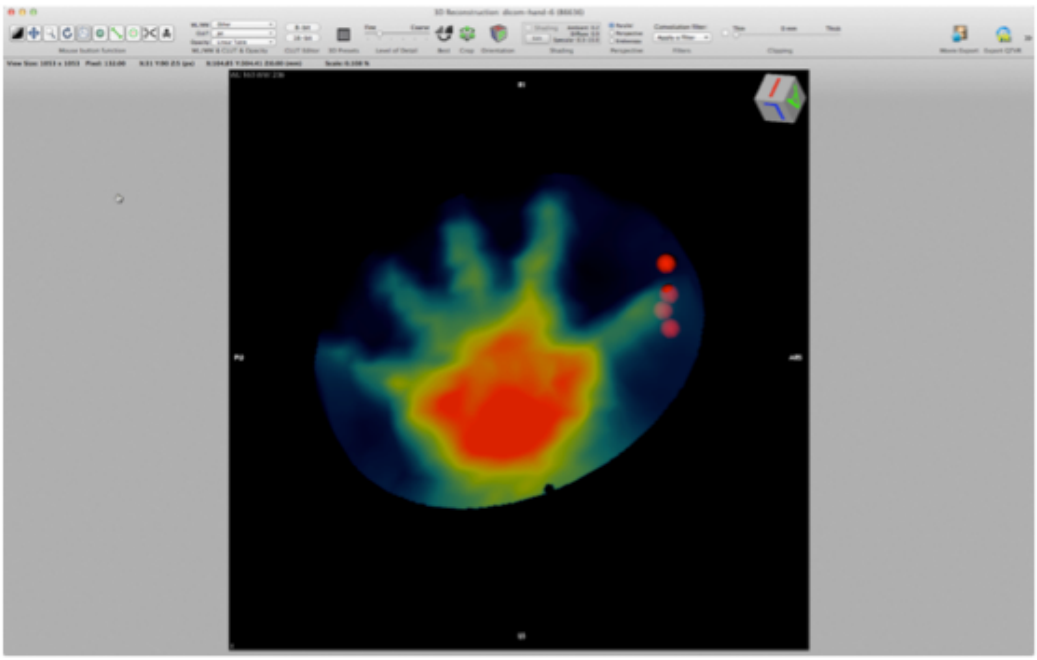

Figure 6.33. 3D reconstruction in DICOM of the EIM Mk4 hand scan data.

More conversion and imaging tests were performed in DICOM. Figure 6.34 shows the reconstructed 3D breast phantom scanned in ultrasound.

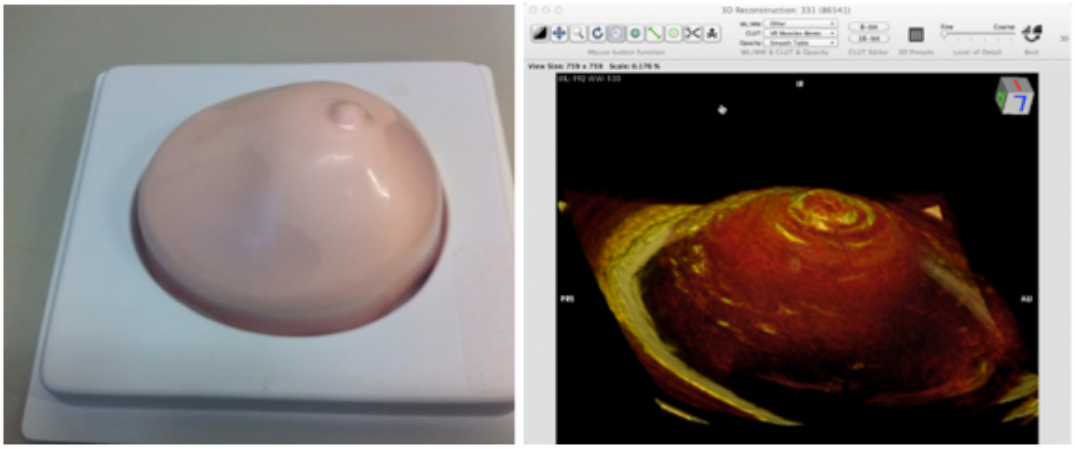

Figure 6.34. Ultrasound breast phantom (left); Reconstruction in DIACOM of the ultrasound scan of the phantom (right).

The screenshots in Figure 6.35 show the breast phantom in 3 different viewing planes and the green line cursor as the locator and coordinate extractor. The 3-frame representation provides valuable visual information that cannot be seen in normal 2D. Note: in the centre of frame 2, there is another small lesion that cannot be seen in any other plane (very visible when the image is displayed larger).

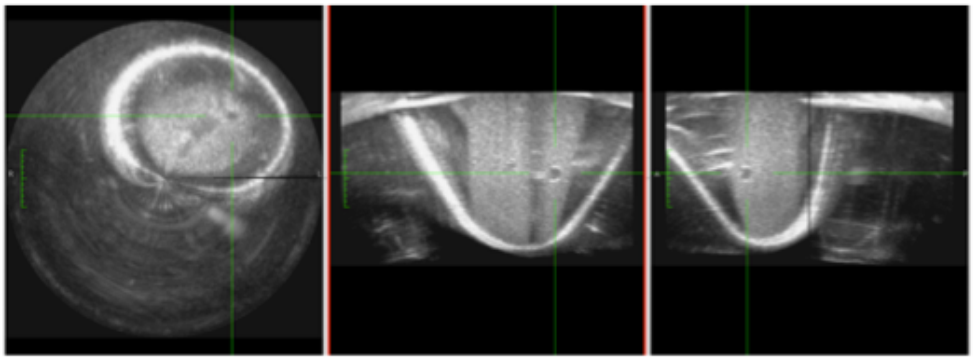

Figure 6.35 Three plane arrangement of the 3D ultrasound matrix data represented in DICOM.

The images can be rendered with different colour maps to enhance any further differences. Colour mapping features are shown in Figure 6.34 (right) and Figure 6.36.

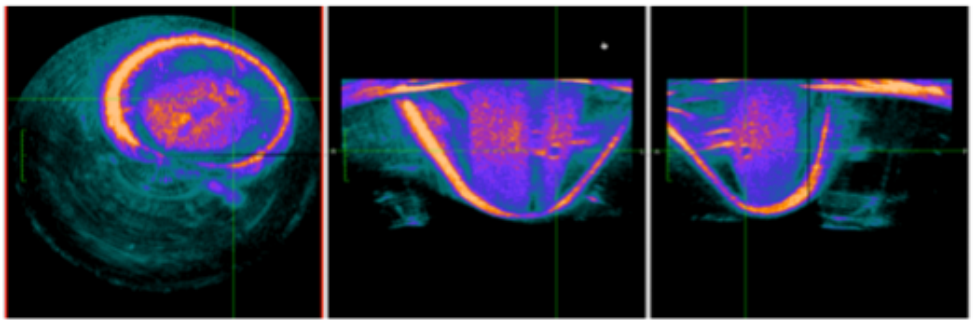

Figure 6.36 Colour mapping feature of three plane arrangement of the 3D ultrasound matrix data represented in DICOM.

6.6 CONCLUSION

This chapter is the pinnacle of the research where both modalities are merged together. The chapter starts with the modification of the PXI based architecture and how the ultrasound and motion (rotation) control modules were integrated in the all-in-one system. It then continues comparing the two scan modalities of ultrasound (sidewall or on the base) and how they integrate and interfere with the current EIM electrode plate and breast position. The scan on base, again is the best choice but introduces a gap of 4 electrodes in the EIM plate. This is overcome by either multiple EIM scans and data fusion or by adding a 'bridge' of electrodes above the ultrasound transducer. For research purposes an interchangeable scanner plate design was introduces even though its manufacturing would be very challenging.

The research uncovered a potential safety risk when the plate rotates and scans the breast. This would twist the breast. Therefore a breast-plate was introduced between the breast and the scanner base. The plate is designed with extrusions that allow it to move up and down in channels of the inner walls (cup size adaptation), but prevent it from rotating with the scanner. Materials and designs of the breast-plate were tested and the results compared in this chapter. The best plate is made from an acrylic ring, holding taught a cotton-polyester cloth. This provides full liquid saturation (i.e. EIT penetration and dead channel elimination) and also high acoustic transparency, while at the same time holding its shape and protecting the breast.

Results of scans and reconstructions in dual modality were presented in this chapter, with the latest evolution of DICOM image porting and visualisation. Presenting the images in DICOM format makes them more acceptable to the medical environment and the clinicians. On its own the spatial resolution of EIT is not to the same standard as other medical imaging modalities (e.g. MRI, X-Ray). Ultrasound on the other hand has very good spatial resolution but lacks the ability to differentiate between tissue types. When combined, these two modalities complement each other by providing the boundary information of ultrasound to the impedance information of EIT. This was successfully proven by the dual modality images of phantoms and even more so by the results of in vivo scans of a human hand, where tissue and bone are visualised with a lot of detail. The next step from this research is to take the device to full clinical trials.

CHAPTER 7

- DISCUSSION CONCLUSIONS AND FUTURE WORK

7.1 DISCUSSION

The aim of this thesis is to present investigations and research accomplished on novel and non-invasive methods for early stage breast cancer detection, based on Electrical Impedance Mammography and Ultrasound. The findings and the innovations derived here will be expedited to fully completed prototype machines for *in-vivo* hospital clinical trials, so that one day in the very near future this technology can be fully deployed in hospitals and save lives.

The thesis expanded on the breast cancer issue and how it is causing almost half a million deaths a year. The current most common imaging and diagnostic modalities were introduced and were statistically compared for their performance. The analysis and the data point out that imaging methods are aiding in saving lives but there is still a lot of room for advancement, be that in the evolution of current imaging methods or the introduction of new ones. From the analysis it is derived that, not considering the side effects and the poor performance of mammography in dense breast, looking at the statistical data, using dual modality in general and adding ultrasound specifically, increased the sensitivity of detecting breast cancer. In general, MRI offers higher specificity but lower sensitivity. Mammography is the opposite with lower specificity but higher sensitivity. Ultrasound on its own seems to be in the middle range for both, but that is not a good thing. MRI is very expensive, while mammography is cheaper but cannot image dense breast. The bottom line is that there is no one-for-all solution, therefore new modalities can overcome the missing gap and dual-modality will complement any diagnostic results.

The data from the investigation of the anatomy of the human breast, the locations and prevalence of cancers, and the ergonomics of breast size and comfort were used to draw up the specifications for a cup size adaptable (cup size A-G) scanning tank, filled with warm water that can scan a patient in the prone position, one breast at a time.

A risk assessment of the system was provided according to medical instrumentation standards. This is in preparation for the next stage when this project is assessed by the

MHRA and progresses to clinical trials in a hospital and further along CE marking. The risk analysis has identified all potentially known risks in the manufacture, use and disposal of the system for the purpose of clinical trial evaluation in identifying breast cancer in a non-invasive manner. In addition Chlorhexidine 0.5% was found to be a suitable clinical cleaning agent for the device. On the basis that the actions stated to mitigate the identified risks are followed, it is concluded that the device is safe to use and that the potential benefits of using the device outweigh any residual risks.

The thesis continued with Electrical Impedance Tomography, its theory and its major applications. It explained how this could be used for detecting breast cancer and the work done so far. The innovative step is the new concept in system architecture for the Mk4 system - the use of an instrumentation industry based PXI platform. This added flexibility and faster prototyping in comparison to standard DSP custom based systems. The system achieved the required specifications. The use of a PXI-based set-up proved successful in building a working system in record time. The module swapping capability proved vital also in the calibration process. Due to the modular nature of the PXI system future improvements will not require major modifications. Based upon this experience it is concluded that a PXI system would be very beneficial to the further study of EIT.

A number of investigations on the performance and problem solving methods for the Mk4 system were also presented; The addition of ringed-gauze or grooved plate to ensure the presence of liquid coupling between electrode-tissue and removal of dead and saturated channels; Fast sweep electrode combination pattern acquisition to ensure that no air bubbles or debris are present on the electrodes. The next stage of this method is the ability to dynamically map the breast position on the plate before a full scan takes place. This dynamic scan method can help in patient positioning and reduce nipple folds that could inherently compromise the acquired raw data and the reconstruction that follows; Mk4 DAS performance tests with saline and phantom load, and comparison of image quality between raw and calibrated data.

Ultrasound was presented as a medical imaging modality. The theory and the properties of ultrasound were explained in preparation for selecting the best setup for breast scanning. The trade off is between resolution and penetration. The higher the ultrasonic frequency, the higher the resolution and the lower the penetration range. The research also focused on, current prototypes or ready to enter the market, new 3D ultrasound scanners for breast cancer detection. All of the above information was then transferred to achieve the best 3D scanner for this research but always bearing in mind the specifications and limitations set by the EIM system.

The designs were based on a cylindrical water tank with a diameter of 180cm. The breast is to be submerged in the tank and a 360-degree scan of the breast will be done by mechanically rotating the ultrasound transducer. There were two major designs; the transducer scanning from the sidewall of the tank; or scanning underneath the tank's base. The best method chosen via experiments, image quality and ease of manufacturing, was scanning from the base. Performance tests of the scanner proved very satisfactory, be that in small feature detection and on penetration testing. The results were certified by industry standard ultrasound phantoms.

The thesis presented the modification of the PXI based architecture and how the ultrasound and motion (rotation) control modules were integrated in the all-in-one system. It then continued comparing the two scan modalities of ultrasound (sidewall or on the base) and how they integrate and interfere with the current EIM electrode plate and breast position. The scan on base, again is the best choice but introduces a gap of 4 electrodes in the EIM plate. This is overcome by either multiple EIM scans and data fusion or by adding a 'bridge' of electrodes above the ultrasound transducer. For research purposes an interchangeable scanner plate design was introduces even though its manufacturing would be very challenging.

The research uncovered a potential safety risk when the plate rotates and scans the breast. This would twist the breast. Therefore a breast-plate was introduced between the breast and the scanner base. The plate is designed with extrusions that allow it to move up and down in channels of the inner walls (cup size adaptation), but prevent it from rotating with the scanner. Materials and designs of the breast-plate were tested and the

results were compared. The best plate is made from an acrylic ring, holding taught a cloth made of cotton-polyester. This provides full liquid saturation (i.e. EIT penetration and dead channel elimination) and also high acoustic transparency, while at the same time holding its shape and protecting the breast.

Results of scans and reconstructions in dual modality were also presented, with the latest evolution of DICOM image porting and visualisation. Presenting the images in DICOM format makes them more acceptable to the medical environment and the clinicians. On its own the spatial resolution of EIT is not to the same standard as other medical imaging modalities (e.g. MRI, x-ray). Ultrasound on the other hand has very good spatial resolution but lacks the ability to differentiate between tissue types. When combined, these two modalities complement each other by providing the boundary information of ultrasound to the impedance information of EIT. This was successfully proven by the dual modality images of phantoms and even more so by the results of *in vivo* scans of a human hand, where tissue and bone are visualised with a lot of detail.

7.2 PROJECT CONCLUSIONS

Combined Electrical Impedance Mammography and Ultrasonic imaging for breast cancer, is the combination of a three-dimensional, automated, ultrasound CT scanner with Electrical Impedance detection capabilities. The resulting product offers a non-invasive scanner with repetitive imaging and diagnostic results by combining the high-resolution images of ultrasound with the tissue type identification information of EIM. The research successfully proved the dual modality scanning capability of such system and the feasibility of such technology for *in vivo* scans; therefore opening the path for full clinical trials for breast scans. For it to succeed this research does conclusively provide: technology and designs platforms, human factors and scanning protocol, risk analysis and platform independent medical imaging.

EIM and Ultrasound use non-ionising radiation, thereby eliminating any potential risk of iatrogenic neoplastic change associated with imaging techniques based on x-rays. Breast positioning during scanning is more on the supportive side rather than full squashing and deformation like in mammography, which is uncomfortable for some

women. The diagnostic acuity of the system is unaffected by young, dense breasts, and so could be used for any age group. Owing to the specific impedance profiles detectable in different tissues, and the use of algorithmic analysis and parametric modelling, it is possible to 'type' tissues into cancerous and non-cancerous, and even by sub-type, in a way not possible with previous imaging modalities. This capability may, in time, allow actual 'virtual histopathology'.

Cost – EIM+Ultrasound will be significantly cheaper than mammography and MRI to manufacture and deploy, the complexity lying largely in the analysis algorithms and software. The tissue signature algorithms give an 'intelligent' yes-no output (indicating need for further investigation), EIM and Ultrasound images have the capability of extracting regions of interest, therefore staffing costs of new screening programmes would be greatly reduced.

The impact would be revolutionary on the diagnosis of breast cancer. It would offer a device that is; non-invasive; identify cancer at an earlier stage; no radiation (as in x-ray); fast (scan time 1-15 minutes); fast results (1-30 minutes); low cost (10-20 times cheaper compared to MRI and other modalities); small form factor (all integrated in a patient trolley bed); high specificity and sensitivity; reduction of subjectivity in diagnosis; reduction in biopsy requirements.

The road to commercialisation of medical devices is a long and arduous one. The next stage is the preparation of the device for *in vivo* clinical trials and the process of transferring from a prototype to a CE and FDA approved device. This will open the door to more developments in other devices based in Electrical Impedance, Ultrasound or combined. As with most medical technologies the potential impact is huge. The technology, if successful, will be able to detect and identify lesions of the breast with a sensitivity and specificity not currently available with conventional x-ray screening technologies. Furthermore the nature of the technology; non-invasive, non-ionising radiation, lends itself to the detection of abnormalities in any human or animal soft tissue where an identifiable "signature" can be found.

The ability of the technology to be used repeatedly with minimal risk opens the opportunity for use as a monitoring tool. An example of this may be in the long-term monitoring of the effects of drug treatments on lesions. In such an application data could be regularly and repeatedly collected for later analysis of, for example, lesion size changes over the drug treatment period. This non-limiting example shows the potential this innovation has to aid researchers in the medical trials field.

7.2.1 EIM+Ultrasound *vs* EIM Only

EIM promises to be a very valuable diagnostic tool for cancer detection. However its resolution is well below other commercial modalities. A current EIM setup promises resolution of 7-17mm in the 2-Dimentional X-Y plane and even worse at 15-25mm in the Z-axis. Ultrasound can offer resolutions of 1mm, however cannot distinguish the type of tissue. Therefore data merger would inform the high-resolution ultrasound image about the tissue type using the EIM data. Ultrasound is a proven technology with a wide customer base. It would be more commercially viable for EIM to be an extra on Ultrasound rather than open a new medical device niche. Ultrasound will not just stop there; it can aid the EIM reconstruction itself by providing external and internal custom mesh information.

NB: The lesson should be learned from the introduction and progression of Elastography, a non-invasive diagnostic method that identifies boundaries and tissue stiffness, tumours being 5-30 times stiffer than normal tissue. The manufacturers tried to break the market with it as a standalone device but found more success when sold it as a feature in Ultrasound systems.

7.2.2 What Has the Project Achieved to Date?

Patented technology – two patents cover methods and apparatus. DICOM – EIM and Ultrasound images have been ported to DICOM and visualized with OsiriX. Merged images – geometry correction, image realignment and dual modality scans have been achieved. Image analysis for: measurement, segmentation, noise reduction, edging etc. 3D pixel matrices of both modalities with an integrated coordinate system. Real stereoscopic (without glasses) 3D visualisation (subject to third party software). Successful

prototype dual modality scanners have been manufactured and tested. This is a very strong base for a clinical trials machine. Taking the project one step further.

7.2.3 What Is Missing?

A steadier 'bridge' on the electrode plate above the ultrasound transducer for the four missing electrodes. Better ultrasound transducer – with higher frequency and bigger active window. Pre-manufactured breast holding plates, so they maybe single use and standardardised tension. The plate has to appear transparent to both the electrical field of the EIM and acoustic field of the ultrasound. Integrate a DC (laptop) based ultrasound system, so that patient scans are all done in battery mode. Motion controller – Port the motor controller software as part of the clinical software for speed and system checks. De-gassed water – investigate methods to reduce ultrasound noise from air bubbles or debris. Fully integrated software, ready for clinical trials and MHRA scrutiny. Partial 60601 testing of the device for the trials.

7.2.4 Why – What is the Market Worth?

The information above demonstrates very clearly that there is a need for a device like this. The benefits are; Diagnostic and medical for the millions of women that cannot be x-rayed; Scientific as the scanning method is non-invasive; Commercial, value to clinic and hospitals, because of its fractional cost; Economical, when fully developed and commercialised due to the high value market of Medical Imaging - Global diagnostic imaging market was $20.7 billion in 2010. Global Ultrasound Market $5 billion. Breast ultrasound is expected to grow due to factors like: drop in price, better systems and a surge in patient numbers due to an aging population.

7.3 Project Derivatives & Future Research

A number of offshoot developments will be discussed in this section. These project derivatives are methods and designs that require more in-depth work but look promising from the initial analysis.

Derivative one is a method to remove the nipple artefact in EIM scans. This is a big issue for other EIT systems as well, as the nipple can saturate the acquisitions and mask the cancers up in the breast.

Derivative two are some proposed designs to achieve real 3D EIM, with the help of Linear Variable Differential Transformers (LVDT) at the electrode pin bases, to measure the displacement from the breast shape, or the use of ultrasound for external and internal shape and mesh reconstruction.

Derivative three is based on the breast-plate design and the translation of the inner cylinder to acquire EIM data in more than one planar position, effectively increasing the information quantity and the resolution of EIM.

Derivative four describes the extraction of lesion coordinates from EIT and Ultrasound. Based on these coordinates, a High Frequency Focused Ultrasound (HIFU) can be used to automatically ablate that lesion, on the same scanner.

Derivative five, describes the designs of an intra-cavity dual modality EIT+Ultrasound scanner for cancer detection in body orifices.

7.3.1 Layer Zero – Skin (Nipple) Reference Calibration

Saline reference extraction according to the Newton-Raphson algorithm is a method that is commonly used to remove known interferences in the calibration of the 2D and 3D images. In the image in Figure 7.1 (left), the phantom is at 7 o'clock, a big artifact is known to be at 1 o'clock, therefore by subtracting the 'saline reference', shown in Figure 7.1 (middle), the phantom is identified more easily as shown in Figure 7.1 (right).

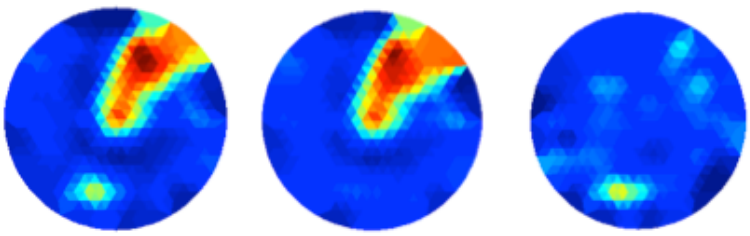

Figure 7.1. Reconstruction of an EIM scan performed on the dual modality plate (missing 4 diagonal electrodes at 1 o'clock); With a phatom at 7 o'clock (left); Saline only/reference (middle); Scan minus reference (right).

Using this principle it could be possible to reduce or even eliminate the effect of skin and nipple from EIM images. If the injection values (current/voltage) are reduced then the penetration power is also reduced, therefore reducing the penetration distortion caused to the very first layer.

Calling it Layer-zero, the idea is to have injection values that only affect height in millimeters from the plate, therefore only the skin on the EIM plate would be visualized, and more importantly the nipple position. Layer-0 should map the skin and the nipple coordinates. Then a standard acquisition can be done with normal injection values, without the patient moving. This acquisition will show the nipple and possibly an object further up in the layers. By referencing it to Layer-0 the other objects could be identified more confidently. Figure 7.2 shows an image from simulated data. Starting from the bottom:

- Layer 0 - very low injection currents: showing the nipple.
- Ventral Layer = Layer 1 - normal injection: showing nipple and distortion in the center.
- Dorsal Layer = Layer 2 - normal injection: showing nipple and the fainted distortion in the center.

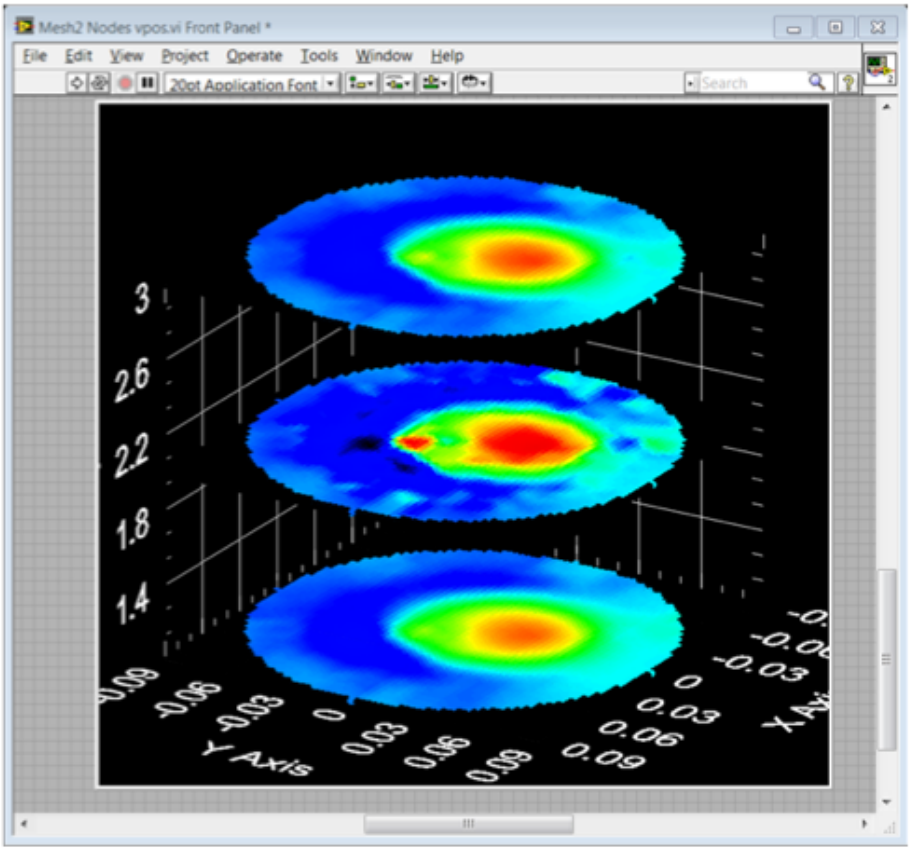

Figure 7.2. Simulated data for Layer-zero visualisation at the bottom; showing the lession feature in the middle layer and still vissible on the top layer. Note the nipple on all three layers. No image subtraction has been done to the other layers.

7.3.2 ADAPTIVE 3D EIM WITH *A PRIORI* INFORMATION

The EIM Mk3-Mk4 scanner plate squashes the breast lightly, shaping it into a cylinder. After the scan, the current EIM reconstruction relies on a fixed mesh geometry, shown in Figure 7.3 (left). Whilst this could speed up and simplify the reconstruction it could also introduce errors and distortion in the position of the cancer. Custom mesh geometry could help reduce this. In the past mesh creation was time consuming and required processing power, but today this can be achieved quite easily (Adler & Lionheart, 2011).

'Distmesh' is a Matlab-based source code released under GNU GPL (General Public Licence) that permits fast custom, tetrahedral, mesh generations and support for implicit functions and geometries (Persson & Strang, 2004). Samples shown in Figure 7.3 (right).

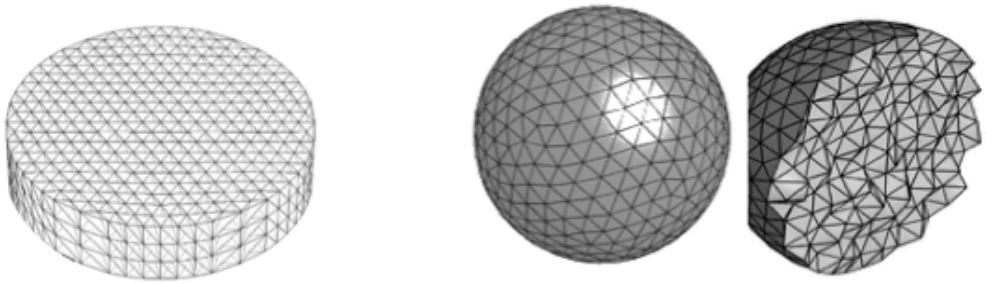

Figure 7.3. Fixed 3D mesh as currenty used in EIM reconstruction (left). Two images of custom half spherical mesh reconstructions in Distmesh (right).

The images in Figure 7.4 show ideal representations of the breast in free form (hemispherical) and squashed in EIM (cylindrical) whilst keeping the same volume.

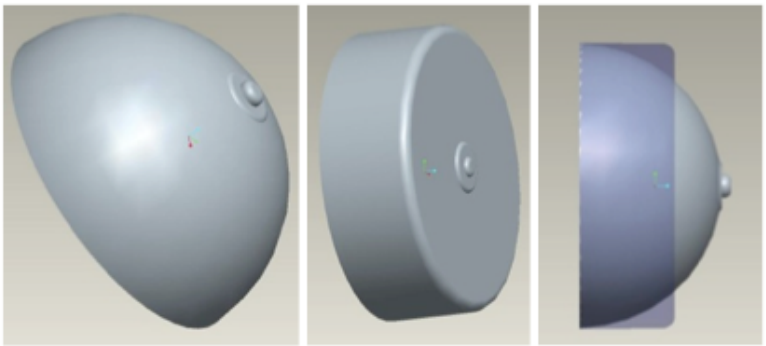

Figure 7.4 CAD representation of an ideal hemispherical breast lighly squished to a cylinder retaining the same volume.

When the breast is compressed at the scanner plate, this will cause a change in localized tissue density. A change in density will translate into a change of conductivity for a given area. Also a change in 'shape' due to the compression will be seen differently. The same shape positioned at different angles to the electrical field lines will cause different disturbance, as seen in Figure 7.5.

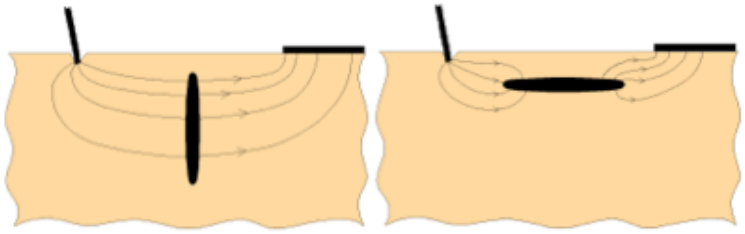

Figure 7.5 Variation of electrical field disturbance from the same object placed at different angles (Martinsen 2011).

To overcome these issues, a possible solution would be the ability to scan the breast in EIM without distorting the breast and using shape information and custom meshing for the EIT algorithm. Figure 7.6 shows an EIM spring electrode plate design, where the spring's sensors provide the displacement and volume information and the electrodes, the EIM data. The pins are based on LVDT (Linear Variable Differential Transformers) to measure the displacement and with a core EIT wire inside a non-conductive outer body, similar to a spark plug design (Figure 7.7).

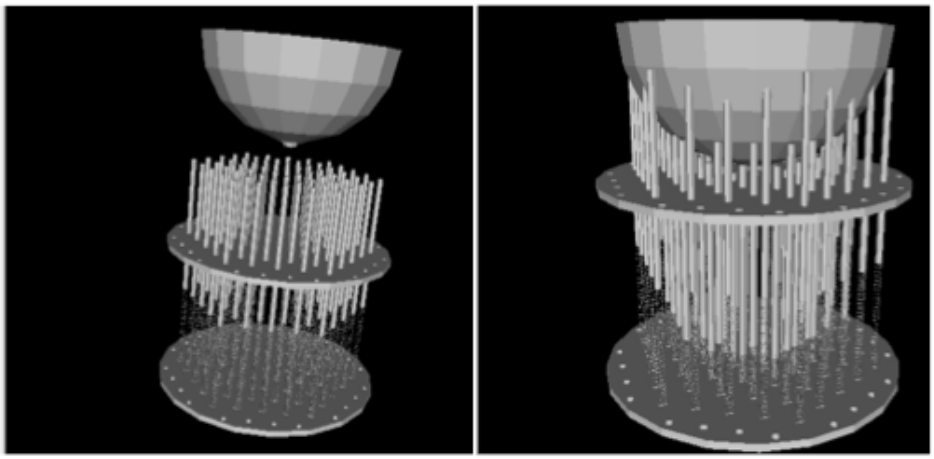

Figure 7.6 CAD prototype of the LVDT electrodes that retaining the outer shape information.

Figure 7.7. The design of the LVDT electrode pin (left); Pin art demonstrating the pin displacement concept and the comparison of resolution of the actual 17mm apart EIM pins (right).

Figure 7.8 shows a comparison of a 'standard' flat distorted EIM reconstruction on the left and in the middle/right the 'correct' (simulated) reconstruction based on the external mesh shape from the spring displacement. Notice the actual shape and location of the lesion (in red).

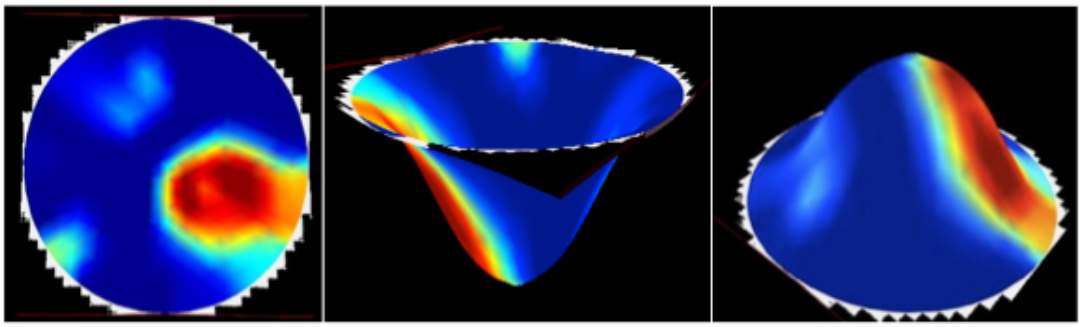

Figure 7.8 Flat distorted EIM reconstruction (left); 3D reconstruction based on the external mesh shape from the spring displacement (middle and right).

Ultrasound imaging can offer the same mesh extracting information for the EIM reconstruction as shown in Figure 7.9 (middle). This was proved by (Soleimani 2006) on ultrasound shape information for a phantom. The outer boundary information can be evaluated using other methods, e.g. optical breast measurement for custom EIM mesh (Forsyth et al, 2011). Autodesk-Photofly software package offers a mesh extraction option from multiple 2D images as shown in Figure 7.9 (right).

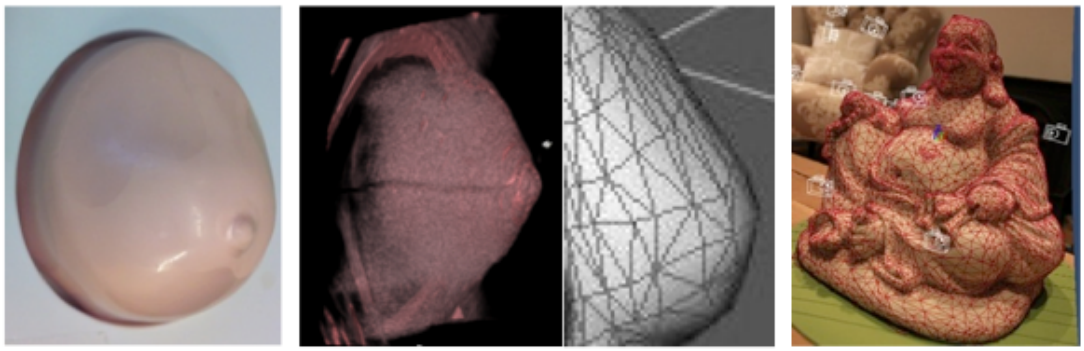

Figure 7.9. Breast shaped phantom (left); 3D ultrasound scan and proposed mesh extraction (middle); Image sample with external mesh created with Autodesk (right).

Mesh information could also be applied to internal structures from the ultrasound data. Figure 7.10 shows images of a breast phantom on the left, its reconstruction in the middle and filtering revealing internal features on the right. The features can provide coordinates and sizes for small internal meshes for the EIM reconstruction.

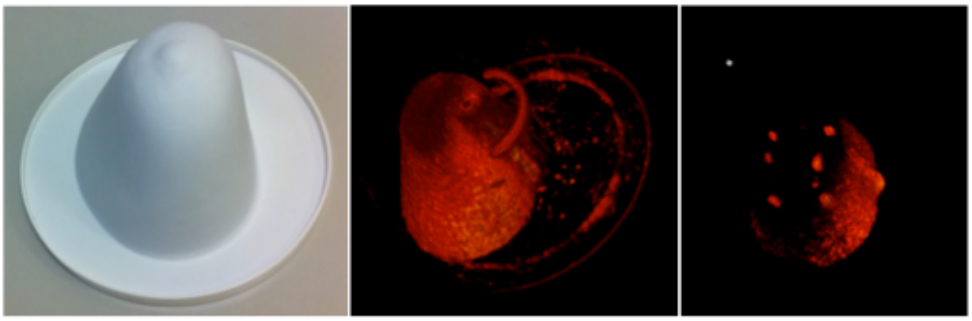

Figure 7.10. Breast phantom with embedded features (left); Ultrasound scan reconstruction of the phantom (middle); External layer removed revealing the embedded features inside the phantom (right).

7.3.3 MK4 PLANAR RESOLUTION INCREASE

In Chapter 6, the electrode superposition method was introduced as a way to compensate for the missing 4 electrodes. The following method takes this a step further and tries to use the current electrodes to increase the EIM resolution by scanning at known consecutive superimposing positions while the breast is held in a fixed position.

The electrodes are positioned in a triangular arrangement from each other and selected in hexagonal patterns selection when scanning, therefore as described in Chapter 4, superposition symmetry happens only at 60-degree rotation.

By holding an object steady, e.g. on the breast plate of the combined scanner, and modifying the inner cylinder to do translations in the X and Y axes, if a scan was to be done twice, once in the normal setup and then in the proposed method, there would be two frames of data slightly offset from each other.

Using the information above and the superposition algorithm previously demonstrated in Chapter 6, Figure 6.21, the number of electrodes just doubled.

In another translation setup, each reconstruction triangular voxel can now be split in 3 sub-voxels, effectively tripling the resolution.

7.3.4 Assisting HIFU Surgery with EIT

The natural evolution of identifying suspicious breast lesions with EIT, could be an all-in-one system that can 'Identify–Diagnose–Treat' carcinomas in humans and more specifically for breast cancer. Once the coordinates of the lesion have been identified and confirmed as tumoral, the 'treating' side of the system can use the coordinates to deliver a targeted treatment using the ablation power of HIFU (High Intensity Focused Ultrasound). Following is a preliminary study of Lobstein-Adams & Beqo in 2011.

The benefits that a system such as this could provide include the possibility of detection, diagnosis and treatment of breast cancer all within a single device. Furthermore the timescales involved will allow the process to be considered as an out-patient procedure such that a patient can be diagnosed and treated all within the same day using the same device, and in fact without the patient having to physically move. Additionally this has the potential to be performed without the use of anaesthetic, thus reducing the costs involved without compromising the patients' comfort.

The use of diagnostic ultrasound as a medical imaging device has been well established, and is a common procedure used in hospitals worldwide. High Intensity Focused Ultrasound (HIFU) utilises a similar technology to diagnostic ultrasound, but with significantly higher power. In addition, the ultrasonic waves are focused in a small volume (in the order of millimetres). This allows the non-destructive propagation of acoustic waves through the tissue overlying the targeted volume. However, at the focal point (i.e. the cancerous region) these waves constructively superimpose, resulting in a very high local acoustic intensity, sufficient to ablate tissue by coagulative necrosis at the cellular level.

The HIFU procedure operates using the fact that when an acoustic wave travels through tissue a portion of the energy of the wave is absorbed and converted to heat. Using focused beams this effect can be exploited deep within tissues, using a very small focus point to localize heating such that surrounding tissues are unaffected (Wu et al, 2006). This occurs due to the energy in the individual waves being of small enough magnitude to not adversely affect the overlying tissue. When focused correctly, however, the areas of high pressure are superimposed at the focal point, thus the acoustic intensity and subsequent energy deposition is much higher in the focal region than in the

surrounding tissue. The focus is adequately defined such that a target tissue volume (such as a cancerous tumour) can be rapidly heated and subsequently necrosed (Haemmerich et al 2009) (given 1-2s at a temperature of 56°C or an equivalent dose (Haar, 2001)) without any permanent damage to the surrounding cells. By focusing consecutively at more than one location, or indeed scanning the beam, a whole portion of tissue can be ablated.

This technology is not new, and in fact has applications spanning back to investigations into the use of HIFU for non-invasive tissue ablation as early as the 1940s. Furthermore in the 1950s and 1960s Francis and William Fry, amongst others, performed work that led to treatments of neurological disorders using the combination of ultrasound and a high precision milling machine to accurately destroy tumours of the brain (Wu et al, 2007). This type of clinical trial however has until recently been difficult to perform due to the problems and complexity associated with the targeting of the ultrasound beams. As both ultrasound technology and general medical imaging have advanced, the use of HIFU for the treatment of tumours has once again become an area of interest in which much research is ongoing.

Currently, HIFU-based surgical treatment devices exist and a number have even gained FDA approved. These devices include the Sonablate 500 produced by Focus Surgery (Indianapolis, US) which has received the CE mark for prostate treatment in Europe and similar approval for use in Japan (Seip et al, 2004). The Sonablate 500 uses ultrasound for both guidance and treatment, the combination of which can be referred to as Ultrasound-guided Focused Ultrasound Surgery (USgFUS). In contrast the company Insightec have developed the Exablate 2000 device that offers Magnetic Resonance guided Focused Ultrasound Surgery (MRgFUS) with treatment centres located worldwide (Jolesz, 2009). These are just two of the many devices that have been developed in recent years, and this is an area that will no doubt be flooded with new devices as advances in the relevant technologies are made.

The Sussex Mk4 EIM device is capable of performing *in-vivo* breast scans, reconstruct 3D image layers (Figure 7.11) and extract coordinates (X,Y,Z) and impedance data values from selected Region of Interests (ROI). The possibility exists to incorporate into the EIM system a HIFU device that would use the extracted coordinates ($X_1Y_1Z_1$) to allow guidance of surgery for accurate ablation of cancerous tumours.

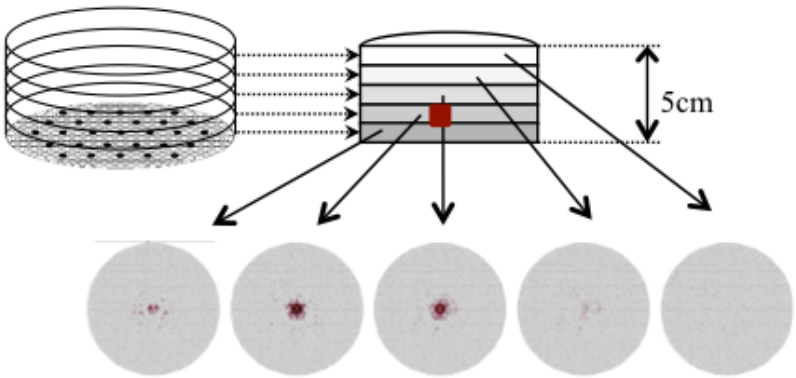

Figure 7.11. 3D reconstruction of layers with the Sussex EIM Mk4 with a ROI.

If the High Intensity Ultrasound already incorporates an ultrasound imaging module as in USgFUS, the diagnostic ultrasound device could be employed to scan again around the EIM defined Region of Interest. Using a method such as this would potentially allow a second three-dimensional image to be reconstructed from the ultrasound scan data, thus increasing the accuracy to interpret the geometry of the malignancy and the coordinates for the HIFU. Given suitably accurate image recognition software this could very well become a semi or even fully automated procedure, using a single device without the need for patient repositioning. Figure 7.12 shows the stages of extracting a Region of Interest and its coordinates from a 3D EIM volume.

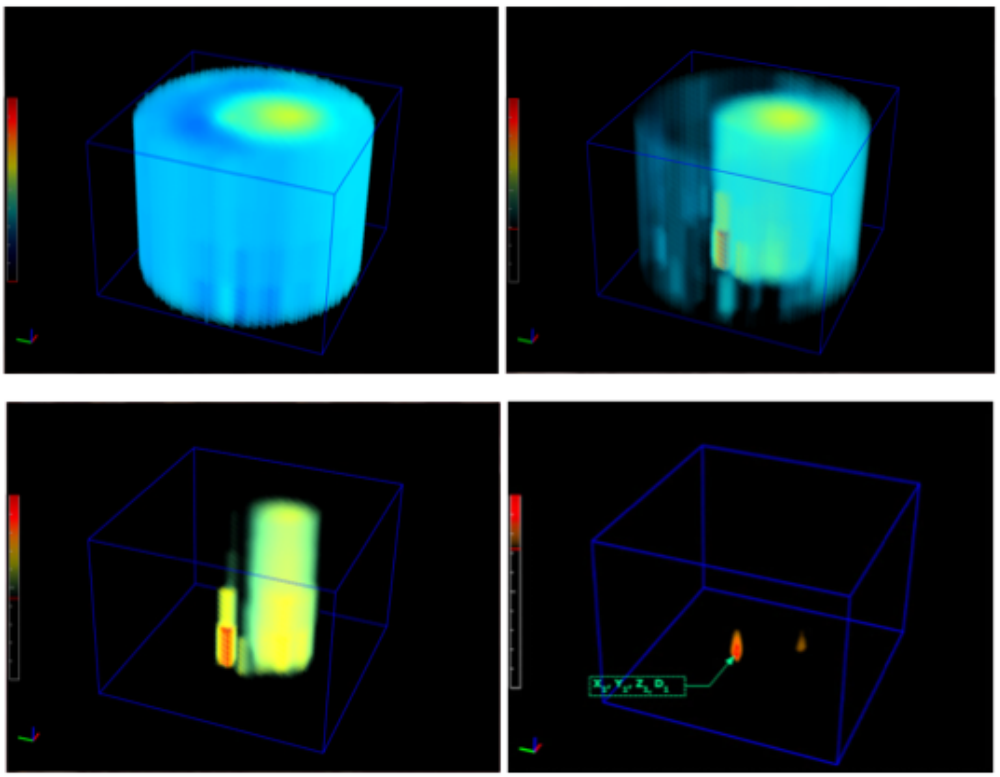

Figure 7.12. Threashholding steps of ROI information extraction from 3D layers in EIM.

One possible configuration to incorporate a HIFU device into the existing system would be to use a planar transducer in conjunction with a suitable acoustic lens (Cervera et al, 2002) as shown in Figure 7.13. This would allow a number of lenses to be used with the same, planar HIFU device, thus allowing flexibility in focal depth, and therefore in the tissue that could feasibly be targeted.

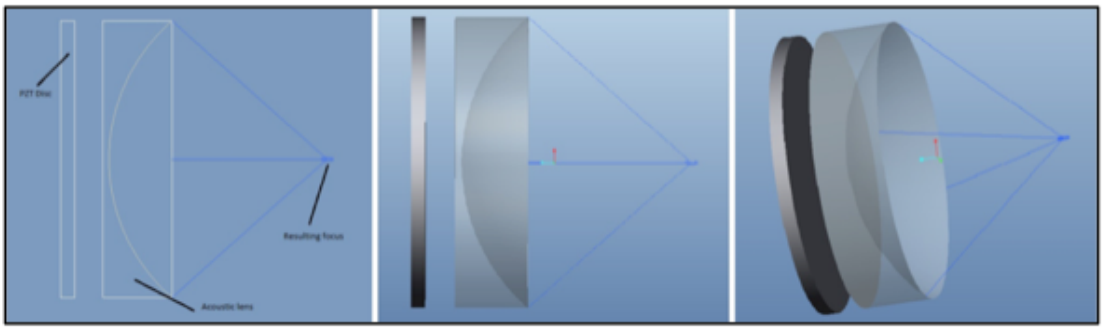

Figure 7.13. A planar HIFU transducer in combination with an acoustic lens.

A number of simulations have been carried out to determine suitable parameters for a device capable of non-invasive localised surgery. Examples of the results of such simulations are presented graphically in Figure 7.14.

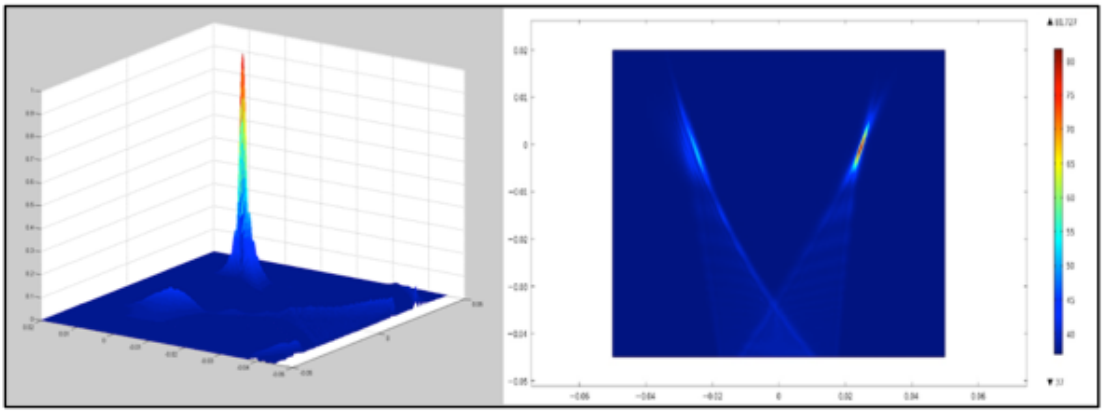

Figure 7.14. Example of the normalised acoustic intensity field (left); Resulting temperature rise (°C) in tissue (right).

Combining HIFU as a treatment methodology with EIM for detection and diagnosis of breast cancer offers huge potential for future research activity. The potential exists to improve the quality of life for a significant portion of the population, and to make this improvement with minimum pain or discomfort for those treated. In addition, with relevant adaptations this process could be modified to treat a larger range of cancers.

7.3.5 Intracavity EIT and Dual Modality Design

In this section is proposed a single or dual modality apparatus for intracavity EIT or combined EIT and Ultrasound scanning. The device dimensions and design could offer variations as standalone scanners for prostate and colon cancer; cervical cancer or throat and esophagous cancer. The device consists of an inner piston with a small ultrasound transducer on the tip, an outer body shell and a latex balloon with embedded electrodes. The inner space is filled with water and the piston functions like a syringe. When the syringe is pushed in, the water inflates the balloon and at the same time acts as ultrasound coupling material with the latex wall. The EIT electrodes on the balloon are arranged in parallel rings, therefore relying on current reconstruction algorithms.

The ultrasound transducer does never come into contact with the tissue and is part of the unibody design of the 'piston'. The ultrasound field of view will depend on the transducer or by additional rotation of the piston. Mapping of the EIT electrodes for the reconstruction mesh can be achieved by the ultrasound imaging.

8

- BIBLIOGRAPHY

Aberg, P., Nicander, I., Hansson, J., Geladi, P., Holmgren & U., Ollmar, S., (2004) Skin cancer identification using multifrequency electrical impedance - A potential screening tool. *IEEE Trans Biomed Eng;* 51(12):2097-102.

Adler, A., Arnold, J. H., Bayford, R., Borsic, A., Brown, B., Dixon, P., Faes, T. J. C., Frerichs, I., Gagnon, H., Garber, Y., Grychtol, B., Hahn, G., R B Lionheart, W. R. B., Malik, A., Patterson, R. P., Stocks, J., Tizzard, A., Weiler, N., & Wolf, G. K., (2009) GREIT: a unified approach to 2D linear EIT reconstruction of lung images. *Physiol. Meas. 30* S35–S55

Adler, A., & R B Lionheart, W. R. B., (2011) Minimizing EIT image artefacts from mesh variability in finite element models. *Physiol. Meas. 32* 823–834

Assenheimer, M., Laver-Moskovitz, O., Malonek, D., Manor, D., Nahaliel, U., Nitzan, R., & Saad, A. (2001). The T-SCAN technology: electrical impedance as a diagnostic tool for breast cancer detection. *Physiol Meast, 22 (1)*, 1–8.

Baert, A. L., (2008) Encyclopedia of diagnostic imaging. *Springer-Verlag Berlin Heidelberg New York* ISBN: 978-3-540-35278-5

Barber, D. C., Brown, B. H., & Freeston, I. L. (1983). Imaging Spatial Distributions of Resistivity Using Applied Potential Tomography. Electronics Letters, 19(22), 933-935.

Barber, D. C., & Brown, B. H. (1984). Applied Potential Tomography. *Journal of Physics E-Scientific Instruments, 17*(9), 723-733.

Barber, D. C., & Seagar, A. D. (1987). Fast reconstruction of resistance images. *Clin Phys Physiol Meas, 8 Suppl A*, 47-54.

Barber, D. C. (1990). Quantification in impedance imaging. *Clin Phys Physiol Meas, 11 Suppl A*, 45-56.

Barber, D. C. (2000). *Electrical Impedance Tomography* (Vol. Chapter 68).

Bayford, R. H. (2006). Bioimpedance tomography (Electrical impedance tomography). *Annual Review of Biomedical Engineering, 8*, 63-91.

Berg, W.A., Blume, J.D., Cormack, J.B., Mendelson, E.B., Lehrer, D., Böhm-Vélez, M., Pisano, E.D., Jong, R.A., Evans, W.P., Morton, M.J., Mahoney, M.C., Larsen, L.H., Barr, R.G., Farria, D.M., Marques, H.S., Boparai, K.; ACRIN 6666 Investigators. (2008) Combined screening with ultrasound and mammography vs mammography alone in women at elevated risk of breast cancer.*Journal of the American Medical Association. 14;299*(18):2151-63.

Bertolini, M., Nitrosi, A., Borasi, G., Botti, A., Tassoni, D., Sghedoni, R., & Zuccoli, G. (2011). Contrast detail phantom comparison on a commercially available unit. Digital Breast Tomosynthesis (DBT) versus full-field digital mammography (FFDM). *J Digit Imaging, 24*(1), 58-65.

Boone, K. G., & Holder, D. S., (1996). Effect of skin impedance on image quality and variability in electrical impedance tomography: a model study. *Med. and Biol. Eng. and Comput.* 34 (5) 351-354

Boone, K., Barber, D., & Brown, B. (1997). Imaging with electricity: report of the European Concerted Action on Impedance Tomography. *J Med Eng Technol, 21*(6), 201-232.

Borsic, A., & Paulsen, K. D., (2009) Safety Study for Induced Current Magnetic Resonance - Electrical Impedance Tomography in Breast Imaging. *Proceedings 10th International Conference on Biomedical Applications of Electrical Impedance Tomography*, Manchester UK.

Boyd, N. F., Guo, H., Martin, L. J., Sun, L., Stone, J., Fishell, E., Jong, R. E., Hislop, G., Chiarelli, A., Minkin, S., & Yaffe. (2007) Mammographic Density and the Risk and Detection of Breast Cancer. M. J. *N Engl J Med*, 356:227-236

Brown, B. H., & Seagar, A. D. (1987). The Sheffield data collection system. *Clin Phys Physiol Meas, 8 Suppl A*, 91-97.

Brown, B. H., Tidy, J., Boston, K., Blackett, A. D., & Sharp, F., (1998) Tetrapolar Measurement of Cervical Tissue structure using Impedance Spectroscopy. IEEE/EMBS International Conference, Hong Kong, 2886-2889.

Brown, B. H., Smallwood, R. H., Barber, D. C., Lawford, P. V., Hose, D. R., (2001) Medical Physics and Biomedical Engineering. *IOP Series in Medical Physics ISBN 0-7503-0368-9.*

Bushberg, J. T., Seibert, J. A., Leidholdt, E. M., Boone, J. M., (2002) The essential physics of medical imaging 2nd Ed. Lippincott Williams & Wilkins, ISBN 0-683-30118-7.

Campbell, A. M., & Land, D. V. (1992). Dielectric properties of female human breast tissue measured in vitro at 3.2 GHz. *Phys Med Biol, 37*(1), 193-210.

Campbell, J., & Dimache, N. (2007). 3D EIT - MEIK in clinical application: observations and preliminary results. *World Congress on Medical Physics and Biomedical Engineering 2006, Vol 14, Pts 1-6, 14*, 3906-3910.

Cervera, F., 2002 Physical Review Letters, *Vol 88, (2) January 2002*

Chauveau, N., Hamzaoui, L., Rochaix, P., Rigaud, B., Voigt, J. J., & Morucci, J. P. (1999). Ex vivo discrimination between normal and pathological tissues in human breast surgical biopsies using bioimpedance spectroscopy. *Electrical Bioimpedance Methods: Applications to Medicine and Biotechnology, 873*, 42-50.

Cherepenin, V. A., Karpov, A. Y., Korjenevsky, A. V., Kornienko, V. N., Mazaletskaya, A., Mazourov, D., & Meister, D. (2001). A 3D electrical impedance tomography (EIT) system for breast cancer detection. *Physiological Measurement, 22*(1), 9-18.

Cherepenin, V. A., Karpov, A. Y., Korjenevsky, A. V., Kornienko, V. N., Kultiasov, Y. S., Ochapkin, M. B., Trochanova, O. V., & Meister, J. D. (2002). Three-dimensional EIT imaging of breast tissues: system design and clinical testing. *IEEE Trans Med Imaging, 21*(6), 662-667.

Cherry, S., R., (2006) Multimodality in Vivo Imaging Systems: Twice the power or double the trouble?, *Annual Review of Biomedical Engineering 8: 35-62*

Cole, K. S. (1940). Permeability and Impermeability of Cell Membranes for Ions. *Cold Spring Harbor Symposia on Quantitative Biology, 8*, 110-122.

Cole, K. S., & Cole, R. H. (1941). Dispersion and absorption in dielectrics I. Alternating current characteristics. *Journal of Chemical Physics, 9*(4), 341-351.

Cook, R. D., Saulnier, G. J., Gisser, D. G., Goble, J. C., Newell, J. C., & Isaacson, D. (1994). ACT3: a high-speed, high-precision electrical impedance tomograph. *IEEE Trans Biomed Eng, 41*(8), 713-722.

Dobbins, J. T. (2009). Tomosynthesis imaging: At a translational crossroads. *Medical Physics, 36*(6), 1956-1967.

Dreyer, K.J., Hirschorn, D. S., Thrall, J. H., & Mehta, A., PACS – A guide to the Digital Revolution 2nd Ed. Springer. ISBN 978-0387-26010-5

Duffy, S.,W., Tabar, L., (2002) Journal of Cancer, 95: 458-469

Faes, T.J., van der Meij, H.A., de Munck, J.C. & Heethaar, R.M. (1999) The electric resistivity of human tissues (100 Hz-10 MHz): a meta-analysis of review studies. *Physiol Meas,* 20 (4)**,** R1-10.

Ferlay, J., Shin, H.R., Bray, F., Forman, D., Mathers, C. & Parkin, D.M., (2010) *GLOBOCAN 2008 v1.2, Cancer Incidence and Mortality Worldwide: IARC Cancer Base No. 10.* Lyon, France.

Fletcher, S.W., & Elmore, J.G., (2003) Mammographic Screening for Breast Cancer. *N Engl J Med 348,* 1672-1680

Forsyth, J., Borsic, A., Halter, R.J., Hartov, A., & Paulsen, K.D. (2011) Optical breast shape capture and finite-element mesh generation for electrical impedance tomography. *Physiol Meas*, 32(7), 797-809.

Fricke, H. M., S. (1925) The electric resistance and capacity of blood for frequencies between 800 and 4.5 million cycles *J. Gen. Physiol. , 9* 153-167.

Gennaro, G., Toledano, A., di Maggio, C., Baldan, E., Bezzon, E., La Grassa, M., Pescarini, L., Polico, I., Proietti, A., Toffoli, A., & Muzzio, P. C. (2010). Digital breast tomosynthesis versus digital mammography: a clinical performance study. *European Radiology, 20*(7), 1545-1553.

Gisser, D. G., Isaacson, D., & Newell, J. C. (1987). Current topics in impedance imaging. *Clin Phys Physiol Meas, 8 Suppl A*, 39-46.

Griffiths, H., & Zhang, Z. (1989). A dual-frequency electrical impedance tomography system. *Phys Med Biol, 34*(10), 1465-1476.

Grimnes, S. & Martinsen, Ø.G. (2008) *Bioimpedance and bioelectricity basics.* 2nd ed. ed. London: Academic.

Haar, G. T., (2001) Acoustic Surgery 2001 Physics Today Volume 54, Issue 12.

Haemmerich, D., Schutt, D.J., Wright, A.W., Webster, J.G. & Mahvi, D.M. (2009) Electrical conductivity measurement of excised human metastatic liver tumours before and after thermal ablation. *Physiol Meas,* 30 (5)**,** 459-66.

Halter, R. J., Hartov, A., & Paulsen, K. D. (2008). A broadband high-frequency electrical impedance tomography system for breast imaging. *IEEE Trans Biomed Eng, 55*(2), 650-659.

Halter, R.J., Schned, A., Heaney, J., Hartov, A., & Paulsen, K.D., (2009a) Electrical properties of prostatic tissues: I. Single frequency admittivity properties. *J Urol.* 182(4), 1600-7.

Halter, R.J., Schned, A., Heaney, J., Hartov, A., & Paulsen, K.D., (2009b) Electrical properties of prostatic tissues: II. Spectral admittivity properties. *J Urol.* 182(4), 608-13

Hartov, A., Mazzarese, R. A., Reiss, F. R., Kerner, T. E., Osterman, K. S., Williams, D. B., & Paulsen, K. D. (2000). A multichannel continuously selectable multifrequency electrical impedance spectroscopy measurement system. *IEEE Trans Biomed Eng, 47*(1), 49-58.

Hartov, A., Paulsen, K. D. (2004). Variation in breast EIT measurements due to menstrual cycle. *Physiol. Meas. , 25*, 295-299.

Hassan, A. M., & El-Shenawee, M., (2011) Review of Electromagnetic Techniques for Breast Cancer Detection. *Biomedical Engineering, IEEE reviews, Vol 4,* 103-118

Hellquist, B., Duffy, S., Abdsaleh, S., Björneld, L., Bordás, P., Tabár, L., Viták, B., Zackrisson, S., Nyström, L., Jonsson, H., (2011) Effectiveness of Population-Based Service Screening With Mammography for Women Ages 40 to 49 Years: Evaluation of the Swedish Mammography Screening in Young Women (SCRY) Cohort, *Journal of Cancer, vol. 117, 4: 714–722.*

Herman, G. T., (2009) *Fundamentals of computerized tomography: Image reconstruction from projection* 2nd Edition (Berlin: Springer)

Hinz, J., Hahn, G., Neumann, P., (2003) End-expiratory lung impedance change enables bedside monitoring of end-expiratory lung volume change. *Intensive Care Med* 29:37-43

Holder, D. S., (2004) *Electrical Impedance Tomography: Methods, History and Applications (Series in Medical Physics and Biomedical Engineering)* IoP Publishing ISBN 0-7503-0952-0

Hua, P., Woo, E. J., Webster, J. G., Tompkins, W. J., (1993) Finite element modeling of electrode-skin contact impedance in electrical impedance tomography *IEEE Trans. Biomedical Engineering* 40 (4) 335-343

Hua, P. (1987). Electrical impedance tomography in medicine. PhD Preliminiary proposal, University of Wisconson, Madison.

Isaacson, D. (1986). Distinguishability of Conductivities by Electric Current Computed Tomography. *Medical Imaging, IEEE Transactions on 5*(2), 91 - 95.

Ji, Z., Dong, X., Shi, X., You, F., Fu, F. & Liu, R. (2009) Novel electrode-skin interface for breast electrical impedance scanning. *Medical & Biological Engineering & Computing,* 47 (10)**,** 1045-52.

Jolesz, F. A., 2009 MRI-Guided Focused Ultrasound Surgery *Annual Review of Medicine Volume 60*: 417-430

Jossinet, J. (1998). The impedivity of freshly excised human breast tissue. *Physiol Meas, 19*(1), 61-75.

Joy, J. E., Penhoet, E. E., & Diana B. Petitti, D. B., (2005) Saving Women's Lives: Strategies for Improving Breast Cancer Detection and Diagnosis. ISBN: 0-309-53209-4,

Kak, C. A., Slaney, M., (2001) Principles of Computerized Tomographic Imaging. SIAM publishing ISBN 0-89871-494-X

Kao, T. J., Boverman, G., Kim, B. S., Isaacson, D., Saulnier, G. J., Newell, J. C., Choi, M. H., Moore, R. H., & Kopans, D. B. (2008). Regional admittivity spectra with

tomosynthesis images for breast cancer detection: preliminary patient study. *IEEE Trans Med Imaging, 27*(12), 1762-1768.

Kao, T.J., Saulnier, G.J., Xia, H.J., Tamma, C., Newell, J.C. & Isaacson, D. (2007) A compensated radiolucent electrode array for combined EIT and mammography. *Physiological Measurement,* 28 (7)**,** S291-S299.

Kelly, K.M., Dean, J., Lee, S.J., & Comulada, W.S., (2010) Breast cancer detection: radiologists' performance using mammography with and without automated whole-breast ultrasound. *Eur Radiol*. 20(11): 2557-64.

Kerner, T. E., Paulsen, K. D., Hartov, A., Soho, S. K., & Poplack, S. P. (2002). Electrical impedance spectroscopy of the breast: clinical imaging results in 26 subjects. *IEEE Trans Med Imaging, 21*(6), 638-645.

Knowles, M.A. & Selby, P. (2005) *Introduction to the cellular and molecular biology of cancer.* Oxford: Oxford University Press.

Kolb, T.M., Lichy, J. and Newhouse, J.H. (2002). Comparison of the Performance of Screening Mammography, Physical Examination, and Breast US and Evaluation of Factors that Influence Them: An Analysis of 27,825 Patient Evaluation. *Radiology*; 225: 165 – 175

Kolb, T.M., Lichy, J., & Newhouse, J.H., (1998) Occult cancer in women with dense breasts: detection with screening US - diagnostic yield and tumor characteristics. *Radiology*; 207:191-199.

Kolehmainen, V., Vaukhonen, M., Karjalainen, P. A., & Kaipio, J. P., (1997). Assessment of errors in static electrical impedance tomography with adjacent and trigonometric current patterns. *Physiol. Meas.* (18) 289-303.

Kopans, D. B. (1999). Breast-cancer screening with ultrasonography. *Lancet, 354*, 2096-2097.

Kourunen, J., Savolainen, T., Lehikoinen, A., Vauhkonen, M., & Heikkinen, L. M., (2009) Suitability of a PXI platform for an electrical impedance tomography system. *Meas. Sci. Technol.* 20 015503.

Kwong, S. L. (2003). Laterality, detailed site, and histology of female breast cancer in California 1988–1999. *Breast Cancer in California, Department of Health Services.*(9)

Lantin, B., (2003). A Weight off my shoulders. *The Daily Telegraph (London). (14 April 2003).* Retrieved Dec 2011.

Lionheart, W.R. (2004) EIT reconstruction algorithms: pitfalls, challenges and recent developments. *Physiological Measurement,* 25 (1)**,** 125-42.

Lobstein-Adams, C., Beqo, N., & Wang, W. (2011). Electrical Impedance assisted Ultrasound guided Focused Ultrasound Surgery: A comprehensive out-patient procedure? *Proceedings of the 12th International Conference in Electrical Impedance Tomography*. 69-72. Bath UK.

Malich, A., Fritsch, T., Anderson, R., Boehm, T., Freesmeyer, M. G., Fleck, M., & Kaiser, W. A. (2000). Electrical impedance scanning for classifying suspicious breast lesions: first results. *European Radiology, 10*(10), 1555-1561.

Markets and Markets (2011) Diagnostic Imaging Market (CT, MRI, X-Ray & Ultrasound) - Competitive Landscape & Global Forecasts 2010 – 2016, *Report Code: MD 1628, July 2011*

McAdams, E.T., Jossinet, J., Lackermeier, A. & Risacher, F. (1996) Factors affecting electrode-gel-skin interface impedance in electrical impedance tomography. *Medical & Biological Engineering & Computing,* 34 (6)**,** 397-408.

McEwan, A., Romsauerova, A., Yerworth, R., Horesh, L., Bayford, R., & Holder, D. (2006). Design and calibration of a compact multi-frequency EIT system for acute stroke imaging. *Physiological Measurement, 27*(5), S199-S210.

Metherall, P., Barber, D. C., Smallwood, R. H., & Brown, B. H. (1996). Three-dimensional electrical impedance tomography. *Nature, 380*(6574), 509-512.

Nissinen, A., Heikkinen, L. M., Kolehmainen, V., & Kaipio, J. P., (2009). Compensation of errors due to discretization, domain truncation and unknown contact impedances in electrical impedance tomography. *Meas. Sci. Technol.* 20 (10).

Office for National Statistics (ONS). (2011). Cancer survival in England: Patients diagnosed 2005-2009 and followed up to 2010. *ONS Publications London.*

Osterman, K. S., Kerner, T. E., Williams, D. B., Hartov, A., Poplack, S. P., & Paulsen, K. D. (2000). Multifrequency electrical impedance imaging: preliminary in vivo experience in breast. *Physiol Meas, 21*(1), 99-109.

Persson, P.-O., & Strang, G., (2004) A Simple Mesh Generator in MATLAB. *SIAM Review, Volume 46 (2), pp. 329-345,* June 2004

Piperno, G. F., & Moshitzky, M. (1990). *Breast cancer screening by impedance measurement. Front Med Biol Eng. , 1990(2(2)),* 111-117.

Pisano, E.D., Gatsonis, C., Hendrick, E., Yaffe, M., Baum, J. K., Acharyya, S., Conant, E. F., Laurie, Fajardo, L. L., Bassett, L., D'Orsi, C., Jong, R., & Rebner, M., (2005) Diagnostic Performance of Digital versus Film Mammography for Breast-Cancer Screening. *N Engl J Med.* 353:1773-1783

Polydorides, N., & Lionheart, W. R. B. (2002). A Matlab toolkit for three- dimensional electrical impedance tomography: a contribution to the Electrical Impedance and Diffuse Optical Reconstruction Software project. *Measurement Science & Technology, 13(12)* 1871-1883.

Qiao, G., Wang, L., Sze, G., Beqo, N., Tunstall, B., Chatwin, C. R., & Wang, W. Investigation of a compact *in-vitro* bio-impedance measurement system. *Asian Journal of Physics.* 2010. Volume 19. Page 79-86.

Saulnier, G. J., Blue, R. S., Newell, J.C., Isaacson, D., & Edic, P. M., (2001) Electrical Impedance Tomography. *IEE Signal Processing Magazine 1053-5888/01.*

Saulnier, G. J., Liu, N., Tamma, C., Xia, H., Kao, T. J., Newell, J. C., & Isaacson, D. (2007). An electrical impedance spectroscopy system for breast cancer detection. *Conf Proc IEEE Eng Med Biol Soc, 2007*, 4154-4157.

Schwan, H. P. (1957). Electrical properties of tissue and cell suspensions. *Adv Biol Med Phys. , 5*, 147-209.

Seip, R., Carlson, R. F., Chen, W., Sanghvi, N. T., Peenna, M. A., Dines, K. A., Pfile, R., Gardner, T. A., Koch, M., (2004) Automated HIFU Treatment Planning and Execustion based on 3D Modeling of the Prostate, Urethra and Rectal Wall *Ultrasonics Symposium 2004 Volume 3* 1781-1784

Sha, L. W., Ward, E. R., & Stroy, B. (2002). A review of dielectric properties of normal and malignant breast tissue. *IEEE Southeastcon 2002: Proceedings*, 457-462.

Sim, L.S., Hendriks, J.H., & Fook-Chong, S.M., (2004) Breast ultrasound in women with familiar risk of breast cancer. *Ann Acad Med Singapore.* 33(5): 600-6.

Smith, A. (2008). Fundamentals of breast tomosynthesis: improving the performance of mammography. *Breast, 2008*, 1-8.

Soleimani, M., (2006) Electrical impedance tomography imaging using a priori ultrasound data. *BioMedical Engineering OnLine 2006*, 5:8

Soni, N. K., Hartov, A., Kogel, C., Poplack, S. P., & Paulsen, K. D. (2004). Multi-frequency electrical impedance tomography of the breast: new clinical results. *Physiol Meas, 25*(1), 301-314.

Stavros, A. T. (2004) *Breast Ultrasound*. Lippincott Williams & Wilkins. ISBN-13:978-0397-51624-7

Stavros A.T., Thickman D., Rapp C.L., Dennis M.A., Parker S.H., Sisney G.A. (1995). Solid breast nodules: use of sonography to distinguish between benign and malignant lesions. *Radiology*;196:123-34.

Steiner, G., Soleimani, M., & Watzenig, D., (2008) A bio-electromechanical imaging technique with combined electrical impedance and ultrasound tomography *Physiol. Meas. 29* S63–S75.

Surowiec, A. J., Stuchly, S. S., Barr, J. R., & Swarup, A. (1988). Dielectric-Properties of Breast-Carcinoma and the Surrounding Tissues. *Ieee Transactions on Biomedical Engineering, 35*(4), 257-263.

Sze, G., (2012). Detection of breast cancer with Electrical Impedance Mammography. PhD Thesis. University of Sussex.

Sze, G., Wang, W., Barber, D. C., Huber, N., (2011). Preliminary study of the sensitivity of the Sussex Mk4 Electrical Impedance Mammography planar electrode system. *Proceedings of the 12th International Conference in Electrical Impedance Tomography EIT*. 77-81.

Tabar, L., & Dean, P., (2010) A new era in the diagnosis and treatment of breast cancer, *J. Breast, vol. 16, S2-4*

Tabar, L., Fagerberg, C., Gad, A., Baldetorp L., (1985) Reduction in mortality from breast cancer after mass screening with mammography: Randomised trial from

the Breast Cancer Screening Working Group of the Swedish National Board of Health and Welfare, *Lancet, vol. 325, no. 8433, 829-832.*

Tingberg, A. (2010). X-ray tomosynthesis: a review of its use for breast and chest imaging. *Radiat Prot Dosimetry, 139*(1-3), 100-107.

Tobias, J.S., Hochhauser, D., Souhami, R.L.C. & its, m. (2010) *Cancer and its management.* 6th ed. ed. Oxford: Wiley-Blackwell.

Trokhanova, O. V., Okhapkin, M. B., & Korjenevsky, A. V. (2008). Dual-frequency electrical impedance mammography for the diagnosis of non-malignant breast disease. *Physiol Meas, 29*(6), S331-344.

Tromberg, B., Pogue, B., Paulsen, K., Yodh, A., Boas, D., & Cerussi, A., (2008) Assessing the future of diffuse optical imaging technologies for breast cancer management, *Medical Physics, vol. 35, 2443-2451.*

Tunstall, B. D., W; Lu, H; Huber, N; Béqo, N; Sze, G; Wang, W (2010). Preliminary findings of a clinical investigation into the use of 3-dimensional impedance imaging for the detection of breast lesions in-vivo. *XIV International Conference on Electrical Bioimpedance and 11th Conference on Biomedical Applications of Electrical Impedance Tomography (ICEBI & EIT 2010) conference proceedings, 224.*

Tunstall, B. Wang, W., McCormick M., Walker, R., Rew, D., (1997) Preliminary in vitro studies of electrical impedance mammography (EIM): a future technique for non-invasive breast tissue imaging ? *The Breast Aug. Vol 6*(4), 253-253.

Udupa, J. K., & Herman, G. T. (1999) *3D Imaging in Medicine* 2nd Ed. CRC Press.

Vauhkonen, P. J., Vauhkonen, M., Savolainen, T., & Kaipio, J. P. (1999). Three-dimensional electrical impedance tomography based on the complete electrode model. *IEEE Trans Biomed Eng, 46*(9), 1150-1160.

Verkooijen, H. M., (2002). Diagnostic accuracy of stereotactic large-core needle biopsy for nonpalpable breast disease: Results of a multicenter prospective study with 95% surgical confirmation. *International Journal of Cancer. 99(6),* 853-859

Viehweg, P., Lampe, D., Buchmann, J., & Heywang-Kobrunner, S.H., (2000) In situ and minimally invasive breast cancer: morphologic and kinetic features on contrast-enhanced MR imaging. *MAGMA. 11(3)*, 129–137.

Wang, W., Gu, D-W., Pelengaris, S., Qiao, G., Cheung, L., Tunstall, B., & Epstein, E. (2008) Preliminary results from a study of pancreatic tissue for cancer identification using electrical impedance measurement. *The 9th Electrical Impedance Tomography (EIT) Conference Hanover, USA*

Wang, L., Wang, W., Huang, T. & Tunstall, B., (2008) In-vitro Study of the Electrical Impedance Characteristics of Human Female Breast Tissues *The 9th Electrical Impedance Tomography (EIT) Conference Hanover, USA*

Wang, W., Wang, L., Qiao, G., Prickett, P., Bramer, B., Tunstall, B., & Al-Akaidi, M. (2007). Study into the repeatability of the electrode-skin interface utilizing electrodes commonly used in Electrical Impedance Tomography. *13th International Conference on Electrical Bioimpedance and the 8th Conference on Electrical Impedance Tomography. 17*, 336-339.

Wang, W., Tang, M., McCormick, M., & Dong, X. (2001). Preliminary results from an EIT breast imaging simulation system. *Physiol Meas, 22*(1), 39-48.

Wang, W., Tunstall, B., Chauhan, D., & McCormick, M. (1998). The design of De Montfort Mk2 electrical impedance mammography system. *Proceedings of the 20th Annual International Conference of the Ieee Engineering in Medicine and Biology Society, Vol 20, Pts 1-6, 20*, 1042-1043.

Wang, W., Brown, B. H., & Barber, D. C. (1995). *Performance of the Sheffield Mk3A multi-frequency system for electrical impedance tomography*. Innovations in Instrumentation for Electrical Tomography, IEE Colloquium.

Wilson, A. J., Milnes, P., Waterworth, A. R., Smallwood, R. H., & Brown, B. H. (2001). Mk3.5: a modular, multi-frequency successor to the Mk3a EIS/EIT system. *Physiological Measurement, 22*(1), 49-54.

Wu, J., Nyborg, W., (2006) Emerging Therapeutic Ultrasound *University of Vermont, USA.*

Wood, K., Cameron, M., & Fitzgerald, K., (2008) Breast size, bra fit and thoracic pain in young women: a correlational study *Chiropractic & Osteopathy*. 16:1

Wu, F., Wang, Z. B., Cao, Y. D., Zhu, X. Q., Zhu, H., Chen, W. Z., Zou, J. Z., (2007) Wide local ablation of localised breast cancer using high intensity focused ultrasound *J Surg Oncol. 2007* Aug 1;96(2):130-6

Xu, G. Z., Wang, R. P., Zhang, S., Yang, S., Justin, G. A., Sun, M. G., & Yan, W. L. (2007). A 128-electrode three dimensional electrical impedance tomography system. *2007 Annual International Conference of the Ieee Engineering in Medicine and Biology Society, Vols 1-16*, 4386-4389.

Ybarra G. A. , L. Q. H., Ye G. Ye, Lim K. H., Lee J. H., Joines W. T., and George R. T. (2007). *Breast Imaging using Electrical Impedance Tomography (EIT)* (Vol. 2008): American Scientific Publishers.

Ye, G., Lim, K. H., George, R., Ybarra, G., Joines, W. T., & Liu, Q. H. (2006). A 3D EIT system for breast cancer imaging. *2006 3rd Ieee International Symposium on Biomedical Imaging: Macro to Nano, Vols 1-3*, 1092-1095.

Ye, G., Lim, K. H., George, R. T., Ybarra, G. A., Joines, W. T., & Liu, Q. H. (2008). 3d EIT for Breast Cancer Imaging: System, Measurements, and Reconstruction. *Microwave and Optical Technology Letters, 50*(12), 3261-3271.

Zou, Y., & Guo, Z. (2003). A review of electrical impedance techniques for breast cancer detection. *Med Eng Phys, 25*(2), 79-90.

9

- APPENDIX

9.1 PATENT 1 - GB AND INTERNATIONAL PCT FILINGS

ELECTRICAL IMPEDANCE DETECTION AND ULTRASOUND SCANNING OF BODY TISSUE

- GB patent application 1020729.8 - December 2010.
- International patent application PCT/GB2011/052418 - December 2011.
- International Publication WO2012076881 – June 2012.

W Wang, N Beqo, H J Gassert, D I Lines, J Wharrie, M McCormick, M C Forman, M Greenwood

INTELLECTUAL PROPERTY OFFICE

Concept House
Cardiff Road
South Wales
NP10 8QQ
United Kingdom

Telephone +44 (0) 1633 814000
Minicom +44 (0) 8459 222250

DX 7226AB41 Clappa Park 3

Website www.ipo.gov.uk

Electronic Filing Receipt

Swindell & Pearson Ltd
48 Friar Gate
Derby
United Kingdom
DE1 1GY

Your Ref: 23475GB

07 December 2010

PATENT APPLICATION NUMBER 1020729.8

We have received your request for grant of a patent and recorded its details as follows:

Filing date(*)	07 December 2010	
Earliest priority date (if any)		
Applicant(s) / contact point	The University of Sussex	
Application fee paid	Yes	
Description (number of pages or reference)	18	
Certified copy of referenced application	Not applicable	
If description not filed	Not applicable	
Claims (number of pages)	6	
Drawings (number of pages)	9	
Abstract (number of pages)	No, file by 07 December 2011	
Statement of inventorship (Form 7)	No, file by 07 April 2012	
Request for search (Form 9A)	Yes	
Request for examination (Form 10)	None	
Priority Documents	None	
Other Attachments Received	Fee Sheet	FeeSheet.pdf
	Validation Log	ValidLog.pdf
Signed by	CN=P. Higgin 9226,O=Swindell & Pearson,C=GB	

INTELLECTUAL PROPERTY OFFICE

Concept House
Cardiff Road
South Wales
NP10 8QQ
United Kingdom

telephone +44 (0) 1633 814000
Minicom +44 (0) 8459 222250

DX 722540/41 Cloppa Park 3

Website www.ipo.gov.uk

Electronic Filing Receipt

Acknowledgement of receipt

We hereby acknowledge receipt of your request for the processing of an international application according to the Patent Cooperation Treaty as follows:

Submission number	1200029482	
PCT application number	PCT/GB2011/052418	
Date of receipt	07 December 2011	
Receiving Office	Intellectual Property Office, Newport	
Your reference	23475PCT1	
Applicant	THE UNIVERSITY OF SUSSEX	
Number of applicants	9	
Country	GB	
Title	ELECTRICAL IMPEDANCE DETECTION AND ULTRASOUND SCANNING OF BODY TISSUE	
Documents submitted	eolf-pkda.xml	eolf-requ.xml
	eolf-appb.xml	eolf-fees.xml
	eolf-vlog.xml	eolf-othd-000001.pdf (24 p.)
	eolf-abst.txt	eolf-appb-P000001.pdf (9 p.)
	eolf-othd-000002.zip	
Submitted by	CN=P. Higgin 9226,O=Swindell & Pearson,C=GB	
Method of submission	Online	
Date and time receipt generated	07 December 2011, 13:00:37 (GMT)	
Digest	10:6D:55:61:BF:18:F1:06:71:84:8C:64:66:A2:6F:7F:CD:59:9F:76	

/Intellectual Property Office, Newport/

(12) INTERNATIONAL APPLICATION PUBLISHED UNDER THE PATENT COOPERATION TREATY (PCT)

(19) World Intellectual Property Organization
International Bureau

(43) International Publication Date
14 June 2012 (14.06.2012)

WIPO | PCT

(10) International Publication Number
WO 2012/076881 A1

(51) International Patent Classification:
A61B 5/053 (2006.01) *A61B 8/08* (2006.01)
A61B 8/14 (2006.01)

(21) International Application Number:
PCT/GB2011/052418

(22) International Filing Date:
7 December 2011 (07.12.2011)

(25) Filing Language: English

(26) Publication Language: English

(30) Priority Data:
1020729.8 7 December 2010 (07.12.2010) GB

(71) Applicant *(for all designated States except US)*: **THE UNIVERSITY OF SUSSEX** [GB/GB]; Sussex House, Brighton BN1 9RH (GB).

(72) Inventors; and

(75) Inventors/Applicants *(for US only)*: **WANG, Wei** [CN/GB]; The University of Sussex, Sussex House, Brighton BN1 9RH (GB). **BEQO, Nevis** [AL/GB]; The University of Sussex, Sussex House, Brighton BN1 9RH (GB). **GASSERT, Hans-Juergen** [DE/GB]; Diagnostic Sonar Limited, Baird Road, Kirkton Campus, Livingston West Lothian EH54 7BX (GB). **LINES, David Ian Arthur** [GB/GB]; Diagnostic Sonar Limited, Baird Road, Kirkton Campus, Livingston West Lothian EH54 7BX (GB). **WHARRIE, James O'Brien** [GB/GB]; Diagnostic Sonar Limited, Baird Road, Kirkton Campus, Livingston West Lothian EH54 7BX (GB). **MCCORMICK, Malcolm** [GB/GB]; Newsplus Media Technologies Limited, Omega Court, 352 Cemetery Road, Sheffield South Yorkshire S11 8FT (GB). **FORMAN, Matthew Charles** [GB/GB]; Newsplus Media Technologies Limited, Omega court, 352 Cemetery Road, Sheffield South Yorkshire S11 8FT (GB). **GREENWOOD, Mark** [GB/GB]; Weedon Electronics, Richmond House, Walkern Road, Stevenage Hertfordshire SG1 3QP (GB).

(74) Agents: **HIGGIN, Paul** et al.; Swindell & Pearson Ltd, 48 Friar Gate, Derby Derbyshire DE1 1GY (GB).

(81) Designated States *(unless otherwise indicated, for every kind of national protection available)*: AE, AG, AL, AM, AO, AT, AU, AZ, BA, BB, BG, BH, BR, BW, BY, BZ, CA, CH, CL, CN, CO, CR, CU, CZ, DE, DK, DM, DO,

[Continued on next page]

(54) Title: ELECTRICAL IMPEDANCE DETECTION AND ULTRASOUND SCANNING OF BODY TISSUE

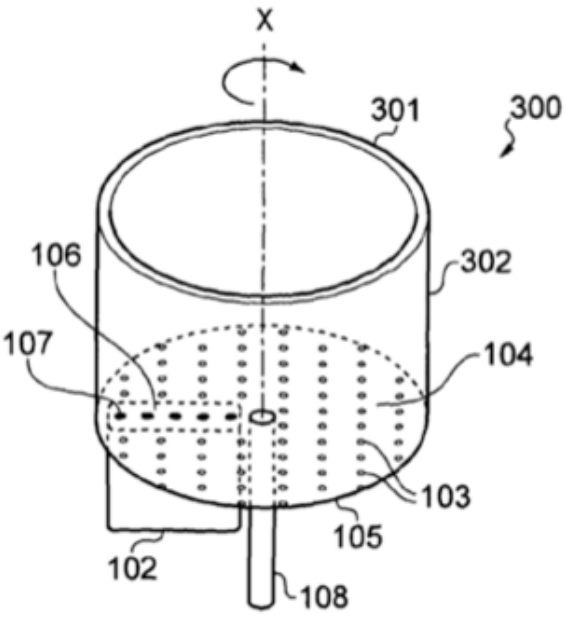

FIG. 3

(57) Abstract: An apparatus for performing electrical impedance detection and ultrasound scanning of body tissue, the apparatus comprising: a container for receiving body tissue comprising, at a depth, a spacing member for contacting the body tissue;an electrode array for performing electrical impedance detection by applying a first electrical signal to the body tissue, receiving an electrical response signal characteristic of the body tissue, and providing a first output signal representative of the electrical response signal; an ultrasound transducer for performing ultrasound detection by applying a first ultrasound signal to the body tissue, receiving an ultrasound response signal characteristic of the body tissue, and providing a second output signal representative of the ultrasound response signal, wherein the ultrasound transducer and the electrode array are mounted on a rotatable element of the apparatus that moves when the depth of the container is varied, and that, is configured in use, to underlie the spacing member and to rotate with respect to the body tissue; and wherein the spacing member comprises apertures.

WO 2012/076881 A1